Paleogeography modulates marine extinction risk over the Phanerozoic

Cooper M. Malanoski[1*], Seth Finnegan[2,4], Edward C. Huang[3], Lila Blake[1], Connal Mac Niocaill[1], Erin E. Saupe[1*]

[1]*Department of Earth Sciences, Oxford University, South Parks Road, Oxford, OX1 3AN, U.K.*

[2]*Department of Integrative Biology, University of California, Berkeley, CA 94720*

[3]*Department of Computer Science, Stanford University, Stanford, CA 94305*

[4]*Smithsonian Tropical Research Institute, Panama City, Panamá Province 0843-03092, Panama*

**Corresponding authors*

Abstract

Understanding the factors that have influenced the intensity and selectivity of extinction throughout Earth history is important for explaining past biodiversity change and forecasting biotic responses to environmental change. Here we investigate the role of coastline geometry and paleogeographic boundary conditions in shaping extinction risk for shallow-marine taxa over the past 540 million years. We show that interactions between the geographic distributions of taxa and the geometric configurations of continental margins consistently predict relative extinction risk—taxa with potential dispersal pathways that are long relative to the range of latitude traversed, such as occurs along east-west oriented coastlines, islands, or inland seaways, consistently exhibit higher extinction risk than taxa with potential dispersal pathways that provide more direct latitude-traversing paths. This dispersal distance selectivity is amplified during mass extinction events and hyperthermal intervals, suggesting that geographic constraints become more important during periods of rapid climate change. Our results provide another mechanism potentially contributing to the generally elevated extinction rates during the Paleozoic, an interval characterized by complex inland seas and a preponderance of east-west coastlines. These insights underscore the importance of considering paleogeographic context when interpreting past extinction patterns and provide empirical support for assumptions underlying extinction risk assessments of extant species.

Introduction

Earth has experienced dramatic fluctuations in biodiversity across time (*1*) and space (*2*, *3*), with relatively quiescent background intervals episodically interrupted by mass extinction events (*4*, *5*). Extinction over geological timescales has been shown to result from the complex interplay of organismal traits (*6–10*), population-level attributes such as geographic range size (*6*, *9*, *11*, *12*), and extrinsic environmental factors such as climate change (*6*, *13*, *14*). We hypothesize that the geographic arrangement of continents and islands (hereafter *paleogeography* (*15*, *16*)) was a significant boundary condition modulating extinction risk by facilitating or inhibiting habitat tracking (*17–21*) during periods of climate change (*14*, *22*). In marine systems, the role of paleogeography should be most important for taxa restricted to relatively shallow habitats (~<200 m depth) tied to continental shelf environments, where

the ability to track preferred climatic conditions in a changing climate may depend in part on availability of continuous dispersal corridors, assuming species do not adapt *in situ* (Fig. 1). If so, taxa inhabiting east-west oriented coastlines, isolated islands, and epicontinental seaways may be more prone to extinction during episodes of rapid climate change than taxa inhabiting continuous north-south oriented coastlines (*16*, *23*).

The influence of paleogeography on past biodiversity dynamics has been investigated previously using simulations (*16*, *24–27*) for limited time intervals (*26*, *26–29*). These models provide proof of principle, but their predictions have not been tested using empirical fossil data. Here we investigate the role of paleogeographic boundary conditions, and specifically coastline geometry, in regulating extinction patterns over the last 540 million years. We additionally test whether the effect of paleogeography on extinction risk was amplified during periods of mass extinction, when the need to disperse to track climate change or avoid perturbations such as anoxia was more critical (*30*, *31*).

We develop a metric for estimating coastline geometries (*32*, *33*) using a parallel pathfinding algorithm to contemporaneously evaluate all possible dispersal paths that would have allowed documented populations of a given taxon to reach a predefined threshold of either 5^{o}, 10^{o} or 15^{o} latitude from any given coastal grid cell. This method is analogous to box counting algorithms used to evaluate modern coastline geometries (*32*) and allows quantification of geometric properties of each coastal grid cell over the Phanerozoic across three different geographic scales (5^{o}, 10^{o} or 15^{o} latitude), potentially reflecting different ecological implications associated with varying intensities of climate-driven latitudinal shifts. For each taxon in a given Stage at each occurrence, we computed the average number of grid-cell steps to the specified latitudinal threshold (5°, 10°, or 15°) north and south, then took the median across occurrences to assign a single coastline-geometry value per taxon. This metric, hereby referred to as '*distance to track'*, represents the average steps required to reach a specified latitudinal change (see SI Methods and Materials (*34*)). To account for uncertainty in paleogeographic reconstructions (*35*), we use four global plate models (GPM) (Scotese and Wright (*36*), Torsvik & Cocks (*37*), Golonka (*38*), and Merdith (*39*)) and two coastline definitions: a simple 1° × 1° grid-based approach, and a more complex definition that includes all shallow marine shelf areas, accounting for continental flooding (*40*).

We analyse per-taxon extinction selectivity at the genus level for shallow-marine-restricted ectotherms (n=12,945) from the Paleobiology Database (PBDB) (*41*), for taxa belonging to the phyla Brachiopoda, Porifera, Echinodermata, Bryozoa, and Mollusca, along with the classes Anthozoa and Polychaeta, and the arthropod clades Trilobita, Xiphosura, and Malacostraca—these taxa were selected for their relatively high preservation potential. We evaluated the effect of coastal geometry on extinction risk for these taxa by employing a generalized linear mixed-effects model (GLMM) approach, accounting for temporal and taxonomic structure with stage and class as random effects. Mass extinction and hyperthermal events were included as interaction terms in some models, allowing us to test how selectivity varies across different evolutionary and climatic regimes (see SI Methods and Materials (*34*)).

Paleogeography Predicts Extinction Risk

Coastline geometry is significantly positively correlated with per-taxon extinction risk across the Phanerozoic (Fig. 2, 3), suggesting that more convoluted coastlines or those that are

east-west oriented impose a greater risk of extinction for marine taxa. Taxa needing to move more than 50 grid cell steps (equating to ~5,500 kilometers) exhibit an increased probability for extinction across all global plate models (GPMs) when considering latitudinal thresholds of 5°, 10°, or 15° (Fig. 3b). Taxa that could not travel 5°, 10°, or 15° latitude north or south in 100 steps were 45% (95% CI: 20%, 100%) more likely to go extinct compared to those that could (Fig. 3). Consistent with expectations, we found the effect of coastline geometry was amplified when accounting for the interaction between dispersal ability (see SI Methods and Materials (*34*)) and coastline geometry, with coastline geometry less important for good dispersers than for taxa with poor or uncertain dispersal ability (fig. S1,S2,S3,S4; table S2).

Coastline geometry remains a significant predictor of relative extinction risk when tested using the post-Triassic record, when paleogeographic configurations are better constrained by existing oceanic crust (*35*, *42*) (fig. S5,S6). A significant positive correlation between extinction risk and paleogeography was maintained for most thresholds and GPMs (15 out of 16, see SI Methods and Materials (*34*); fig. S7,S8,S9,S10,S11,S12), when polar occurrences were excluded to avoid edge effects (11 of 16; see SI Methods and Materials (*34*); fig. S13-S14,S15,S16,S17,S18), and when a Haversine distance was used instead of grid cell steps (fig. S10).

We explored different definitions of coastlines, comparing narrow coastlines that are defined as the interface between continental landmasses and broader definitions based on coastal shelves (See SI Methods and Materials (*34*); fig. S19). Both approaches yielded similar results, although broader coastal shelves showed slightly stronger associations between coastline geometry and per-taxon extinction risk. To account for sampling biases, we employed bootstrap and jackknife subsampling methods, which produced results consistent with those based on raw unsubsampled occurrence data (fig. S19). We additionally tested the effect of coastline geometry on extinction risk while accounting for uncertainty in true time of extinction using the approach developed by Reddin et al. (*7*, *43*) and found coastline geometry remained an important predictor (fig.S20).

To assess the robustness of our findings to Type I and Type II statistical errors, we implemented power analyses and permutation- and simulation-based null models (see SI Methods and Materials (*34*)). These analyses indicated high power to detect the observed effect sizes and showed that comparable signals did not emerge under null expectations, suggesting the effect of coastline geometry is unlikely to be a statistical artifact on Phanerozoic timescales.

Our results support the hypothesis that paleogeography, and specifically coastline geometry, played a role in modulating extinction risk for marine invertebrate taxa throughout the Phanerozoic (*16*). Taxa inhabiting north-south oriented coastlines were likely able to better track their thermal tolerance range when climate changed (Fig. 1c, 3b), whereas taxa inhabiting east-west oriented coastlines, islands, convoluted coastlines, or elongated epicontinental seas likely experienced significant barriers to dispersal, contributing to heightened extinction risk.

Epicontinental seaways were generally more extensive during the Paleozoic (*40*) compared to the subsequent Mesozoic and Cenozoic, and differences in continental configuration may help explain the elevated extinction of the early to mid Paleozoic, particularly when

compounded by the effects of other factors, such as low oxygenation and climate change (*6*, *15*, *44*). We find a significant positive correlation between our distance to track metric and eustatic sea level (*45*) (fig. S21), suggesting that increased continental flooding may limit species' abilities to track climate change and thereby lead to increased extinction risk, consistent with the common cause hypothesis (*46*).

We focus here on skeletonized marine invertebrates because of the relative completeness of their fossil record. Paleogeography has likely played a similarly-consistent role in modulating extinction risk for marine vertebrates, but it is possible the effect is dampened by the greater mobility of many nektonic and pelagic vertebrates relative to the benthic groups that dominate the marine invertebrate record.

The role of paleogeography is amplified during mass extinctions

The influence of coastline geometry on extinction risk was amplified during mass extinction events (Fig. 4a) and hyperthermals (Fig. 4b) compared to background intervals (Fig. 4c, table S1), suggesting differing selectivity signals dependent on macroevolutionary regime (*4*, *5*, *8*, *9*, *12*, *47–49*). Marginal effects for mass extinctions versus background intervals (Fig. 4a, fig. S20a), and hyperthermals versus non hyperthermals (Fig. 4b, fig. S22b), show that the probability of extinction is similarly-low, regardless of extinction regime or threshold, until a divergence in odds of extinction at ~25 grid cell steps for both mass extinctions (Fig. 4a) and hyperthermals (Fig. 4b). Taxa with longer distances to track had an increased risk of extinction of up to 400% during mass extinctions compared to only a 60% increase during background intervals. Thus, the geographic constraints imposed by paleogeography become even more significant in driving extinction during periods of elevated environmental stress.

This amplified effect is particularly notable when considering the interaction between paleogeography and hyperthermals (Fig. 4; fig. S22) (*7*, *43*), providing a potential mechanism contributing to differences in extinction severity observed between events such as the Paleocene–Eocene Thermal Maximum **(**PETM; 56 Ma) and the Permian-Triassic mass extinction at ~252 Ma (*50*, *51*). Although both intervals were characterized by rapid climate change on geologic timescales, differences in paleogeography, and thus coastline geometries, may have played a role in modulating the different extinction magnitudes, alongside other factors such as ocean oxygenation (*15*, *44*, *52*). The heightened importance of paleogeography during rapid or extreme climate change highlights the role of boundary conditions in shaping the severity of mass extinction or hyperthermal events (16, 63), and contrasts with other extinction risk factors, whose influence is typically weakened during mass extinctions (4, 5, 8, 9, 12, 32–34, 46).

Paleogeography predicts risk alongside other known determinants

To test the importance of paleogeography in the context of other known determinants of extinction risk (*6*, *7*, *9*, *12*, *53*), we included coastline geometry alongside five other predictors analysed in Malanoski et al. (*6*) (geographic range size, body size, realized thermal preference, realized thermal breadth, and the temperature change experienced by individual taxa) in a GLMM. Unsurprisingly, coastline geometry played a relatively minor role in mediating extinction risk (0.05 log odds, compared to geographic range size, with a log odds of -0.44; fig. S23, table S3-S9) but was included alongside the five other well-established extinction predictors in the best supported model (*6*, *7*, *9*, *12*). The overall effect

of coastline geometry on extinction risk, while significant, is therefore modest compared to other measured correlates.

Model considerations

Several sources of uncertainty need to be considered when contextualising our model results. Although we used multiple plate models to account for variability in paleogeographic reconstructions (*36–40*); Fig. 3; fig. S7,S8,S9,S11), the inherent uncertainty in these models, particularly for periods older than 300 Ma (*35*, *42*), introduces potential error (*35*). This uncertainty is compounded by the scaling issues associated with reconstructing coastline geometries (*33*), as the resolution of these models may affect the precision of our coastline metric and relatively local coastline features can have a large influence on dispersal and provinciality of marine species (*54*).

Dispersal is another potential critical confounding factor in our analyses. Many taxa, especially those with planktotrophic larvae, would have been able to traverse vast distances (*21*), potentially rendering paleogeographic constraints less important. The temporal scale of our analysis, which averages over millions of years, may compound this potential issue, introducing uncertainty regarding how accurately our metric reflects real-time dynamics. The presence of these sources of uncertainty, however, would generally tend to weaken the selectivity signal for coastline geometry, so the recovery of any signal on such broad timescales may highlight its importance in modulating extinction patterns.

Dispersal is also mediated largely via ocean circulation dynamics in the modern (*55*), and climate change can lead to shifts in these dynamics (*55*). Unfortunately, there is a dearth of paleo-ocean current models and large errors associated with estimating these changes in the geologic past. Our metric is therefore unlikely to be reflective of the true dispersal potential for a species, but rather serves as a proxy for coastline geometry. To address this, we excluded taxa that are hypothesized to have poorer dispersal abilities (See SI Methods and Materials (*34*)), but accurately delineating the dispersal potential of every taxon in our dataset is difficult, especially for the Paleozoic. Coastline geometry, however, remained significant despite the likely inclusion of taxa with high dispersal potential, suggesting the importance of coastline geometry might be underestimated, not overestimated, in our analysis.

We additionally assume all coastal grid cells are habitable, and that a taxon can track its habitat both north and south. In reality, some coastal regions, despite being geographically accessible, would have been ecologically unsuitable due to differences in salinity, temperature, or other biotic or environmental factors that could affect a species' survival and dispersal (*23*, *30*). Depending on the direction of climate change, species may be restricted to tracking their habitat either north or south.

To account for dispersal uncertainties, we used two coastline definitions: a simplified version that only allows dispersal along a 1°x1° coastline, even though a single dispersal event can cross 10's of kilometers (*29*, *56*), and an expanded definition (*40*), which allowed for dispersal across shallow seas and along the continent-ocean interface. We focused on calculating the average distance to track as a proxy for coastline geometry, rather than calculating the distance to track climatic niches through time, since we were focused here on the role of paleogeography, and not the intersection of abiotic tolerances, rates of climate change, and paleogeography.

Finally, accurately quantifying the timing of extinction is challenging, as true extinction events may postdate the last appearance datum due to the Signor-Lipps effect and other vagaries of sampling (*57*). Although we attempt to correct for this uncertainty using a probabilistic extinction approach (*7*, *43*) (fig. S20), some uncertainty inevitably remains.

Paleogeographic Boundary Conditions Impact Extinction Trajectories

In conclusion, our study provides compelling evidence that paleogeography, and specifically coastline geometry, played a role in shaping extinction patterns over the Phanerozoic. Our coastline geometry metric, which quantifies the difficulty a taxon would have in tracking environmental shifts based on (paleo)geographic configurations, emerged as an important predictor of per-taxon extinction risk over 540 million years.

The amplified effect of paleogeography during mass extinction and hyperthermal events highlights the increased importance of geographic barriers during periods of extreme and rapid climate change on geologic timescales, suggesting present-day species with restricted dispersal abilities or those in isolated habitats may be especially vulnerable to the current anthropogenic-driven climate crisis (*17*). Our results provide empirical support for assumptions underlying extinction risk assessments of extant species, which is crucial in an era of accelerating climate change (*58*).

References

1. J. Alroy, M. Aberhan, D. J. Bottjer, M. Foote, F. T. Fürsich, P. J. Harries, A. J. W. Hendy, S. M. Holland, L. C. Ivany, W. Kiessling, M. A. Kosnik, C. R. Marshall, A. J. McGowan, A. I. Miller, T. D. Olszewski, M. E. Patzkowsky, S. E. Peters, L. Villier, P. J. Wagner, N. Bonuso, P. S. Borkow, B. Brenneis, M. E. Clapham, L. M. Fall, C. A. Ferguson, V. L. Hanson, A. Z. Krug, K. M. Layou, E. H. Leckey, S. Nürnberg, C. M. Powers, J. A. Sessa, C. Simpson, A. Tomašových, C. C. Visaggi, Phanerozoic Trends in the Global Diversity of Marine Invertebrates. *Science* **321**, 97–100 (2008).

2. R. A. Close, R. B. J. Benson, E. E. Saupe, M. E. Clapham, R. J. Butler, The spatial structure of Phanerozoic marine animal diversity. *Science* **368**, 420–424 (2020).

3. J. T. Flannery-Sutherland, D. Silvestro, M. J. Benton, Global diversity dynamics in the fossil record are regionally heterogeneous. *Nat. Commun.* **13**, 2751 (2022).

4. D. M. Raup, J. J. Sepkoski, Mass Extinctions in the Marine Fossil Record. *Science* **215**, 1501–1503 (1982).

5. D. Jablonski, Background and Mass Extinctions: The Alternation of Macroevolutionary Regimes. *Science* **231**, 129–133 (1986).

6. C. M. Malanoski, A. Farnsworth, D. J. Lunt, P. J. Valdes, E. E. Saupe, Climate change is an important predictor of extinction risk on macroevolutionary timescales. *Science* **383**, 1130–1134 (2024).

7. C. J. Reddin, M. Aberhan, N. B. Raja, Á. T. Kocsis, Global warming generates predictable extinctions of warm- and cold-water marine benthic invertebrates via thermal habitat loss. *Glob. Change Biol.* **28**, 5793–5807 (2022).

8. P. M. Monarrez, N. A. Heim, J. L. Payne, Mass extinctions alter extinction and origination dynamics with respect to body size. *Proc. R. Soc. B Biol. Sci.* **288**, 20211681 (2021).

9. P. M. Monarrez, N. A. Heim, J. L. Payne, Reduced strength and increased variability of extinction selectivity during mass extinctions. *R. Soc. Open Sci.* **10**, 230795 (2023).

10. C. J. Reddin, P. S. Nätscher, Á. T. Kocsis, H.-O. Pörtner, W. Kiessling, Marine clade sensitivities to climate change conform across timescales. *Nat. Clim. Change* **10**, 249–253 (2020).

11. J. L. Payne, A. M. Bush, E. T. Chang, N. A. Heim, M. L. Knope, S. B. Pruss, Extinction intensity, selectivity and their combined macroevolutionary influence in the fossil record. *Biol. Lett.* **12**, 20160202 (2016).

12. J. L. Payne, S. Finnegan, The effect of geographic range on extinction risk during background and mass extinction. *Proc. Natl. Acad. Sci.* **104**, 10506–10511 (2007).

13. G. H. Mathes, J. van Dijk, W. Kiessling, M. J. Steinbauer, Extinction risk controlled by interaction of long-term and short-term climate change. *Nat. Ecol. Evol.* **5**, 304–310 (2021).

14. H. Song, D. B. Kemp, L. Tian, D. Chu, H. Song, X. Dai, Thresholds of temperature change for mass extinctions. *Nat. Commun.* **12**, 4694 (2021).

15. A. Pohl, R. G. Stockey, X. Dai, R. Yohler, G. Le Hir, D. Hülse, A. Brayard, S. Finnegan, A. Ridgwell, Why the Early Paleozoic was intrinsically prone to marine extinction. *Sci. Adv.* **9**, eadg7679 (2023).

16. E. E. Saupe, H. Qiao, Y. Donnadieu, A. Farnsworth, A. T. Kennedy-Asser, J.-B. Ladant, D. J. Lunt, A. Pohl, P. Valdes, S. Finnegan, Extinction intensity during Ordovician and Cenozoic glaciations explained by cooling and palaeogeography. *Nat. Geosci.* **13**, 65–70 (2020).

17. E. S. Poloczanska, C. J. Brown, W. J. Sydeman, W. Kiessling, D. S. Schoeman, P. J. Moore, K. Brander, J. F. Bruno, L. B. Buckley, M. T. Burrows, C. M. Duarte, B. S. Halpern, J. Holding, C. V. Kappel, M. I. O'Connor, J. M. Pandolfi, C. Parmesan, F. Schwing, S. A. Thompson, A. J. Richardson, Global imprint of climate change on marine life. *Nat. Clim. Change* **3**, 919–925 (2013).

18. J. M. Sunday, A. E. Bates, N. K. Dulvy, Thermal tolerance and the global redistribution of animals. *Nat. Clim. Change* **2**, 686–690 (2012).

19. C. E. Brett, A. J. W. Hendy, A. J. Bartholemew, J. R. Bonelli, P. I. McLaughlin, Resoponse of shallow marine biotas to sea-level fluctuations: A review of faunal replacement and the process of habitat tracking. *PALAIOS* **22**, 228–244 (2007).

20. A. Clarke, J. A. Crame, J. -o. Strömberg, P. F. Barker, D. J. Drewry, R. M. Laws, J. A. Pyle, The Southern Ocean benthic fauna and climate change: a historical perspective. *Philos. Trans. R. Soc. Lond. B. Biol. Sci.* **338**, 299–309 (1997).

21. D. Jablonski, R. A. Lutz, Larval Ecology of Marine Benthic Invertebrates: Paleobiological Implications. *Biol. Rev.* **58**, 21–89 (1983).

22. E. J. Judd, J. E. Tierney, D. J. Lunt, I. P. Montañez, B. T. Huber, S. L. Wing, P. J. Valdes, A 485-million-year history of Earth's surface temperature. *Science* **385**, eadk3705 (2024).

23. S. M. Stanley, Thermal barriers and the fate of perched faunas. *Geology* **38**, 31–34 (2010).

24. O. Hagen, B. Flück, F. Fopp, J. S. Cabral, F. Hartig, M. Pontarp, T. F. Rangel, L. Pellissier, gen3sis: A general engine for eco-evolutionary simulations of the processes that shape Earth's biodiversity. *PLOS Biol.* **19**, e3001340 (2021).

25. I. Keller, O. Seehausen, Thermal adaptation and ecological speciation. *Mol. Ecol.* **21**, 782–799 (2012).

26. G. F. A. Donati, V. Parravicini, F. Leprieur, O. Hagen, T. Gaboriau, C. Heine, M. Kulbicki, J. Rolland, N. Salamin, C. Albouy, L. Pellissier, A process-based model supports an association between dispersal and the prevalence of species traits in tropical reef fish assemblages. *Ecography* **42**, 2095–2106 (2019).

27. T. Gaboriau, C. Albouy, P. Descombes, D. Mouillot, L. Pellissier, F. Leprieur, Ecological constraints coupled with deep-time habitat dynamics predict the latitudinal diversity gradient in reef fishes. *Proc. Biol. Sci.* **286**, 20191506 (2019).

28. F. Leprieur, P. Descombes, T. Gaboriau, P. F. Cowman, V. Parravicini, M. Kulbicki, C. J. Melián, C. N. de Santana, C. Heine, D. Mouillot, D. R. Bellwood, L. Pellissier, Plate tectonics drive tropical reef biodiversity dynamics. *Nat. Commun.* **7**, 11461 (2016).

29. M. Álvarez-Noriega, S. C. Burgess, J. E. Byers, J. M. Pringle, J. P. Wares, D. J. Marshall, Global biogeography of marine dispersal potential. *Nat. Ecol. Evol.* **4**, 1196–1203 (2020).

30. T. J. Algeo, J. Shen, Theory and classification of mass extinction causation. *Natl. Sci. Rev.* **11**, nwad237 (2023).

31. M. Aberhan, T. K. Baumiller, Selective extinction among Early Jurassic bivalves: A consequence of anoxia. *Geology* **31**, 1077 (2003).

32. A. Husain, J. Reddy, D. Bisht, M. Sajid, Fractal dimension of coastline of Australia. *Sci. Rep.* **11**, 6304 (2021).

33. G. McNamara, G. V. da Silva, The Coastline Paradox: A New Perspective. *J. Coast. Res.* **39**, 45–54 (2022).

34. Materials and methods are available as supplementary materials.

35. L. Buffan, L. A. Jones, M. Domeier, C. R. Scotese, S. Zahirovic, S. Varela, Mind the uncertainty: Global plate model choice impacts deep-time palaeobiological studies. *Methods Ecol. Evol.* **n/a**.

36. PaleoDEM Resource – Scotese and Wright (2018) – EarthByte (2021). https://www.earthbyte.org/paleodem-resource-scotese-and-wright-2018/.

37. T. H. Torsvik, L. R. M. Cocks, Earth history and palaeogeography (2017).

38. N. Wright, S. Zahirovic, R. D. Müller, M. Seton, Towards community-driven paleogeographic reconstructions: integrating open-access paleogeographic and paleobiology data with plate tectonics. *Biogeosciences* **10**, 1529–1541 (2013).

39. A. S. Merdith, S. E. Williams, A. S. Collins, M. G. Tetley, J. A. Mulder, M. L. Blades, A. Young, S. E. Armistead, J. Cannon, S. Zahirovic, R. D. Müller, Extending full-plate tectonic models into deep time: Linking the Neoproterozoic and the Phanerozoic. *Earth-Sci. Rev.* **214**, 103477 (2021).

40. Á. T. Kocsis, C. R. Scotese, Mapping paleocoastlines and continental flooding during the Phanerozoic. *Earth-Sci. Rev.* **213**, 103463 (2021).

41. Paleobiology Database (2023). https://paleobiodb.org.

42. C. Vérard, Plate tectonic modelling: review and perspectives. *Geol. Mag.* **156**, 208–241 (2019).

43. C. J. Reddin, Á. T. Kocsis, M. Aberhan, W. Kiessling, Victims of ancient hyperthermal events herald the fates of marine clades and traits under global warming. *Glob. Change Biol.* **27**, 868–878 (2021).

44. R. G. Stockey, A. Pohl, A. Ridgwell, S. Finnegan, E. A. Sperling, Decreasing Phanerozoic extinction intensity as a consequence of Earth surface oxygenation and metazoan ecophysiology. *Proc. Natl. Acad. Sci.* **118**, e2101900118 (2021).

45. C. M. Marcilly, T. H. Torsvik, C. P. Conrad, Global Phanerozoic sea levels from paleogeographic flooding maps. *Gondwana Res.* **110**, 128–142 (2022).

46. S. E. Peters, Geologic constraints on the macroevolutionary history of marine animals. *Proc. Natl. Acad. Sci.* **102**, 12326–12331 (2005).

47. J. A. Kitchell, "Biological selectivity of extinction" in *Extinction Events in Earth History*, E. G. Kauffman, O. H. Walliser, Eds. (Springer, Berlin, Heidelberg, 1990), pp. 31–43.

48. R. Lockwood, Abundance not linked to survival across the end-Cretaceous mass extinction: Patterns in North American bivalves. *Proc. Natl. Acad. Sci.* **100**, 2478–2482 (2003).

49. E. A. Orzechowski, R. Lockwood, J. E. K. Byrnes, S. C. Anderson, S. Finnegan, Z. V. Finkel, P. G. Harnik, D. R. Lindberg, L. H. Liow, H. K. Lotze, C. R. McClain, J. L. McGuire, A. O'Dea, J. M. Pandolfi, C. Simpson, D. P. Tittensor, Marine extinction risk shaped by trait–environment interactions over 500 million years. *Glob. Change Biol.* **21**, 3595–3607 (2015).

50. Y. Zhou, Y. Li, W. Zheng, S. Tang, S. Pan, J. Chen, X.-F. He, J. Shen, T. J. Algeo, The role of LIPs in Phanerozoic mass extinctions: An Hg perspective. *Earth-Sci. Rev.* **249**, 104667 (2024).

51. D. P. G. Bond, S. E. Grasby, On the causes of mass extinctions. *Palaeogeogr. Palaeoclimatol. Palaeoecol.* **478**, 3–29 (2017).

52. E. A. Sperling, T. H. Boag, M. I. Duncan, C. R. Endriga, J. A. Marquez, D. B. Mills, P. M. Monarrez, J. A. Sclafani, R. G. Stockey, J. L. Payne, Breathless through Time: Oxygen and Animals across Earth's History. *Biol. Bull.*, 000–000 (2022).

53. M. M. Casey, E. E. Saupe, B. S. Lieberman, The effects of geographic range size and abundance on extinction during a time of "sluggish"' evolution. *Paleobiology* **47**, 54–67 (2021).

54. M. D. Spalding, H. E. Fox, G. R. Allen, N. Davidson, Z. A. Ferdaña, M. Finlayson, B. S. Halpern, M. A. Jorge, A. Lombana, S. A. Lourie, K. D. Martin, E. McManus, J. Molnar, C. A. Recchia, J. Robertson, Marine Ecoregions of the World: A Bioregionalization of Coastal and Shelf Areas. *BioScience* **57**, 573–583 (2007).

55. L. J. Wilson, C. J. Fulton, A. M. Hogg, K. E. Joyce, B. T. M. Radford, C. I. Fraser, Climate-driven changes to ocean circulation and their inferred impacts on marine dispersal patterns. *Glob. Ecol. Biogeogr.* **25**, 923–939 (2016).

56. B. A. Grantham, G. L. Eckert, A. L. Shanks, Dispersal Potential of Marine Invertebrates in Diverse Habitats. *Ecol. Appl.* **13**, 108–116 (2003).

57. P. Signor, J. Lipps, Gradual extinction patterns and catastrophes in the fossil record. *Geol. Soc. Am. Spec. Pap.* **190**, 291–296 (1982).

58. G. L. Foster, P. Hull, D. J. Lunt, J. C. Zachos, Placing our current 'hyperthermal' in the context of rapid climate change in our geological past. *Philos. Trans. R. Soc. Math. Phys. Eng. Sci.* **376**, 20170086 (2018).

59. A. M. Bush, R. K. Bambach, Sustained Mesozoic–Cenozoic diversification of marine Metazoa: A consistent signal from the fossil record. *Geology* **43**, 979–982 (2015).

60. Á. T. Kocsis, C. J. Reddin, J. Alroy, W. Kiessling, The r package divDyn for quantifying diversity dynamics using fossil sampling data. *Methods Ecol. Evol.* **10**, 735–743 (2019).

61. F. Gradstein, J. Ogg, "The Chronostratigraphic Scale" (2020), pp. 21–32.

62. J. T. Flannery-Sutherland, N. B. Raja, Á. T. Kocsis, W. Kiessling, fossilbrush: An R package for automated detection and resolution of anomalies in palaeontological occurrence data. *Methods Ecol. Evol.* **13**, 2404–2418 (2022).

63. G. T. Antell, R. B. J. Benson, E. E. Saupe, Spatial standardization of taxon occurrence data—a call to action. (2023).

64. J. J. Sepkoski, A Kinetic Model of Phanerozoic Taxonomic Diversity. III. Post-Paleozoic Families and Mass Extinctions. *Paleobiology* **10**, 246–267 (1984).

65. S. Mondal, P. J. Harries, The Effect of Taxonomic Corrections on Phanerozoic Generic Richness Trends in Marine Bivalves with a Discussion on the Clade's Overall History. *Paleobiology* **42**, 157–171 (2016).

66. J. R. Hendricks, E. E. Saupe, C. E. Myers, E. J. Hermsen, W. D. Allmon, The Generification of the Fossil Record. *Paleobiology* **40**, 511–528 (2014).

67. R Interface for the GPlates Web Service and Desktop Application. https://gplates.github.io/rgplates/.

68. A. T. Kocsis, N. B. Raja, chronosphere: Evolving Earth System Variables, (2019); https://doi.org/10.32614/CRAN.package.chronosphere.

69. B. Vaes, D. J. J. van Hinsbergen, Slow true polar wander around varying equatorial axes since 320 Ma. (2024).

70. P. V. Doubrovine, B. Steinberger, T. H. Torsvik, Absolute plate motions in a reference frame defined by moving hot spots in the Pacific, Atlantic, and Indian oceans. *J. Geophys. Res. Solid Earth* **117** (2012).

71. Z. Jiang, S. Li, Q. Liu, J. Zhang, Z. Zhou, Y. Zhang, The trials and tribulations of the Hawaii hot spot model. *Earth-Sci. Rev.* **215**, 103544 (2021).

72. T. H. Torsvik, L. R. M. Cocks, The integration of palaeomagnetism, the geological record and mantle tomography in the location of ancient continents. *Geol. Mag.* **156**, 242–260 (2019).

73. J. P. Snyder, *Map Projections--a Working Manual* (U.S. Government Printing Office, 1987).

74. R. J. Hijmans, J. van Etten, M. Sumner, J. Cheng, D. Baston, A. Bevan, R. Bivand, L. Busetto, M. Canty, B. Fasoli, D. Forrest, A. Ghosh, D. Golicher, J. Gray, J. A. Greenberg, P. Hiemstra, K. Hingee, A. Ilich, I. for M. A. Geosciences, C. Karney, M. Mattiuzzi, S. Mosher, B. Naimi, J. Nowosad, E. Pebesma, O. P. Lamigueiro, E. B. Racine, B. Rowlingson, A. Shortridge, B. Venables, R. Wueest, raster: Geographic Data Analysis and Modeling, version 3.6-26 (2023); https://cran.r-project.org/web/packages/raster/index.html.

75. sf package - RDocumentation. https://www.rdocumentation.org/packages/sf/versions/1.0-13.

76. parallel package - RDocumentation (2019). https://www.rdocumentation.org/packages/parallel/versions/3.6.2.

77. ggplot2 package - RDocumentation. https://www.rdocumentation.org/packages/ggplot2/versions/3.5.0.

78. dplyr package - RDocumentation. https://www.rdocumentation.org/packages/dplyr/versions/1.0.10.

79. data.table package - RDocumentation. https://www.rdocumentation.org/packages/data.table/versions/1.16.0.

80. D. J. Marceau, The Scale Issue in the Social and Natural Sciences. *Can. J. Remote Sens.* **25**, 347–356 (1999).

81. R. B. Stoa, The Coastline Paradox. *Rutgers Univ. Law Rev.* **72**, 351–400 (2019).

82. C. J. Reddin, Á. T. Kocsis, W. Kiessling, Marine invertebrate migrations trace climate change over 450 million years. *Glob. Ecol. Biogeogr.* **27**, 704–713 (2018).

83. I. Yang, W. H. Jeon, J. Moon, A study on a distance based coordinate calculation method using Inverse Haversine Method. *J. Digit. Contents Soc.* **20**, 2097–2102 (2019).

84. M. Kowalewski, Kowalewski—Analytical Methods 3 the Fossil Record of Predation: An Overview of Analytical Methods.

85. S. Gavirneni, L. C. Ivany, C. J. Reddin, Burning calories, burning ocean: metabolic rate in bivalves as a predictor of extinction selectivity through time and during rapid global warming. *Paleobiology*, 1–13 (2025).

86. lme4 package - RDocumentation. https://www.rdocumentation.org/packages/lme4/versions/1.1-33.

87. A. Purvis, J. L. Gittleman, T. M. Brooks, 1 Phylogeny and conservation. *Camb. Univ. Press* (2005).

88. D. Lüdecke, ggeffects: Tidy Data Frames of Marginal Effects from Regression Models. *J. Open Source Softw.* **3**, 772 (2018).

89. F. Hartig, L. Lohse, DHARMa: Residual Diagnostics for Hierarchical (Multi-Level / Mixed) Regression Models, version 0.4.6 (2022); https://cran.r-project.org/web/packages/DHARMa/index.html.

90. Kowalewski, P. Novack-Gottshall, Resampling Methods in Paleontology. *Paleontol. Soc. Spec. Pap.* **16**, 19–54 (2010).

91. C. J. Reddin, Á. T. Kocsis, W. Kiessling, Climate change and the latitudinal selectivity of ancient marine extinctions. *Paleobiology* **45**, 70–84 (2019).

92. D. Jablonski, "Evolutionary Consequences of Mass Extinctions" in *Patterns and Processes in the History of Life*, D. M. Raup, D. Jablonski, Eds. (Springer, Berlin, Heidelberg, 1986), pp. 313–329.

93. H. Kappes, P. Haase, Slow, but steady: dispersal of freshwater molluscs. *Aquat. Sci.* **74**, 1–14 (2012).

94. X. Bi, Q. Zhu, Numerical investigation of cephalopod-inspired locomotion with intermittent bursts. *Bioinspir. Biomim.* **13**, 056005 (2018).

95. R. de Campos, F. M. Lansac-Tôha, E. de O. da Conceição, K. Martens, J. Higuti, Factors affecting the metacommunity structure of periphytic ostracods (Crustacea, Ostracoda): a deconstruction approach based on biological traits. *Aquat. Sci.* **80**, 16 (2018).

96. E. Loken, A. Gelman, Measurement error and the replication crisis. *Science* **355**, 584–585 (2017).

97. J. P. A. Ioannidis, Why Most Published Research Findings Are False. *PLOS Med.* **2**, e124 (2005).

98. P. Green, C. J. MacLeod, SIMR: an R package for power analysis of generalized linear mixed models by simulation. *Methods Ecol. Evol.* **7**, 493–498 (2016).

99. S. Zhang, S. Shen, D. H. Erwin, Two cosmopolitanism events driven by different extreme paleoclimate regimes. *Glob. Planet. Change* **216**, 103899 (2022).

Acknowledgements

We thank B. Shipley, R. Close, T. Smith, and B. Vaes for informative discussions, M. Kouvari for figure preparation, and three anonymous reviewers for greatly improving our manuscript. We are grateful to the contributors of the Paleobiology Database who provided the occurrence data used in our analyses. **Funding**: This research was supported by the Leverhulme Trust grant RPG-201170, the Leverhulme Prize, and NERC grants NE/V011405/1 and UKRI1340. This is Paleobiology Database publication no. 542. **Author contributions**: E.E.S. and S.F. conceptualized the study. C.M.M., E.E.S., E.C.H., and L.B. devised the methodology. C.M.M., E.E.S., E.C.H., and L.B. conducted the investigation. C.M.M. performed visualization. E.E.S. acquired funding and conducted project administration. E.E.S. supervised the study. C.M.M. and E.E.S. wrote the original draft of the manuscript. All authors (C.M.M., E.E.S., S.F., E.C.H., C.M., and L.B.) reviewed and edited the manuscript. **Competing interests**: The authors declare no competing interests. **Data and materials availability**: All data and code required to reproduce the analyses in this study is available in Data S1.

Supplementary Materials

Materials and Methods
Figs. S1 to S26
Tables S1 to S9
References (*58–99*)

Data S1

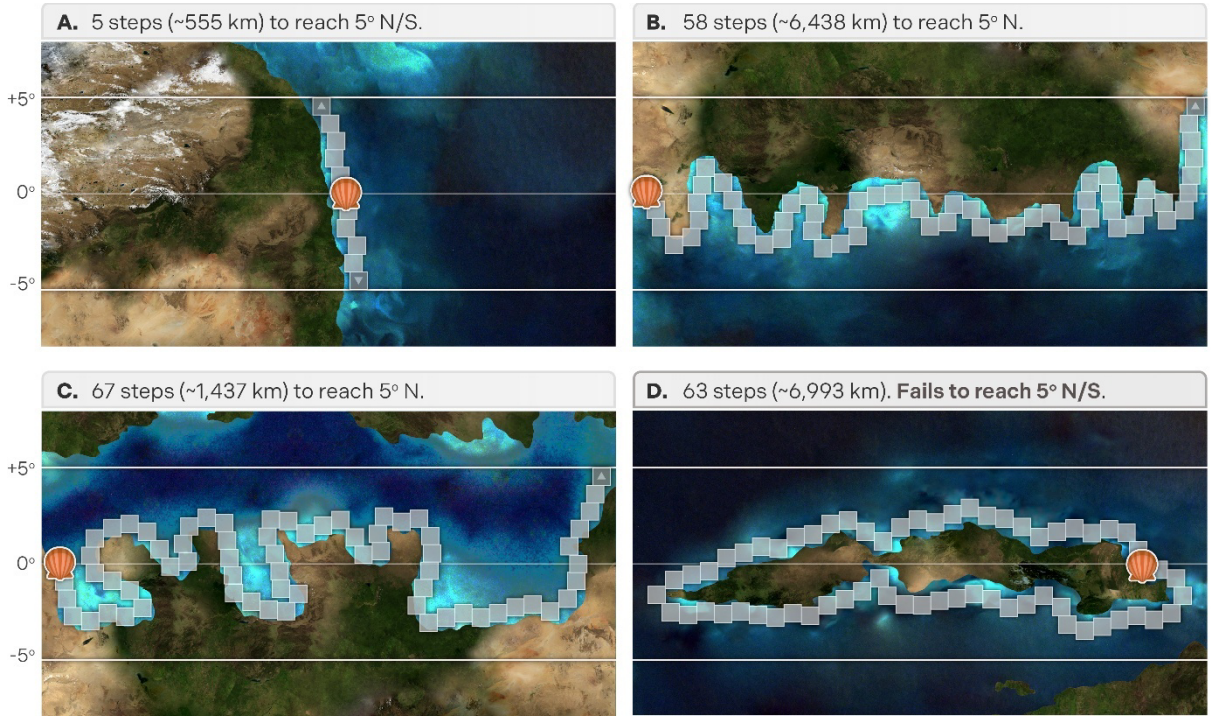

Fig. 1. **The relationship between coastline geometry and dispersal potential.** Each map represents a hypothetical dispersal scenario and the shortest continuous dispersal distance required to reach a 5° change in latitude north and south for a hypothetical marine invertebrate and paleogeographical scenario. The taxon is restricted to grid cells along shallow marine margins, but we also considered an expanded continental shelf region in our simulations. (**A**) A north-south oriented coastline that facilitates a short dispersal distance of five grid cell steps to reach a 5° latitudinal change. (**B**) A convoluted, east-west-oriented coastline showing a fossil genus that must move 58 grid cells, or ~6,438 km at the equator, to reach a 5° latitudinal shift north. (**C**) An east-west oriented interior seaway, typical of the Paleozoic and some intervals of the Mesozoic. In this scenario, the genus must move 67 grid cell steps, or ~7,437 at the equator, to reach a 5° latitudinal threshold. (**D**) An east-west oriented island. Islands can greatly restrict the dispersal ability of taxa. In this case, the genus was unable to disperse 5° north or south within 100 grid cell steps, or roughly ~11,100 km distance. These four maps highlight the potential role of coastline geometry in mediating dispersal through time, where north-south coastlines would allow species to track preferred conditions more easily than east-west orientated coastlines.

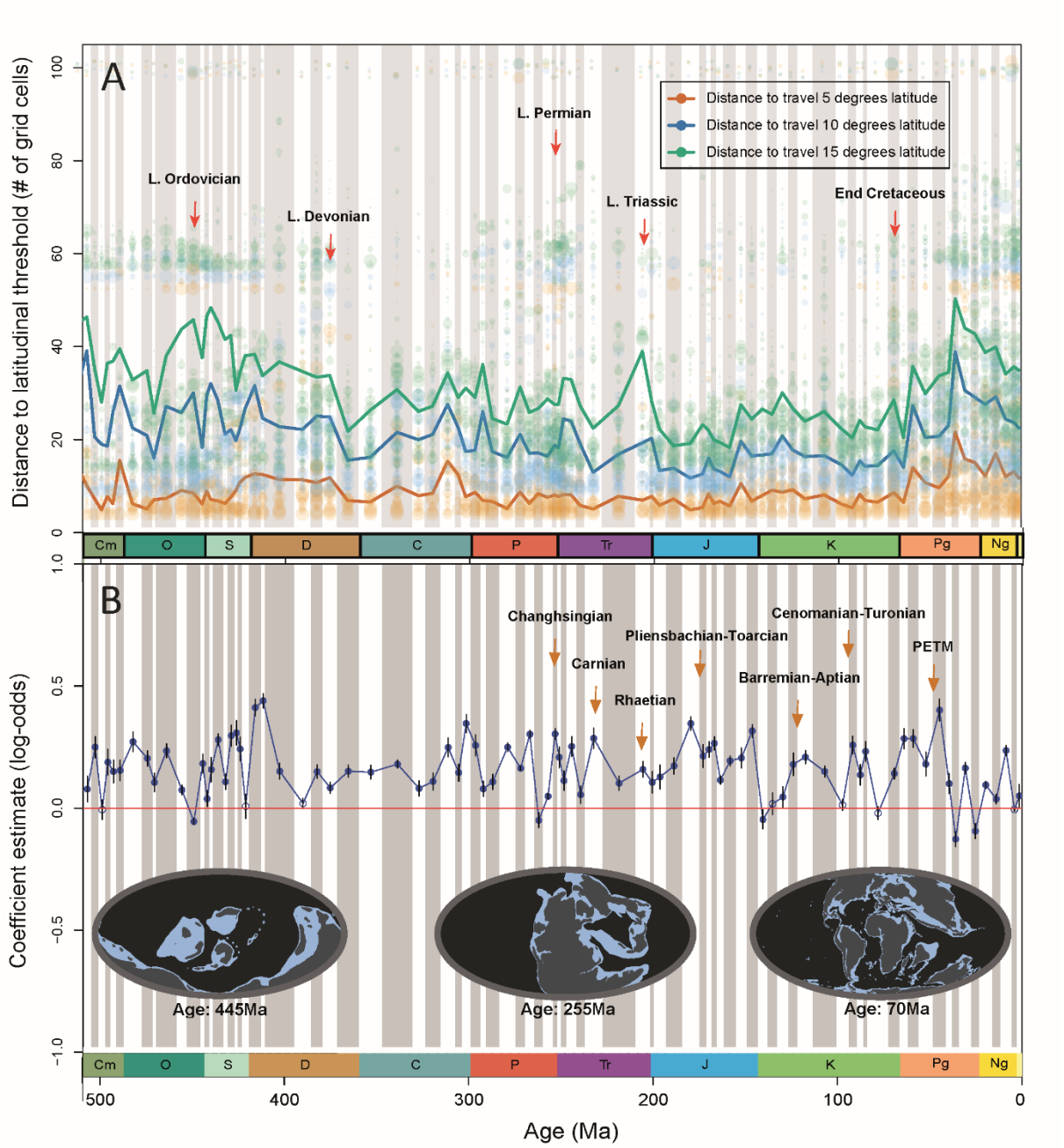

Fig. 2. Temporal trends in coastline geometry and extinction risk across the Phanerozoic. (**A**) Distance (grid cell steps) required to reach thresholds of 5°, 10°, and 15° latitude (orange, blue, and green lines, respectively), plotted over 540 million years of Earth history. Each line represents the mean value for a given time interval across taxa. The Late Ordovician (445 Ma), Devonian (372 Ma), Permian (251 Ma), Triassic (201 Ma), and Cretaceous (66 Ma) extinctions are marked. The distance required to reach each of these thresholds was elevated in the Ordovician (445 Ma), likely due to the high frequency of east-west oriented coastlines. This metric is also elevated in the Paleogene due to the preponderance of islands and isolated subcontinents, such as India. (**B**) Modelled relationship between distance to track and extinction risk derived from a single random-slope, random-intercept GLMM, reflecting changes in extinction selectivity measured in log odds over the Phanerozoic. Positive values indicate increased extinction risk associated with greater distances to track, and points are empty if the 95% confidence interval intersects 0, suggesting no significant selectivity. Note that four stages show a significant negative relationship, which may be due to other

confounding predictors of extinction that are inversely correlated with coastline geometry, while 8 (of 90) stages show no significant relationship with coastline geometry. Insets show paleogeographic reconstructions for three key time slices associated with extinction events (445 Ma, 255 Ma, and 70 Ma), which have distinct continental configurations. Horizontal time axes at the bottom mark geological periods from Cambrian to Holocene. Hyperthermal events (*43*, *58*) are marked here, with the Induan and Olenekian pulses of the Late Permian hyperthermal included in our analysis.

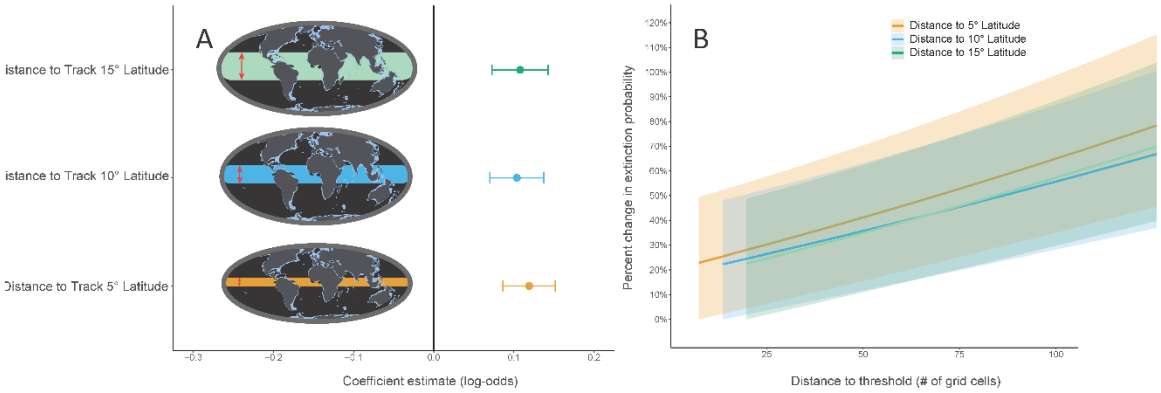

Fig. 3. The effect of coastline geometry on extinction risk. (**A**) Extinction risk associated with each distance to track latitudinal threshold in log odds with 95% confidence intervals. Insets show the different latitudinal thresholds depicted on a present-day map. (**B**) Marginal effects plots showing the percent change in predicted extinction risk as a function of the distance (grid cell steps) to a given latitudinal threshold (15°, 10°, and 5°). Shaded regions represent the 95% confidence intervals for three different distance thresholds, reflecting how changes in distance to track affect extinction risk across space and time.

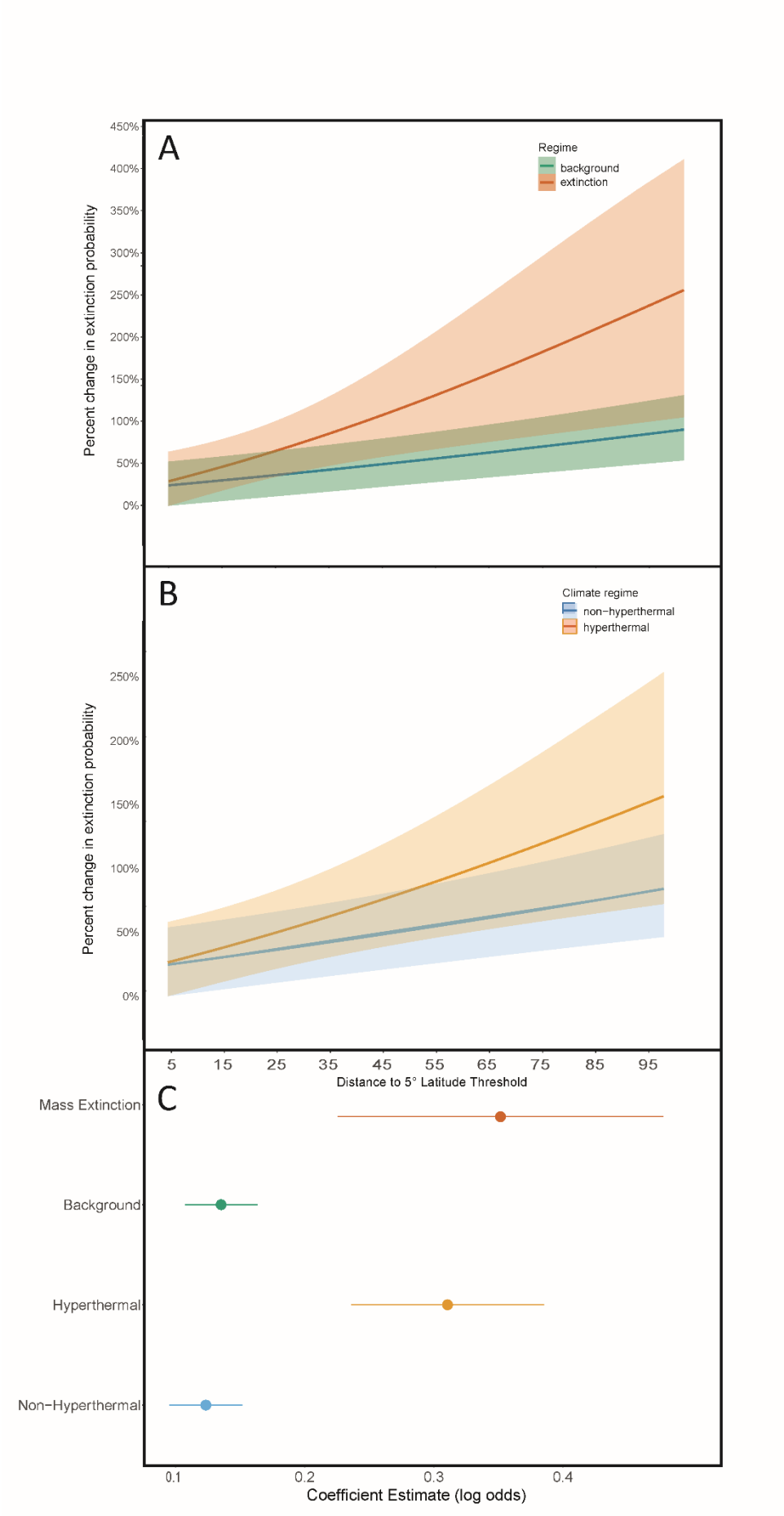
A
Regime
background
extinction
Percent change in extinction probability
450%
400%
350%
300%
250%
200%
150%
100%
50%
0%
B
Climate regime
non−hyperthermal
hyperthermal
Percent change in extinction probability
250%
200%
150%
100%
50%
0%
5
15
25
35
45
55
65
75
85
95
Distance to 5° Latitude Threshold
C
Mass Extinction
Background
Hyperthermal
Non−Hyperthermal
0.1
0.2
0.3
0.4
Coefficient Estimate (log odds)

Fig. 4. **The relationship between coastline geometry and extinction risk across geological regimes and hyperthermal events.** (**A**) The marginal effects for the distance (grid cell steps) to a latitudinal threshold of 5^{o} for the Big Five mass extinctions versus background intervals, showing the change in extinction probability from 5 to 101 steps (the maximum allowed), with 95% confidence intervals. (**B**) The marginal effects for the distance (grid cell steps) to a latitudinal threshold of 5^{o} for 12 hyperthermal versus non-hyperthermal intervals, showing the change in extinction probability from 5 to 101 steps (the maximum allowed), with 95% confidence intervals. (**C**) Model coefficients and 95% confidence intervals for mass extinction versus background intervals, and hyperthermal versus non-hyperthermal periods, capturing the effect of coastline geometry on extinction risk.

Supplementary Materials for

Paleogeography modulates marine extinction risk over the Phanerozoic

Cooper M. Malanoski[1*], Seth Finnegan[2,4], Edward C. Huang[3], Lila Blake[1], Connal Mac Niocaill[1], Erin E. Saupe[1*]

Corresponding authors: cooper.malanoski@wolfson.ox.ac.uk, erin.saupe@earth.ox.ac.uk

The PDF file includes:

Materials and Methods

Figs. S1 to S26

Tables S1 to S9

References (*58–99*)

Other Supplementary Materials for this manuscript include the following:

Data S1

Materials and methods

Taxon occurrence data

Fossil occurrence data were retrieved from the Paleobiology Database (*41*) (PBDB) on October 13th 2023. The data were filtered to retain only marine ectotherms that belong to the phyla Brachiopoda, Porifera, Echinodermata, Bryozoa, and Mollusca; the classes Anthozoa and Polychaeta; and the arthropod clades Trilobita, Xiphosura, and Malacostraca. Terrestrial occurrences were removed using the 'environment' variable from the PBDB. We further removed terrestrial taxa using the terrestrial taxonomic list from Bush and Bambach (*59*). Subgeneric occurrences were elevated to the generic level. The PBDB data were processed and cleaned based on the pipeline used in Kocsis et al. (*60*) and binned into discrete stages using the Gradstein and Ogg (*61*) geologic timescale. We used a strict approach for temporal binning where any occurrences with uncertainty spanning multiple stages were discarded. The taxonomy was further vetted and cleaned using the fossilbrush R package v1.0.5 (*62*), resulting in 673,090 occurrences that were reduced to 325,991 after: (i) only retaining taxa with three or more occurrences, (ii) removing non-spatially-unique occurrences using uniquify() from the Divvy R package v1.0.0 (*63*), and (iii) removing deep water occurrences that were more than 200 km from a coastline grid cell. Our final dataset consisted of taxa in 90 stages from the Cambrian to Recent.

We ran analyses at the genus-level due to uncertainties associated with species-level taxonomy and temporal ranges over Phanerozoic timescales (*64*, *65*). Although species-level dynamics do not always scale up to the genus-level (*66*), previous studies on extinction selectivity studies have found congruence in results across taxonomic levels (*6*).

Paleocoordinate preparation

To accurately assess paleogeographic patterns, such as changes in coastline geometry through deep time, it is necessary to reconstruct the paleogeographic locations of fossil occurrences based on their modern coordinates and age of deposition. We used four different global plate models (GPMs) to reconstruct paleocoordinates, including Scotese and Wright (*36*), GOLONKA (*38*), Torsvik and Cocks (*37*), and Merdith (*39*). These reconstructions were performed using GPlates software v2.3.0 (*67*) and the R packages *chronosphere* v0.6.1 (*68*) and *rgplates* v0.4.0 (*67*).

We matched fossil records to their geological stages using the divDyn R package and applied stage midpoints from the Gradstein and Ogg (*61*) timescale. Reconstructions were performed for all four models across 90 stages, as defined in Scotese and Wright (*36*), using the local GPlates software. We used the default reference frames for the basis of all rotations and GPMs, including a mantle reference frame in Torsvik and Cocks (*37*). All rotation files used for these analyses are available as supplemental files.

We matched the filtered dataset to the unique plate model ages using the matchtime() function from chronosphere (*68*), generating a list of unique latitude and longitude coordinates for each age. Each set of spatio-temporally unique coordinates was then rotated using the reconstruct() function from rgplates (*67*), with validtime set to FALSE to

ensure continuity beyond the model's plate durations, and enumerate set to FALSE to align all coordinates with the corresponding age for each plate model. All coordinates that were within the 200 km cutoff from the nearest coastline were retained.

Paleogeography: isolating coastlines

We reconstructed and isolated coastlines for each stage of the Phanerozoic using raster data for the four GPMs. These GPMs encompass a range of methodologies for reconstructing Earth's tectonic history, reflecting uncertainties that increase for time periods older than 300 million years (*35*). During these deep-time intervals, different models diverge due to limited data, and the methods used to reconstruct plate boundaries and tectonic motions vary significantly (*35*, *42*). A major challenge in deeper time is the subduction of oceanic crust, which erases much of the evidence needed to accurately reconstruct ancient plate movements (*35*). One of the main differences between plate models is in their reference frames. GPM's can incorporate a combination of paleomagnetic and hot spot or mantle reference frames. The choice of reference frame remains controversial, as some argue that paleomagnetic reference frames should be used for paleotological and paleoclimate studies (*69*, *70*), whilst others argue for utilizing a hot spot or mantle reference frame, especially to infer longitudinal position in deep time (*71*, *72*).

The inclusion of multiple plate models in this study aimed to address the uncertainties inherent in deep-time reconstructions. Each model employs a distinct approach: Merdith et al. (*39*) integrates paleomagnetic data alongside tectonic reconstructions (*39*), while Torsvik & Cocks (*37*) incorporates paleomagnetic and hot spot data, and the Scotese and Wright (*36*) model offers widely-recognized paleo-digital elevation models (PaleoDEMs) for consistent baseline reconstructions. By utilizing all four models, we capture varying interpretations of Earth's tectonic history and incorporate the uncertainties inherent in the reconstruction of Phanerozoic coastlines, especially for older time intervals. This multi-model approach ensures that the conclusions drawn from the data are not overly-dependent on a single model, but rather reflect a broader consideration of varying tectonic reconstructions.

To ensure comparability among GPMs and coastline definitions, all paleogeographic raster reconstructions were resampled to a 1°×1° degree resolution. By resampling, we ensured the spatial extent and resolution were consistent, making it possible to directly compare coastlines across different models and time intervals.

We used a latitude and longitude projection (EPSG:4326) over an equal-area projection to maintain geometric accuracy. Although equal-area projections preserve area proportions, they can distort the geometry of coastlines (*73*). By using latitude-longitude projections, we preserved the true relationships between features, allowing us to examine north-south versus east-west orientation without distortion. However, we additionally ran our analyses using Haversine distance to account for the distortion of grid cell distances based on latitude (see *Haversine distance approach*; fig. S10).

Three different approaches were used to estimate coastline geometries from the four GPMs, to represent shallow marine regions around continental margins to which continental-shelf-dwelling marine invertebrates would be confined, detailed below.

Scotese and Wright (*36*) *PaleoDEM-Based Coastline Model*. The first approach was based on the PaleoDEM from Scotese and Wright (*36*). These PaleoDEMs provide land surface elevation and ocean basin depth data for various time intervals, with coastlines defined by isolating the interface between land and sea. We selected coastline grid cells by setting elevation values below or equal to zero (representing underwater areas) to NA, and values with a distance greater than $\sqrt{2 + 0.0001}$ from these areas were excluded to focus on shallow marine regions near continental margins.

Once the coastline data were isolated, the clump() function from the raster R package v3.6-26 (*74*) was used to identify clusters of connected pixels representing continuous coastline segments. Clusters with fewer than five connected cells were removed to reduce noise and eliminate potentially-erroneous edge effects or processing artifacts. We retained clusters of five grid cells or more since this was the minimum distance to track. The exclusion of small clusters was a critical step to ensure data quality; small clusters were more likely to represent noise or artifacts near the edges of the reconstructions.

A 5-grid-cell edge buffer was also applied to each raster to remove spurious coastline pixels along map margins for select models. The 5-grid-cell buffer ensured only valid coastline data remained, removing artifacts generated during processing. The processed coastlines resulted in maps with 1°x1° grid cells along coastline margins across 90 time intervals spanning 540 Ma.

Kocsis et al. (*40*) *Coastline Model.* In the second method to define coastline geometries, we used the GPM of Kocsis et al. (*40*), which is an adaptation of the Scotese and Wright model (*36*) enhanced by fossil data. In this model, continental flooding and continental margins were redefined by Kocsis to reflect periods of maximum transgression, when shallow seas extended furthest over the continents (*40*). Kocsis integrated fossil occurrence data into the process, fine-tuning the positions of the coastlines to ensure they aligned with evidence from marine and non-marine fossils.

The Kocsis coastline models were originally provided in Equirectangular projection and downloaded in GTiff format. These models were re-projected to a latitude and longitude projection (EPSG:4326) using the R packages rgplates (*67*) and sf (*75*) v1.0-1.4, ensuring consistency with the other models. After projection conversion, the same isolation steps were applied, including setting non-continental-margin oceanic grid cells to NA, removing clusters smaller than five grid cells with clump(), and applying a 5-grid-cell edge buffer. In comparison to the four global plate models that identified coastlines as the interface between the continent and the ocean, this model included all marine shelf and continental margin cells.

Merdith, Torsvik & Cocks, Golonka Models: Reconstructed Coastlines. For the Merdith, Torsvik & Cocks, and Golonka models, coastline geometries were directly extracted from the global tectonic models using the reconstruct() function in the *rgplates* R package (*67*). This

allowed us to reconstruct the positions of coastlines at 90 specific time intervals based on tectonic reconstructions. Since there is no true coastline data for these GPMs, we inferred the position of paleo-coastlines using the positions of modern coastlines. These coastlines therefore represent the interface between oceanic and continental tectonic blocks based on modern coastlines, rather than true coastlines. Once the coastlines were extracted, the same data processing steps were applied to ensure consistency across GPMs. Oceanic regions were set to NA, the clump() function was used to isolate continuous coastline segments, and small clusters with fewer than five connected grid cells were removed. A 5-grid-cell edge buffer was applied to remove spurious features near the map margins, and the final coastlines were resampled to a 1°×1° resolution grid.

Quantifying coastline geometry

Grid cell step approach. We quantified coastline geometry by applying a novel pathfinding algorithm approach to the paleogeographic coastline raster data, utilizing the R packages parallel v4.3.2 (*76*), raster v3.6.26 (*74*), ggplot2 v3.4.4 (*77*), dplyr v1.1.4 (*78*), and data.table v1.14.10 (*79*). For a given coastal grid cell, the algorithm finds the minimum path length required to travel a certain degrees latitude north and south using neighboring raster grid cells. We tested three different latitudinal thresholds: 5°, 10°, 15°. This metric serves as a proxy for coastline complexity, providing insights into the structure and variation of ancient coastlines.

The pathfinding algorithm systematically explores all possible paths from each grid cell on the coastline, moving through neighbouring raster grid cells while tracking the number of grid cells (i.e., 'steps' or distance) taken. The algorithm identifies the shortest path that would result in a predefined latitudinal shift, akin to placing a car on each unique 1°x1° grid cell of the coastline and allowing the car to drive in all possible directions until it finds the shortest route to achieve the desired, predefined destination (in this case, a latitudinal shift).

The number of 'steps' (grid cells) required to reach the predefined latitudinal threshold serves as a proxy for a coastline's complexity and orientation. A shorter path suggests a more direct route, reflecting a less complex or more north-south oriented coastline (Fig. 1a), while a longer path may indicate either a more convoluted coastline or an east-west oriented paleogeography (Fig. 1b-d). We set a maximum threshold of 100 grid cell steps, equivalent to a distance of ~11,100 km at the equator. If the algorithm terminated after reaching this 100-grid-cell limit, it suggests isolated regions such as islands or an extremely complex and long pathway to reach the specified latitudinal threshold.

Non-null raster values for isolated coastline GPMs were indexed sequentially, and each raster layer was converted into a data table using the rasterToPoints function in the raster v 3.6-26 R package (*74*). This conversion enabled more efficient handling of the data, after which the pathfinding algorithm was applied. The algorithm accounted for the Earth's spherical geometry by incorporating a wrap-around adjustment at the 180° meridian. This adjustment ensured geographic continuity by correctly identifying points near the International Date Line (e.g., 179°E and -179°W) as neighbors, which is important for accurate pathfinding on a global scale. Longitudinal position is difficult to estimate in deep

time and comes with large scale uncertainties (*42*), but is needed to calculate geometries here.

To quantify the grid cell steps required to reach a given latitudinal threshold of 5°, 10°, or 15°, we calculated the shortest path both northward and southward from each starting point along the coastline. We initially tested a range of latitudinal thresholds from 3° to 20°, finding broad-scale significance across this spectrum. However, we focused our primary analyses on the 5°, 10°, and 15° thresholds for clarity and interpretability. These thresholds were chosen to assess coastline geometry across spatial extents. The minimum threshold of 5° was selected because small, potentially spurious island fragments (fewer than four grid cells) were excluded from our gridded models, making the 5° threshold a reasonable lower bound. The concept of spatial extent in geography highlights how measurements and observations can change when viewed over different areas. Varying the latitudinal threshold allowed us to assess how patterns changed depending on the broader spatial context. For example, a coastline might appear predominantly north-south oriented using a 5° threshold. However, when the threshold is extended to 10° or 15° latitude, the same coastline might appear more east-west oriented, necessitating a greater number of steps to reach the threshold due to the increased complexity and changing coastline orientation over the larger area. Although this pattern differs from the coastline paradox and scale dependence (*33*, *80*, *81*), where the measured length of a coastline increases with finer measurement scales, it similarly illustrates how changing the spatial extent (in this case, the magnitude of latitudinal climate shifts) could impact our results.

The grid cell step length in our algorithm remained constant at a 1°x1° resolution, which meant we could not capture finer spatial scale details of the coastline itself, but rather how its broad geometry influenced the distance required to meet different latitudinal thresholds. The varying latitudinal thresholds may have relevance to contextualizing different levels of climate change. For instance, as global temperatures rise, we can expect isotherms (lines of constant temperature) to shift poleward. The extent of this poleward shift depends on the severity of the climate change scenario. A 5° latitudinal threshold might represent a moderate climate change scenario, while a 10° latitudinal threshold might correspond to more significant warming. The 15° latitudinal threshold may be analogous to the most extreme climate change scenarios, such as those that occurred during the End Permian mass extinction (*82*), when dramatic shifts in climate and temperature zones fundamentally altered global environments. It is important to note, however, that we focus here on a proxy for coastline geometry, rather than the distance to track climatic niches through time, as we were interested in the role of paleogeography and not the intersection of abiotic tolerances, rates of climate change, and paleogeography.

The algorithm recorded the total number of grid cell steps required to reach the threshold both northward and southward, denoted as S_N for northward steps and S_S for southward steps. The algorithm continued to explore neighboring grid cells until the cumulative latitude change ($y_f - y_i$) was met or exceeded the threshold (T_h) in either direction. For any given grid cell, the final estimate of the grid cell steps required to meet the threshold was

calculated as the average of S_N and S_S, providing a balanced measure of the coastline's complexity:

$$\bar{S} = \frac{S_N + S_S}{2}$$

The average of northward and southward distances was used to provide a generalized, direction-agnostic metric to quantify coastline geometry, avoiding assumptions about directional climate forcing and enabling consistent comparisons across geological stages. However, we also explored the distance to track north, south, and poleward and found a similarly important effect of coastline geometry on extinction.

If the algorithm failed to meet the threshold within a predefined maximum number of grid cell steps ($S_{max,}$ capped at a threshold of 100), the number of grid cell steps was set to 1 + S_{max}, indicating the threshold was not reached. We also ran analyses setting grid cells that could not track to a value of S_{max} + $Q_{0.05}$, which is the 5% quantile estimate from all grid cells.

The algorithm was applied to 90 maps, from the Cambrian to Recent. This process was repeated across five different reconstructions, resulting in a total of 405 map analyses, amounting to 1,215 total pathfinding algorithm runs for each coastline cell. Considering the scope and computational demands of these analyses, the algorithm was optimized for maximum efficiency, and all analyses were run in parallel on the computing cluster housed in the Department of Earth Sciences, University of Oxford. Information on the specific job duration, computer specifications, and associated batchfiles are included in data S1.

Haversine distance approach. Since the above analyses to define coastline geometry were performed using latitude and longitude projections, a potential problem could arise in that the distance between grid cell steps is variable and significantly smaller at the poles. Since we used the number of grid cell steps as a proxy for the complexity and orientation of ancient coastlines, the skew in distance represented by each step should not overly-limit our interpretations, and we partially circumvented this issue by removing polar occurrences in some variations of the analyses (fig. S13- S18). However, to address this potential bias, we explored an alternative method of calculating coastline geometry using the Haversine distance formula (*83*). The Haversine approach provides a more accurate calculation of the great-circle distance between two points on the Earth's surface by considering the oblate spheroid shape of the Earth. The formula used was:

$$(1)\ \mathrm{d} = 2\mathrm{R} \cdot \mathrm{atan2}(\sqrt{\alpha}, \sqrt{1-\alpha})$$

$$(2)\ \ \alpha = sin^2\frac{\Delta\Phi}{2} + \cos(\phi_1) \cdot \cos(\phi_2) \cdot sin^2\frac{\Delta\lambda}{2}$$

Where d is the Haversine distance, R is the radius of the Earth in meters (6,371,000), ΔΦ and Δλ are the changes in latitude and longitude, respectively, between y_i and y_f, and Φ_1 and Φ_2 are the latitudes of the two points. Degrees latitude and longitude were converted to radians by multiplying by $\frac{\pi}{180}$.

This formula calculates the shortest path along the Earth's surface as a great circle distance, providing a more precise measure of distance, particularly in regions closer to the poles

where the distance between longitudinal lines decreases significantly. We were interested in the total distance of each path, so instead of computing the Haversine distance between y_i and y_f, we instead computed the distance between each grid cell in every possible path and took the sum of all distances within each path to find the shortest path to each latitudinal threshold.

Although the Haversine method offers greater precision, it is also computationally intensive. Even with optimizations and use of parallel computing, running the Haversine-based algorithm often took several weeks to complete for a single GPM reconstruction. This computational cost made it impractical for widespread use across all the analyses in this study, and thus we used this model only for the 15^{o} latitudinal threshold. However, the general correspondence between the Haversine and grid cell step results (fig. S10) suggests our results are not affected by the distance method used.

Assigning coastline geometry metrics to taxonomic occurrences

To assign a coastline geometry to each individual taxon for each stage of the Phanerozoic, we calculated the number of grid cell steps required for a taxon to travel a predefined latitudinal shift (average minimum number of steps north and south) for each of its occurrences (see 'Quantifying coastline geometry for taxa'), then took the median of these values across the occurrences to assign a single coastline-geometry value to each taxon and time period, detailed below. This method serves as a proxy for coastline geometry since east-west coastlines, islands, and restrictive inland seaways would be represented by a larger number of grid cell steps, and would potentially hinder a taxon's ability to track climate change.

To assign a single distance-to-track metric for each taxon in each time interval, reconstructed coastlines for each GPM were matched with the taxon occurrence dataset using the matchtime() function from the *chronosphere* R package (*68*). This allowed us to link the age of the occurrences to the 90 ages used in the five GPM reconstructions. Some of the shallow-water taxon occurrences did not correspond to a coastal grid cell due to continental flooding, transgression, and other factors discussed in Kocsis et al. (*40*), and due to slight incongruencies between the rotated occurrences and GMP models. We therefore wrote a function called move_occurrences() to relocate taxon occurrences to the nearest coastal grid cell. We only considered occurrences up to 200 kilometres away from a coastal cell. This cutoff was chosen because 200 km corresponds to roughly two 1°x1° grid cells, and cells beyond this threshold likely represent deep water occurrences. The associated coastline geometry values were then extracted for each taxon occurrence.

Taxa included in our analysis always had at least three spatially unique occurrences within each stage, as this was our minimum sampling threshold. To ensure a representative estimate of each taxon's spatial context, whilst accounting for spatial and sample size heterogeneities across time and taxa, we used three different approaches to assign a single distance to track value for each taxon by stage combination: (i) the median coastline geometry value from the distance-to-track estimates for each occurrence of a given taxon by stage combination, without subsampling (fig. S19); (ii) the median value derived from

jackknife subsampling; and (iii) the median value derived from bootstrap subsampling (*84*). The latter two subsampling methods, modified from Malanoski et al. (*6*), are designed to mitigate the potential inflation of our grid cell step estimate due to spatial outliers, sample size disparities, and erroneous occurrences, which could distort results (*84*).

For jackknife subsampling, we iteratively removed one occurrence for a given taxon within a stage and took the median distance-to-track value from the remaining occurrences. This procedure was then repeated until all occurrences were removed once. The median of the median distance-to-track values was then taken as the estimate across the jackknife iterations. We chose median as the preferred method to estimate central tendency, since it is better for addressing potential outliers.

For the bootstrap subsampling approach, we identified the smallest number of generic occurrences per stage, which was three, and subsampled each genus by stage combination down to this sample size. For each subsample, we took the median (i.e., middle) distance-to-track estimate across the three occurrences. We iteratively subsampled without replacement 100 times to account for potential sample size biases. Our bootstrapped grid cell step estimate for a given taxon by stage combination was then quantified by taking the median of the 100 subsampled median distance-to-track values. We chose 100 iterations to strike a balance between ensuring adequate subsampling to obtain stable 95% confidence intervals and limiting pseudoreplication, which can arise with larger numbers of replicates (e.g., 1000) given the structure of the data.

Defining extinction

Extinction was treated as a binary factor of 0 or 1, depending on whether a genus went extinct or not during a stage. We determined when each genus went extinct using the modeltab() function within the R package divDyn (*60*) to estimate first and last occurrence datums. The Fortunian and Holocene were only included in range calculation to remove edge effects but were excluded from analyses. The range-through method was used to estimate the last occurrence datum for each genus. ~~The dataset was then filtered to include genera with at least three spatially unique occurrences, and to exclude stratigraphic singletons.~~

In addition to a binary extinction estimate, we employed a probabilistic extinction estimate to explicitly account for the Signor–Lipps effect (*57*), which recognizes that the observed last occurrence datum typically underestimates the true timing of extinction. To address this, we conducted a supplemental analysis (fig. S20) in which the estimated stage of extinction was treated as probabilistic rather than definite. In this approach, extinction was assigned a probabilistic value derived from the mean three-timer sampling completeness of the temporal stage of interest and the clade sampling completeness across stages using the methods described in (*7*, *43*, *85*).

Macroevolutionary regime definitions

We hypothesise that coastal geometry has a greater influence on taxon extinction risk during mass extinctions and hyperthermal intervals due to the severity of climate change

that occurs during these intervals. Selectivity is almost always muted during mass extinction intervals for known determinants of extinction risk, such as geographic range size (*9*, *12*), likely due to increased stochasticity (*5*, *12*), but coastal geometry may be an exception to this pattern. To test this hypothesis, we used two mass extinction definitions: (i) the Big Five mass extinctions, used in the main text (Fig. 4), and (ii) extinctions defined by Bond and Grasby (*51*) (fig. S22). The Big Five definition includes five events assigned to the Frasnian, Hirnantian, Changhsingian, Rhaetian, and Maastrichtian stages (and not the subsequent stages; e.g., the Permian-Triassic extinction is assigned to the Changhsingian, not the Induan). The other definition includes all first and second order mass extinction events that occurred throughout the Phanerozoic that are associated with a large igneous province (n=17) (*51*). This variable was treated as an interaction term with the coastal geometry variable to assess whether there were significant differences in selectivity between evolutionary regimes.

Hyperthermals were defined as stages with considerable increases in temperature as defined by Reddin et al. (*7*). We coded non hyperthermals versus hyperthermals as a factor of 0 or 1. This variable was included as an interaction term with coastline geometry to assess the differences in selectivity based on climatic regime.

Statistical model framework

We assessed the impact of paleogeography on per-taxon extinction risk across the Phanerozoic using both univariate and multivariate generalized linear mixed effects models (GLMMs). Our primary focus was to understand how coastline geometry influenced extinction risk for taxa, and how this extinction selectivity differed based on evolutionary (mass extinction versus background) and climatic regime (hyperthermal events). To model this, we employed GLMMs via the glmer() function in the lme4 R package v1.1-33 (*86*). Mixed effects models are ideal for paleontological studies, since they account for the hierarchical nature of paleontological data.

Paleontological data can be grouped by space, time, and taxonomic group. We accounted for the temporal grouping structure of fossil data by including stage as a random effect, which allowed for the effect of coastline geometry to vary for each stage over the Phanerozoic. This is important, since we hypothesize that the effect of coastline geometry on extinction may not be constant over the Phanerozoic due to differences in climate, extinction intensity, sea level (fig. S21), marine shelf area, and other factors that vary among stages. We tested for autocorrelation in our model using a Durbin-Watson test and found no statistical support for the need to account for autocorrelation in addition to including stage as a random effect.

Evolutionary history also plays an important role in regulating extinction patterns on macroevolutionary timescales (*87*). To account for the influence of phylogenetic grouping on our extinction model, we included class as a random effect (fig. S4). We used class as opposed to family, which has been used previously (*6*, *53*), since many families were missing or indeterminate, whereas class could be more readily identified for all taxa. Physiology, life history, and ecology are more likely to be similar within classes relative to distantly-related

groups. Although difficult to quantify in the geologic past, modelling coastline geometry across classes should account for some differences in the proportion of good versus bad dispersers within clades (for example, the class Ammonoidea is thought to have a higher proportion of good dispersers than rhynchonellid brachiopods).

Univariate models. Univariate models were run for each of the three latitudinal thresholds (5°, 10°, and 15°) to test the robustness of the variable to coastline definitions at different spatial scales. We found our steps to threshold variable to have a significant impact on extinction risk at all three spatial scales, with $\alpha < 0.05$ in most instances except for the Golonka 10^{o} latitudinal threshold (fig. S7).

Model fit was tested by comparing AICc values between each univariate model and a null model with only the intercept and random effects.

We computed the marginal effects using the ggeffect() function from the ggeffects v1.2 R package (*88*) to assess the relationship between the predictor and extinction risk across all random effect levels. This allowed us to evaluate extinction risk associated with each unique distance (grid cell steps) for a given latitudinal threshold, which was repeated for each threshold x GPM model.

All univariate models were fit as generalized linear mixed models (GLMMs) with random intercepts for both stage and class, modeled as (1|stage) and (1|class), to account for background variation in extinction intensity across time and taxa. We initially tested all plausible random-effects structures, including random slopes and nested effects, and found that results were qualitatively similar. However, the random intercept models were more stable and interpretable, particularly for the interaction and multivariate analyses, and we therefore report them in the main text. Models with random intercepts for class were included in the main text because slope variance was consistently low ($\sigma^2 \approx 0.05–0.06$), indicating that the effect of coastline geometry was relatively consistent across clades. In contrast, intercept variance was substantial, capturing meaningful differences in baseline extinction risk among taxa. While genera are nested within classes, and thus not strictly independent, each genus occurs only once per stage, and temporal structure is accounted for by the stage-level random effect. Models with nested random effects, such as (1|class/genus), or random slopes on genus, often failed to converge or produced singular fits, largely due to the limited number of time bins per genus. The two exceptions were Fig. 2B, which presents a univariate model with a random slope and random intercept for stage, and Fig. 4, which uses the same random slope and random intercept structure in the interaction models. Additional comparisons of alternative random-effect structures are shown in fig. S26.

We ensured each model met the assumptions required for GLMMs. To do so, we used residual plots and tested for dispersion and uniformity in the residuals using the DHARMa R package v0.4.6 (*89*), which is tailored for hierarchical model frameworks. All models met the assumptions required for GLMMs, as indicated by residual diagnostic tests yielding non-significant p-values. ~~For these univariate models, we allowed the intercept to vary for each level of the random effect with random effects modelled as (1|stage), (1|class).~~

We evaluated potential nonlinearity by fitting generalized additive mixed models (GAMMs; mgcv v. 1.8-42) with cubic regression splines on the scaled coastline-geometry predictor while retaining the GLMM random-effects structure. For the 5° threshold, the GAMM AICc (22,593.16) was only marginally higher than the linear GLMM (22,591.03; ΔAICc = +2.13), and similarly negligible differences occurred at 10° and 15°. More flexible spline specifications and alternative random-effects structures often underperformed based on AICc and sometimes suffered convergence or stability issues.

We also tested for potential non-linearity in the relationship between coastline geometry and extinction across macroevolutionary and climatic regimes (Fig. 4) and again found no significant improvement with a GAMM approach. As an additional nonlinearity diagnostic, we overlaid partial (marginal) residuals on the marginal-effects panels using the ggeffects package v1.2 (e.g., show_residuals = TRUE, show_residuals_line = TRUE); in every case, the residual loess line closely tracked the marginal-effect curve, with no discernible structure beyond random scatter, indicating no missed nonlinearity or unmodeled interaction beyond regime. Together, these results support the use of the simpler and more stable linear GLMM framework for modeling extinction risk.

To test for the effects of climatic and evolutionary regime on the relationship between coastline geometry and extinction, we used the following formula:

$$exinction \sim steps\ to\ threshold : regime + (steps\ to\ threshold | stage) + (1 | class)$$

We included mass extinctions versus background as an interaction term between our coastline geometry variable in a model. We also included hyperthermals versus non-hyperthermals as an interaction term, by replacing regime with conditional hyperthermal variable in the above model, between our coastline geometry metric in a separate model:

However, in random intercept models, only the intercept, which is extinction intensity, can vary across all levels of the random effect, and the influence of coastline geometry is assumed to be constant. Therefore, to assess the effect of coastline geometry across temporal groupings, such as stage or macroevolutionary regime, we must allow both the slope and the intercept to vary over time. We used ggeffect() to analyse the difference in slope between each level of the interaction and plotted each level of the interaction with confidence intervals to evaluate differences in selectivity. We additionally compared the difference in coefficients and AIC weight to evaluate whether there is differential selectivity between regimes. Based on a higher AIC weight and an increase in model coefficients for both hyperthermals and mass extinctions (Fig. 4), we saw support that coastline geometry increased in importance during mass extinctions and hyperthermal times (Fig. 4; fig. S22; table S8-S9).

Multivariate models. Finally, to evaluate our novel coastline geometry metric in the broader context of other known determinants of extinction on geologic timescales, we compared our paleogeography metric to geographic range size, body size, realized thermal preference, realized thermal breadth, and absolute temperature change experienced by individual taxa,

from Malanoski et al. (6). We merged the published dataset of these variables with our current dataset by matching stage and genus occurrences, resulting in a dataset that contained 16,722 spatio-temporally unique generic occurrences spanning nine different classes, including Cephalopoda, Gastropoda, Echinoidea, Crinoidea, Trilobita, Ostracoda, Bivalvia, and the brachiopods Rynchonellata and Strophemenata. These occurrences and classes are consistent with those used in previous studies (6, 8, 96).

We tested for multicollinearity in our variables using Variance Inflation Factors (VIF). We retained all predictors in our model, since VIFs were <2.5. We also tested the correlation between coastline geometry and the other variables using a Spearman Rank Correlation. Coastline geometry was not significantly correlated with any of the five variables (e.g., a Rho = –0.12 with geographic range size).

We employed an exhaustive model selection approach using the dredge() function from the MuMIn R package v1.4 (97). This approach compared all possible models, including a null model with only the intercept, based on AICc and AICc weights. We found coastline geometry was included in the best model, which incorporated all six predictors based on an AICc weight percent of 86% (fig. S21; tables S1–S5). The selectivity of coastline geometry in the most saturated model was similar for different taxonomic classes over the Phanerozoic (fig. S24). Relative to the other predictors, coastline geometry played a minor role in mediating extinction risk (0.05 log odds, compared to geographic range size, with a log odds of –0.44; table S3). Although the relative effect size was lower, the strength of coastline geometry was nevertheless greater than expected due to chance compared to permuted and Monte Carlo simulated data under the null hypothesis of no selectivity (see Null models and power analyses below).

We performed an additional model selection procedure using the same six predictors, plus an interaction term between the coastline geometry metric and either hyperthermals or mass extinctions as a seventh predictor. Therefore, we ran 64 unique models without interactions (table S3), and 320 models including interactions (tables S8–S9). Hyperthermals and mass extinctions are retained in the best model when included as interaction terms (tables S7–S9), providing further support for the increased effect of coastline geometry during these events.

Marginal effects were evaluated for the top-ranked models to interpret the influence of coastline geometry on extinction risk in relation to other known predictors. We also assessed model assumptions using the DHARMa R package. The inclusion of coastline geometry alongside the five other well-established extinction predictors (6, 7, 9, 12) highlights that extinction risk is modulated by a complex interplay of both intrinsic biological traits, population-level attributes, and extrinsic environmental factors (6). Although paleogeography is a critical determinant of a taxon’s ability to respond to climate change, this boundary condition interacts with other factors, such as a species' geographic range (9, 12, 56, 58) and physiological tolerance (6, 7), to shape overall extinction outcomes (6). By quantifying the relative importance of coastline geometry compared to known extinction determinants, we provide a comprehensive evaluation of its role in shaping extinction dynamics across the Phanerozoic.

Sensitivity tests

We conducted several sensitivity tests to evaluate the robustness of our results. These tests are important for addressing potential biases introduced by the choice of plate model, spatial scale, subsampling methods, and the inherent variability in paleogeographic data, and show that coastline geometry provides a consistent and reliable signal of extinction selectivity over the Phanerozoic.

1. Plate model choice

Considerable uncertainty exists in paleogeographic reconstructions (*35*, *42*), discussed above. To partially account for this, we ran our analyses using four different plate models: Torsvik & Cocks (2017) (*37*), Wright et al. (2013) (*38*), Merdith et al. (2021) (*39*), and Scotese (2018) (*40*) (fig. S12). For each plate model, we computed coastal geometry at 5°, 10°, and 15° latitudinal thresholds and ran separate GLMMs to assess its impact on extinction risk. Coastline geometry was significant in most plate models for most thresholds (15 out of 16), with positive associations across the different reconstructions (Fig. 3; fig. S7,S8,S9,S11,S12).

2. Spatial threshold: 5°, 10°, and 15° latitudinal thresholds

Measurements and observations can change when viewed over different spatial scales in geography, a concept called 'scale-dependence' (*80*). We therefore tested the effect of coastline geometry over three different spatial scales: 5°, 10°, and 15° of latitude. The steps to threshold metric remained significant across all three thresholds, except for the Golonka 10^{o} latitudinal threshold (fig. S7), although the strength of the association was variable (Fig. 3; fig. S7,S8,S9,S11).

3. Coastline definition: complex shelf areas vs. strict coastlines

We investigated the effect of different coastline definitions. We compared two approaches: a strict 1°x1° grid cell definition and a more complex, larger coastal shelf area derived from Kocsis et al. (*40*). The latter included broader dispersal pathways, such as shallow and inland seas, which are more ecologically-realistic for marine organisms. Our analysis showed that the steps to threshold variable was significant using both definitions, but the strength of the association was slightly higher with the broader coastal shelf definition (Fig. 3; fig. S9).

4. Subsampling approaches: bootstrap, jackknife, and raw data

To address concerns over spatial and sample size biases in fossil data, we employed two subsampling approaches: bootstrap and jackknife (*90*). Each method was designed to test the robustness of our results to variations in sample size and spatial distribution. The subsampling approaches were consistent with the raw results (fig. S19), with the coastline geometry variable remaining significantly positively correlated with extinction risk in all analyses. This consistency underscores the robustness of the metric to different subsampling strategies, supporting its reliability as a predictor of extinction risk.

5. Polar bias: excluding polar occurrences (>60° latitude)

Species that reside at high latitudes are more likely to return higher grid cell step values, especially for the 15° threshold, as they are closer to the poles and may not reach their northern or southern latitudinal thresholds given edge effects. Polar species are also more vulnerable to extinction due to the potential loss of their climatic niches due to climate change (*7*, *91*). By excluding polar occurrences, defined as occurrences at greater than 60^{o} absolute latitude, we aimed to isolate the effect of coastline geometry for species residing in more temperate and tropical regions. We found that the distance to threshold variable remained significant after the exclusion of polar taxa for most plate models and distance thresholds (11 out of 16). However, there was some uncertainty for some of the thresholds in the Golonka, Merdith, and Torsvik and Cocks plate models, evidenced by the confidence intervals intersecting zero. Overall, the majority of our sensitivity tests reveal that the relationship between our paleogeography metric and extinction risk is not likely driven by a polar bias (fig. S13-S14,S15,S16,S17,S18,S25).

6. Dispersal ability: good vs. poor dispersers

Dispersal ability is a key factor influencing extinction risk (*21*, *92*) and is critical in allowing species to shift latitudinally. Although it is difficult to categorize the dispersal abilities of many ancient taxa, we tested the impact of removing taxa categorised as 'good' dispersers on results. We identified 703 unique genera reported from the literature (*21*, *92*–*95*) to be capable of dispersing longer distances (often due to having planktonic larvae or an active nektonic lifestyle), of which Cephalopods comprise a substantial portion (see table S). After removing known good dispersers, including all Cephalopods, the relationship between coastline geometry and extinction risk was strengthened for the remaining taxa, which may represent poorer dispersers (fig. S1,S2-S3). However, coastline geometry remained significant even when including good dispersers, suggesting its broad importance across taxa with varying dispersal capacities.

7. Temporal restriction: post Triassic

The accuracy of paleogeographic reconstructions improves significantly after the break-up of Pangaea (*35*, *42*), allowing for more reliable estimates of latitudinal shifts and extinction dynamics. We therefore tested whether patterns held when we restricted our analysis to the Jurassic and more recent stages (fig. S5-S6). Coastline geometry remained significant for these more recent time periods, reinforcing the robustness of our results.

8. Probabilistic extinction model

We assessed the sensitivity of our results to the Signor-Lipps effect by implementing the probabilistic model described in Reddin et al. (2021) (*43*). We used the probability that the observed time of extinction represents the true time of extinction using the code and framework of Reddin et al. (2021) (*43*). Coastline geometry remained significant, although there was greater uncertainty in the effect size (fig. S20).

9. Random effects structure

We investigated the influence of different random effects structures on the results. We ran both (i) random intercept and (ii) random slope and random intercept models with regards

to both stage and class, and we included a nested model for class to account for non-independence. We found results to be consistent with the random intercept models used in the main text, although the coefficients and uncertainty were higher for the more complex random slope and random intercept models (fig. S26).

Null models and power analyses

We used power analysis and null models to evaluate the robustness and validity of our extinction models. These approaches tested for both Type I and Type II statistical errors, ensuring the effects observed in our analysis were reliable and unlikely due to chance. While the size of our dataset may give us the power to detect minute selectivity signals, it might also increase the risks for type I statistical error (*96*, *97*).

The power analysis was conducted using Monte Carlo simulations, a widely-used method in generalized linear mixed models (GLMMs), using simr v1.0 (*98*). Monte Carlo simulations allow for the estimation of statistical power by repeatedly simulating new response data based on the parameters of a fitted statistical model. For our GLMMs, which assessed the relationship between the coastline geometry metric and extinction risk, the process involved simulating new data using the fitted model's coefficients, variance components, and hierarchical structure. The model was then refitted to this simulated data, and we assessed how often the simulated results identified a significant effect for our coastline geometry metric. By running this simulation for 100 iterations, we calculated the proportion of simulations where the model correctly detected a significant effect. This proportion represents the statistical power of our models to identify true effects, and provided us with an estimate of how likely we were to detect real relationships between our predictor variables and extinction risk. We detected a significant relationship between coastline geometry and extinction risk for 100/100 simulated datasets based on an $\alpha<0.05$.

We also used both Monte Carlo simulations and permutation-based null models to assess the risk of type I errors, raising confidence that our observed relationships were not simply artifacts of chance. The Monte Carlo approach, implemented using the simulate() function in the lme4 R package v1.133, generated datasets under the null hypothesis that coastline geometry had no effect on extinction risk. By simulating response variables with the same structure as our original data but without any real effect, we were able to test the probability of detecting a signal when one does not exist. We simulated 100 datasets and ran the GLMM for each, determining the number of times that a significant signal was detected, and how many times this selectivity was greater than the empirical selectivity signal. We did not find a significant ($\alpha<0.05$) selectivity signal in 100/100 simulations, suggesting our result is likely not due to type I statistical error.

We also used a permutation-based approach, which complemented the Monte Carlo simulation, by directly shuffling the predictor values within the taxonomic and stage groupings using the permute() function in simr (*98*). By randomly reassigning coastline

1205 geometry values to different taxa, we maintained the same data structure but removed any
1206 genuine relationship between the predictor and extinction. This shuffling process was
1207 repeated 100 times, and for each permutation, we refit the extinction model and calculated
1208 the resulting effect size. The distribution of these permuted effect sizes allowed us to
1209 construct a null distribution against which we compared the observed effect size. We found
1210 that 100/100 permuted datasets resulted in no significant ($\alpha<0.05$) association between
1211 coastline geometry and extinction risk, which further corroborates our results that coastline
1212 geometry has a significant effect on extinction risk and is not likely an artifact of type I error.
1213 (*40*).

1214

1215

1216

SUPPLEMENTARY MATERIALS

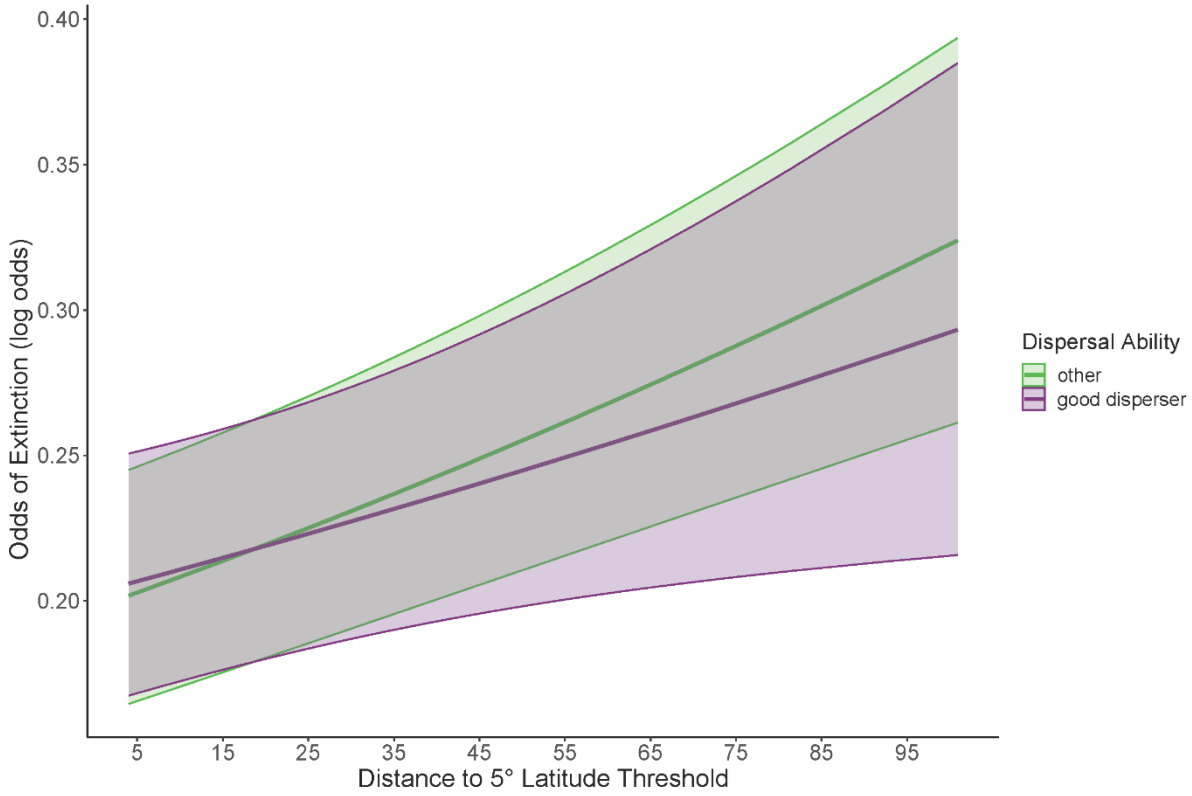

Fig. S1. Marginal effects plot showing the probability of extinction for distance (grid cell steps) to the 5° latitudinal threshold for taxa classed as good dispersers vs. others. All species regardless of dispersal ability are included in the model, with dispersal ability included as an interaction term. Model results are for the 5° latitudinal threshold using the Kocsis et al. (2021) plate model. Shaded regions represent 95% confidence intervals. See Fig. S2 for results when good dispersers are excluded from the model.

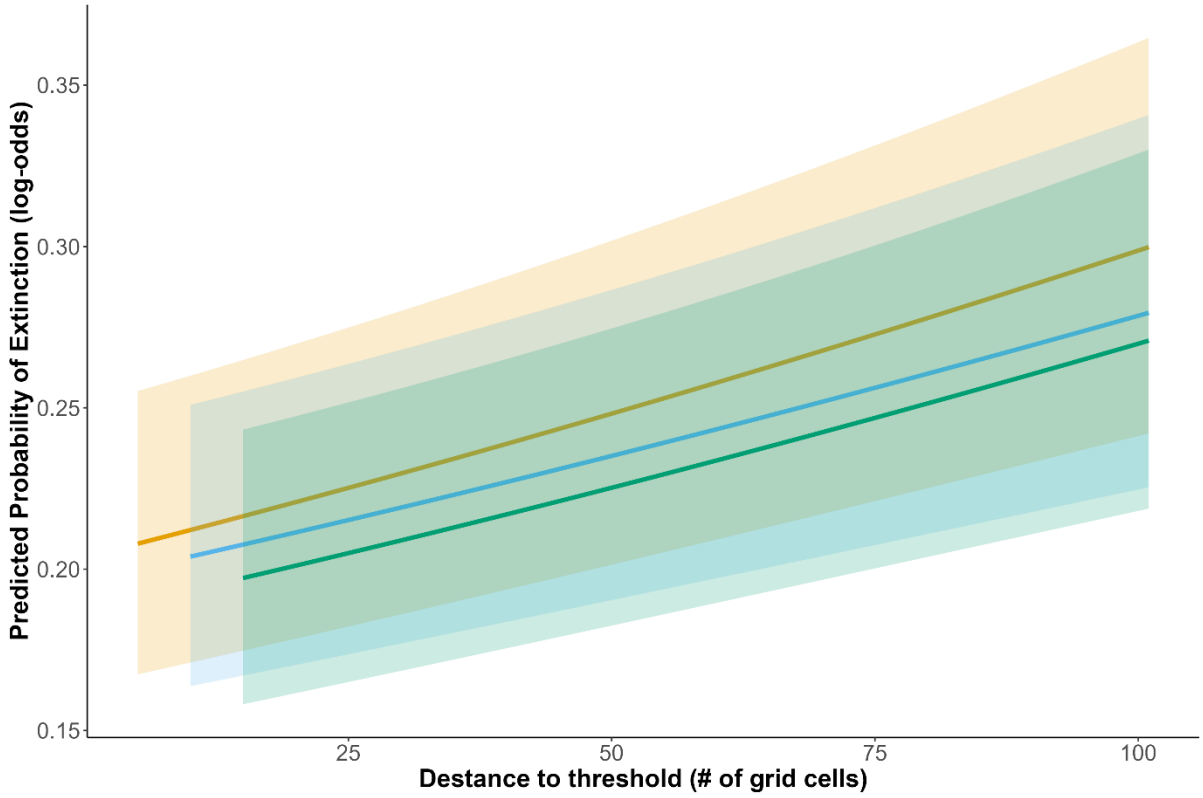

Fig. S2. **Marginal effects plots for the distance (grid cell steps) to travel 5°, 10°, and 15° latitude, using the Kocsis et al. (2021) plate model with the removal of taxa that are known good dispersers**. Shaded regions represent 95% confidence intervals.

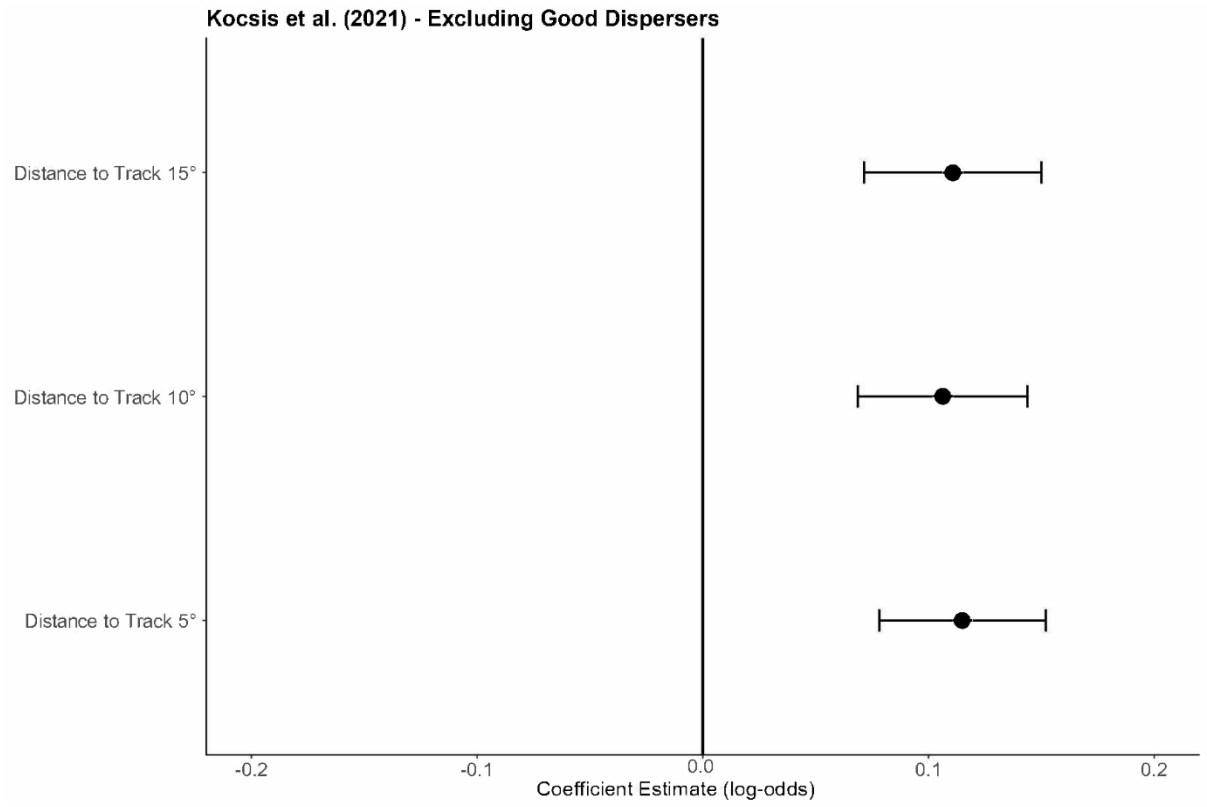

1234

1235 **Fig. S3. Coefficient plots for the distance (grid cell steps) required to travel 5°, 10°, and 15°**
1236 **latitude, using the Kocsis et al. (2021) plate model, with the removal of taxa that are known good**
1237 **dispersers.** Bars represent 95% confidence intervals.

1238

1239

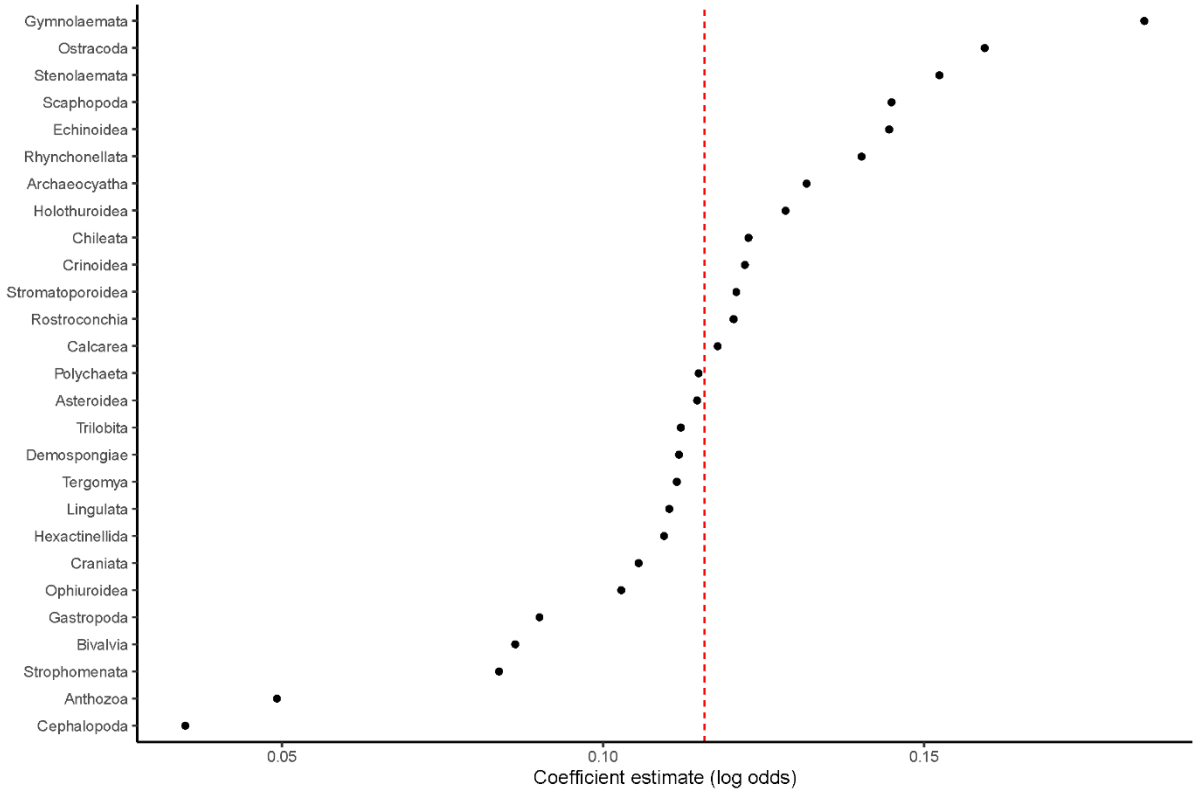

1240

1241 **Fig. S4. Relationship between coastline geometry and extinction risk for each level of the random**
1242 **effect class**. This model was run using a random slope and random intercept term for taxonomic
1243 class, with a random intercept for stage. Class-specific random effect slope coefficients are plotted in
1244 black, and the average slope estimate was plotted at ~0.11 in red.

1245

1246

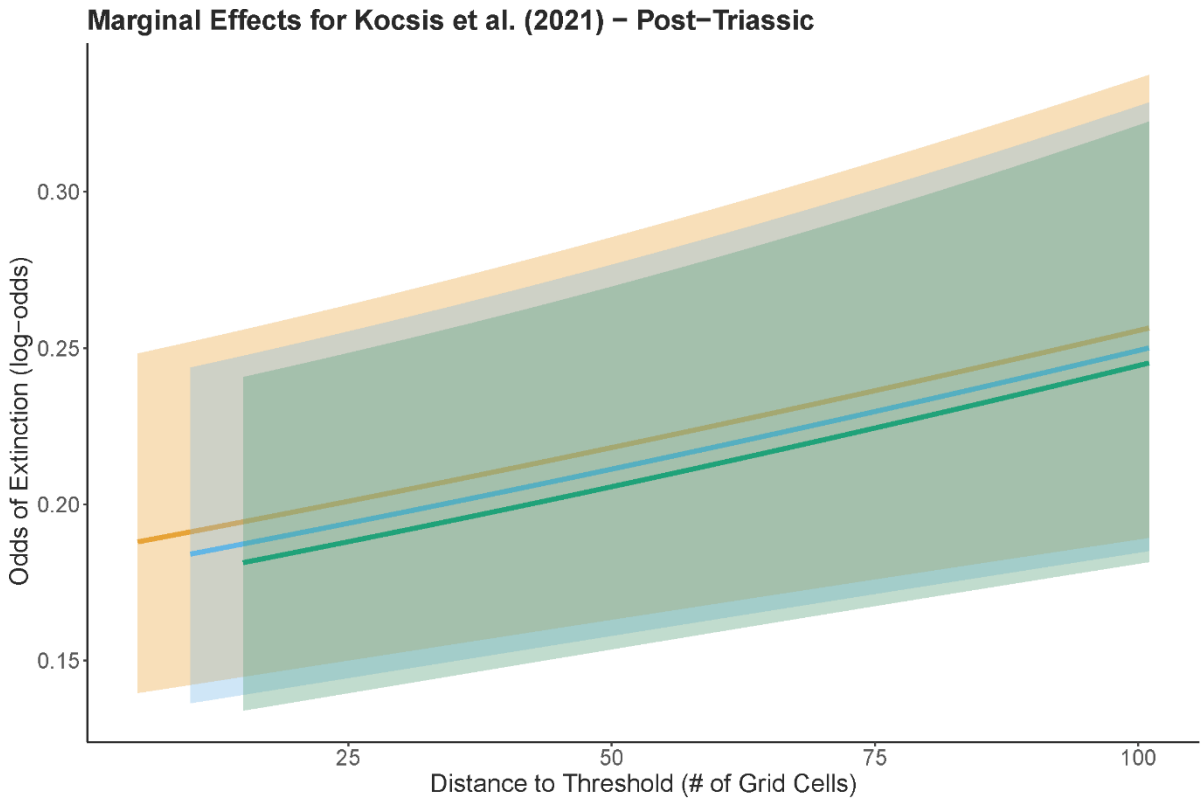

Fig. S5. **Marginal effects plots for the distance (grid cell steps) to a latitudinal threshold of 5°, 10°, and 15° latitude, using the Kocsis et al. (2021) paleogeographic model for post Triassic occurrences only**. Shaded regions represent 95% confidence intervals.

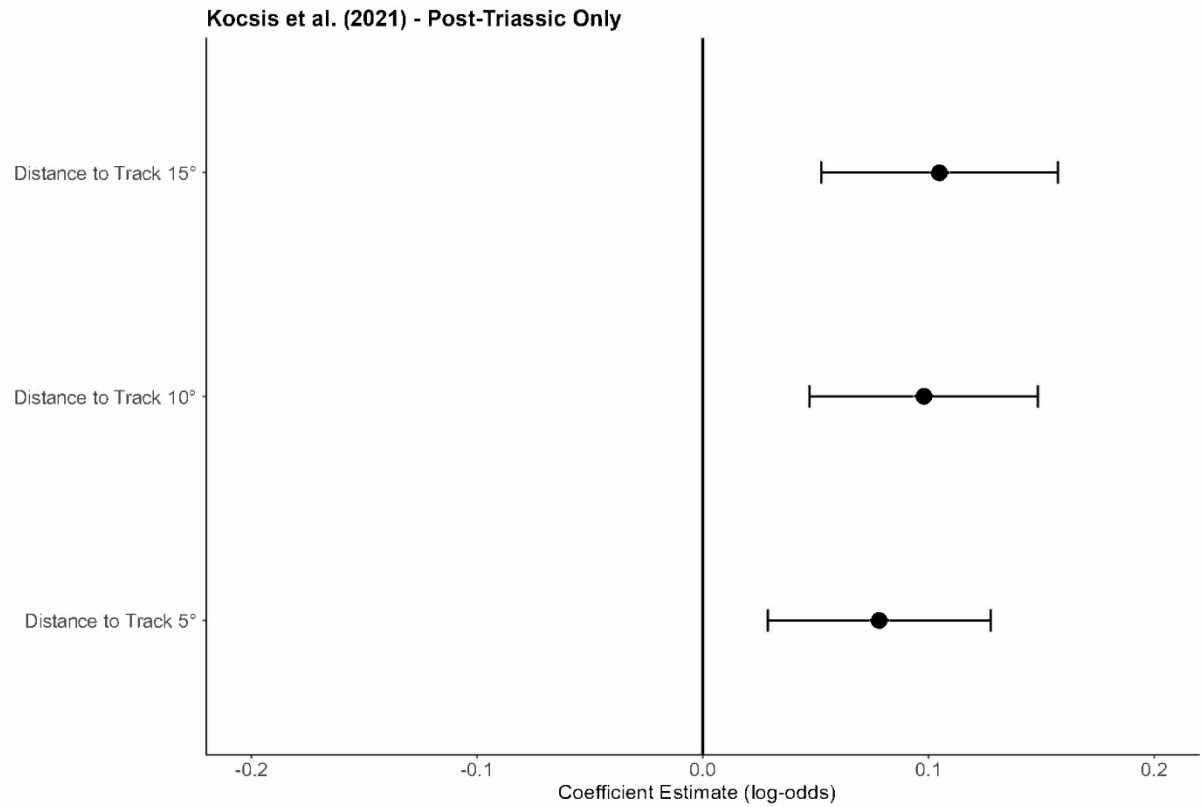

1253

1254 **Fig. S6. Coefficient estimates (log-odds) for extinction risk associated with the coastline geometry**
1255 **metric for a latitudinal threshold of 5°, 10°, and 15° latitude, using the Kocsis et al. (2021)**
1256 **paleogeographic model on post Triassic occurrences.** Each point represents the estimated
1257 coefficient for extinction risk associated with three different latitudinal thresholds, with horizontal
1258 lines representing 95% confidence intervals.

1259

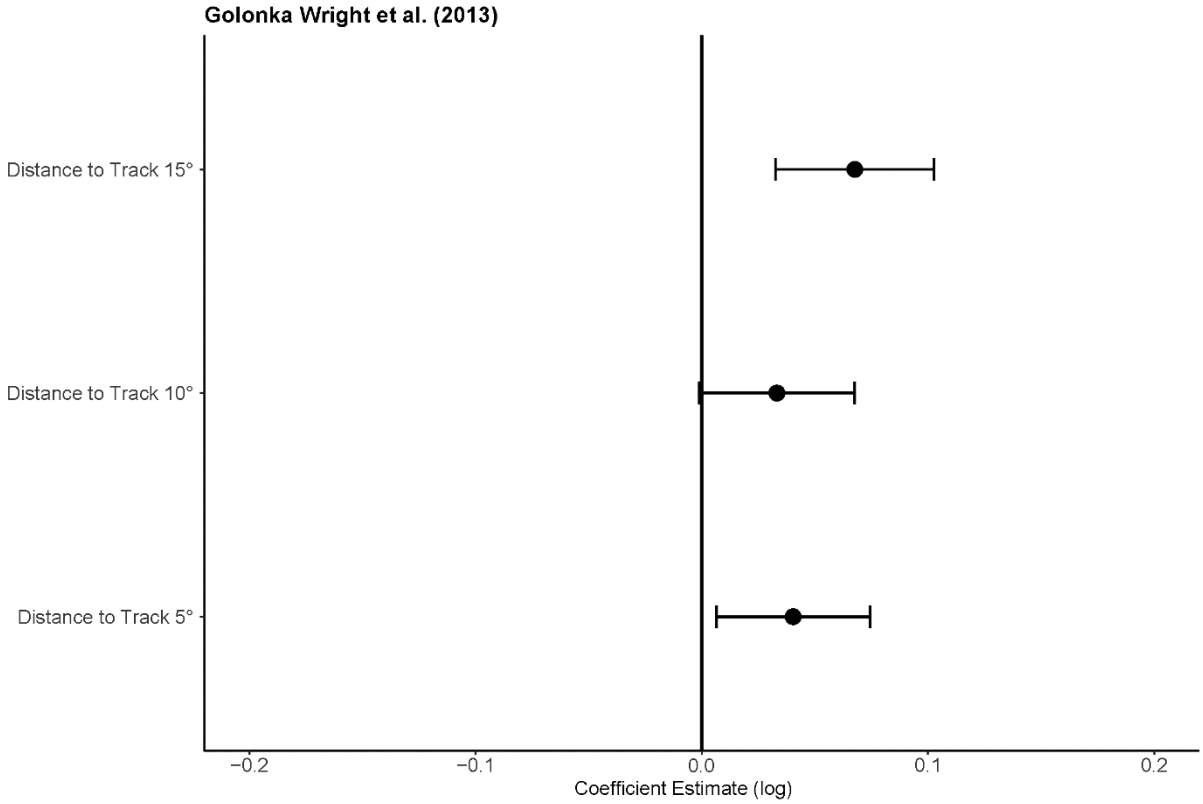

Fig. S7. **Coefficient estimates (log-odds) for extinction risk associated with the coastline geometry metric for latitudinal thresholds of 5°, 10°, and 15°, using the Golonka Wright et al. (2013) paleogeographic model**. Each point represents the estimated coefficient for extinction risk associated with three different latitudinal thresholds, with horizontal lines representing 95% confidence intervals.

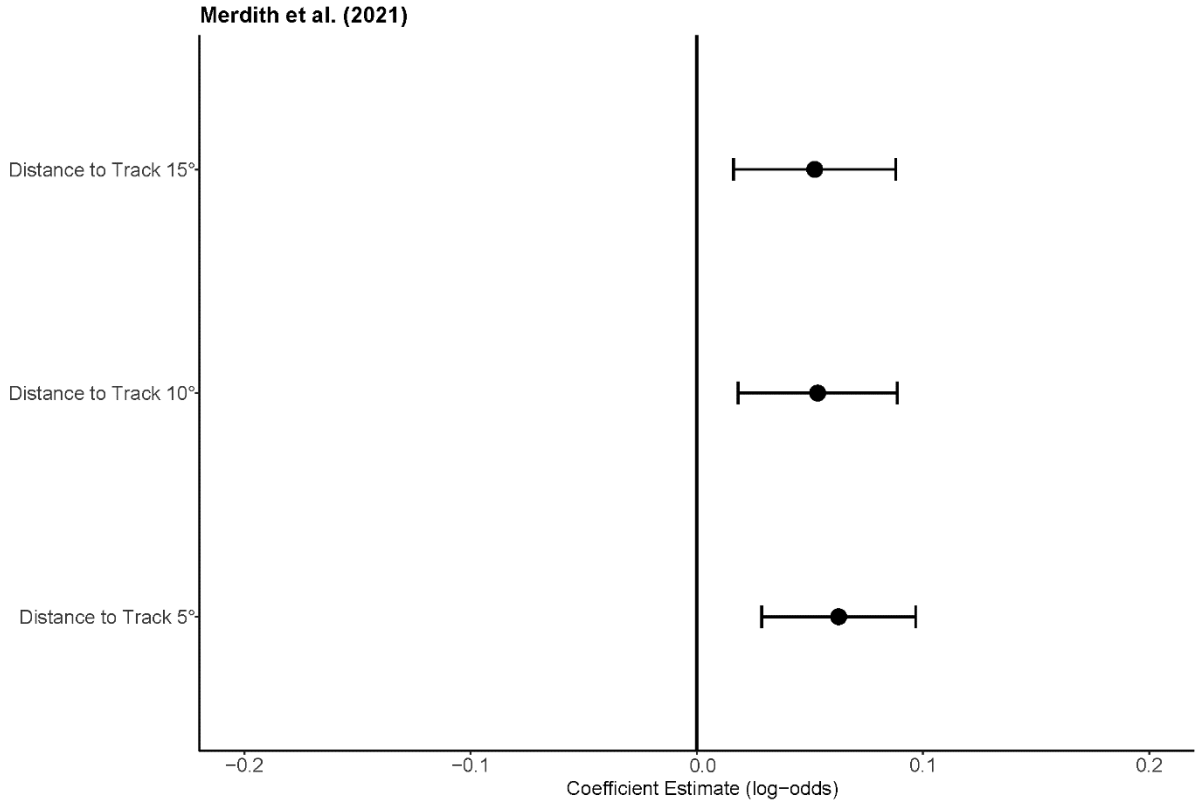

Fig. S8. Coefficient estimates (log-odds) for extinction risk associated with the coastline geometry metric for latitudinal thresholds of 5°, 10°, and 15°, using the Meredith et al. (2021) paleogeographic model. Each point represents the estimated coefficient for extinction risk associated with three different latitudinal thresholds, with horizontal lines representing 95% confidence intervals.

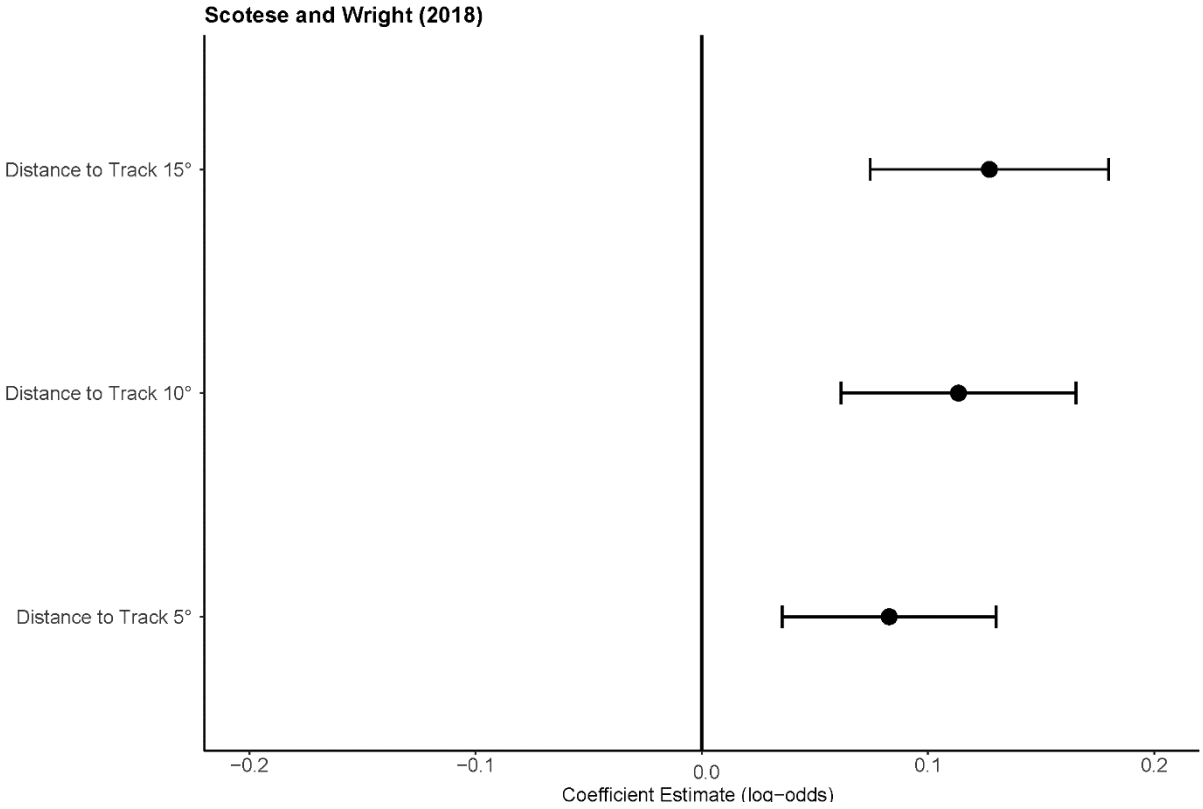

Fig. S9. Coefficient estimates (log-odds) for extinction risk associated with the coastline geometry metric for latitudinal thresholds of 5°, 10°, and 15°, using the Scotese and Wright (2018) model. Each point represents the estimated coefficient for extinction risk associated with three different latitudinal thresholds, with horizontal lines representing 95% confidence intervals.

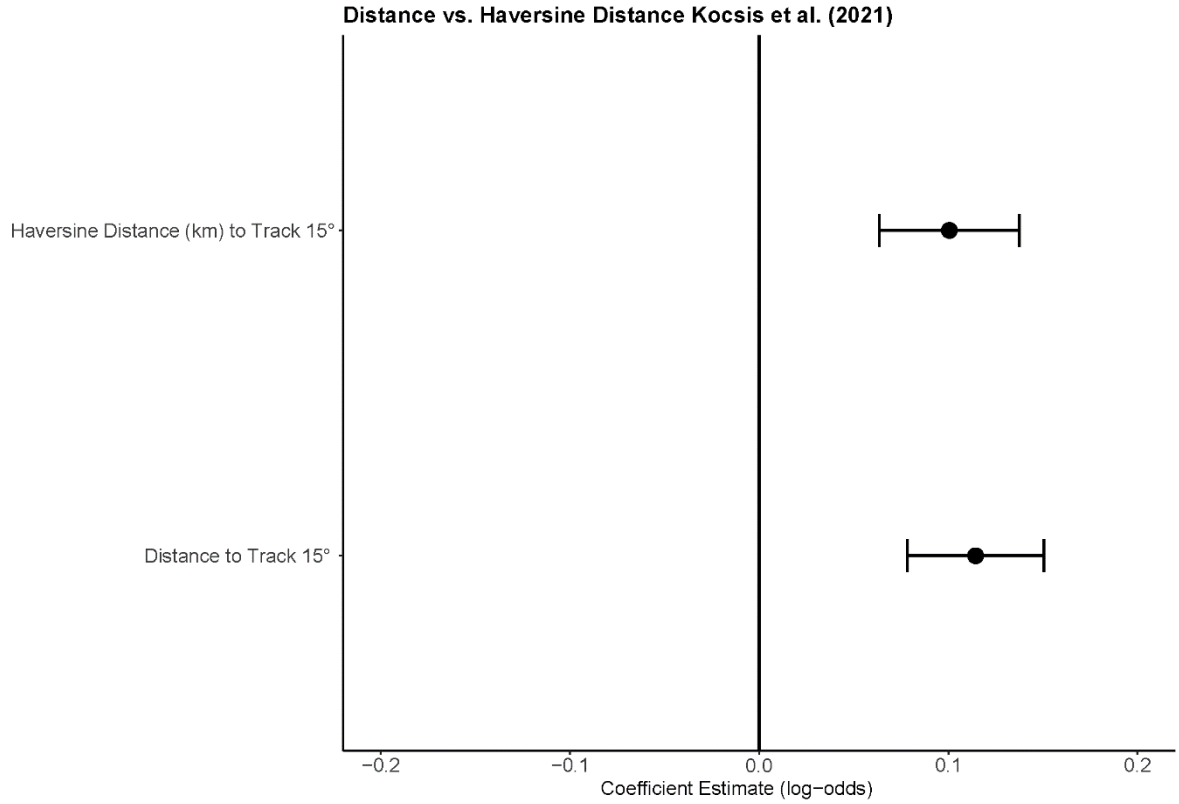

1280

1281 **Fig. S10**. **Coefficient estimates (log-odds) for extinction risk associated with the coastline geometry**
1282 **metric for a latitudinal threshold of 15°, using the Kocsis et al. (2021) paleogeographic model**
1283 **showing similarities between the grid cell steps metric and haversine distance metric**. Each point
1284 represents the estimated coefficient for extinction risk associated with three different latitudinal
1285 thresholds, with horizontal lines representing 95% confidence intervals.

1286

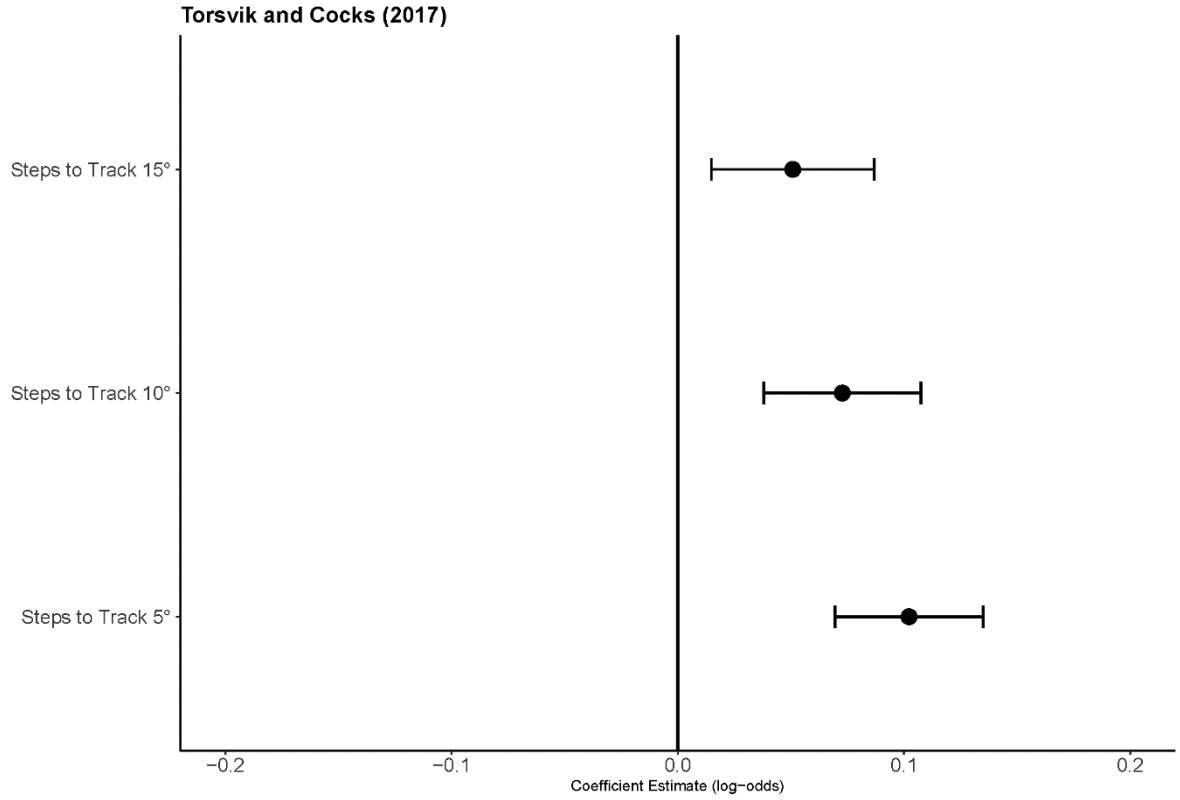

1287

1288 **Fig. S11. Coefficient estimates (log-odds) for extinction risk associated with the coastline geometry**
1289 **metric for latitudinal thresholds of 5°, 10°, and 15°, using the Torsvik and Cocks (2017)**
1290 **paleogeographic model with polar occurrences (absolute latitude > 60) excluded**. Each point
1291 represents the estimated coefficient for extinction risk associated with three different latitudinal
1292 thresholds, with horizontal lines representing 95% confidence intervals.

1293

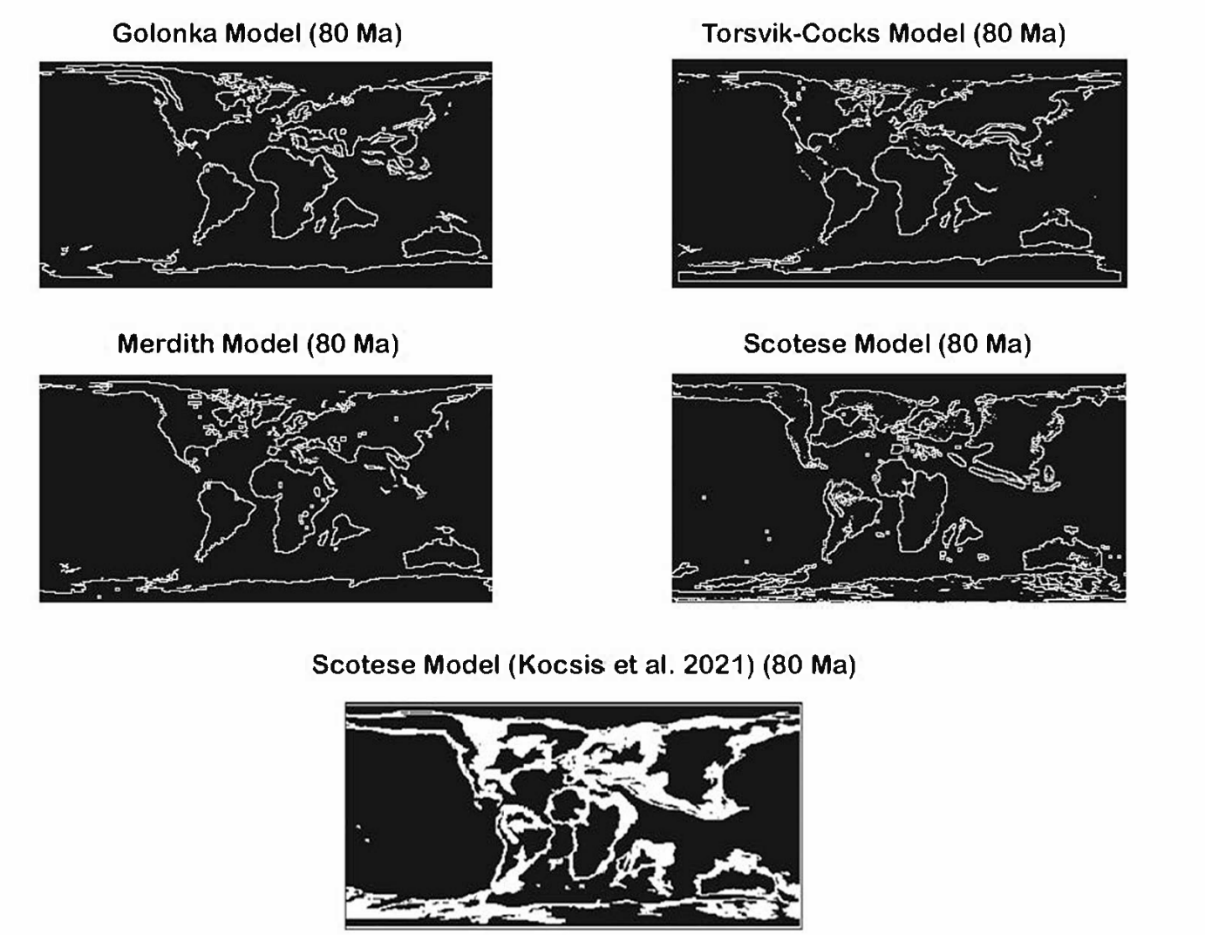

Fig. S12. Latitude-longitude maps for 80 Ma using 5 different global plate models (GPMs). We reconstructed and isolated coastlines for 80 Ma using the Golonka (*38*), Torsvik and Cocks (*37*), Meredith (*39*), and Scotese and Wright (*36*) global plate models. We additionally used an expanded coastline definition (shallow marine shelf area, rather than continental margins) of the Scotese and Wright (*36*) GPM from Kocsis et al. (*40*).

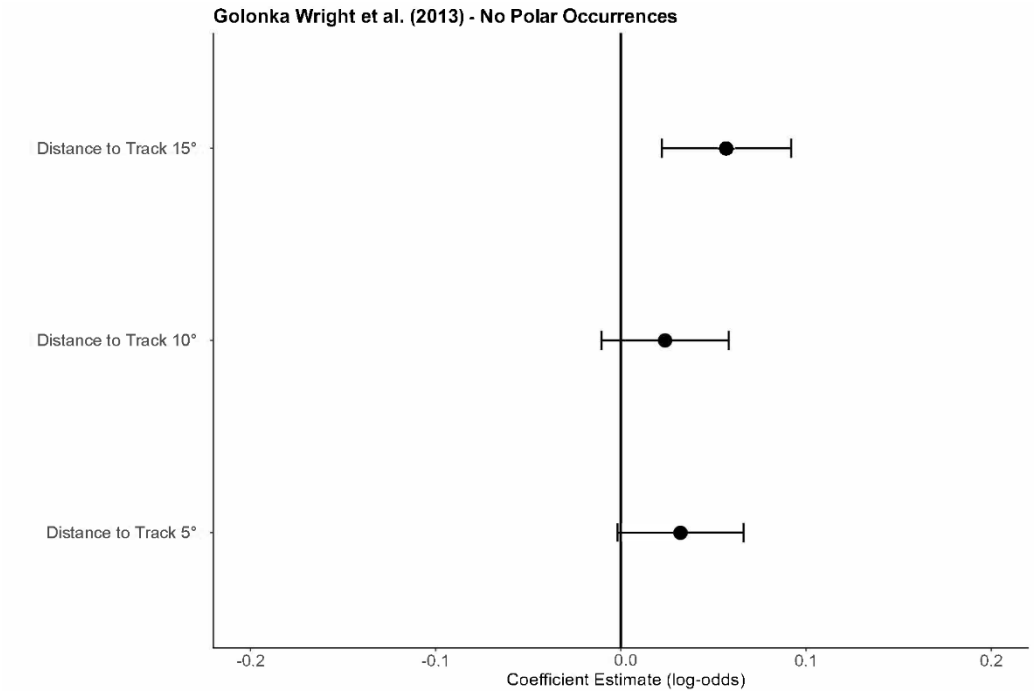

Fig. S13. Coefficient estimates (log-odds) for extinction risk associated with the coastline geometry metric for latitudinal thresholds of 5°, 10°, and 15°, using the Golonka Wright et al. (2013) paleogeographic model with polar occurrences (absolute latitude > 60) excluded. Each point represents the estimated coefficient for extinction risk associated with three different latitudinal thresholds, with horizontal lines representing 95% confidence intervals.

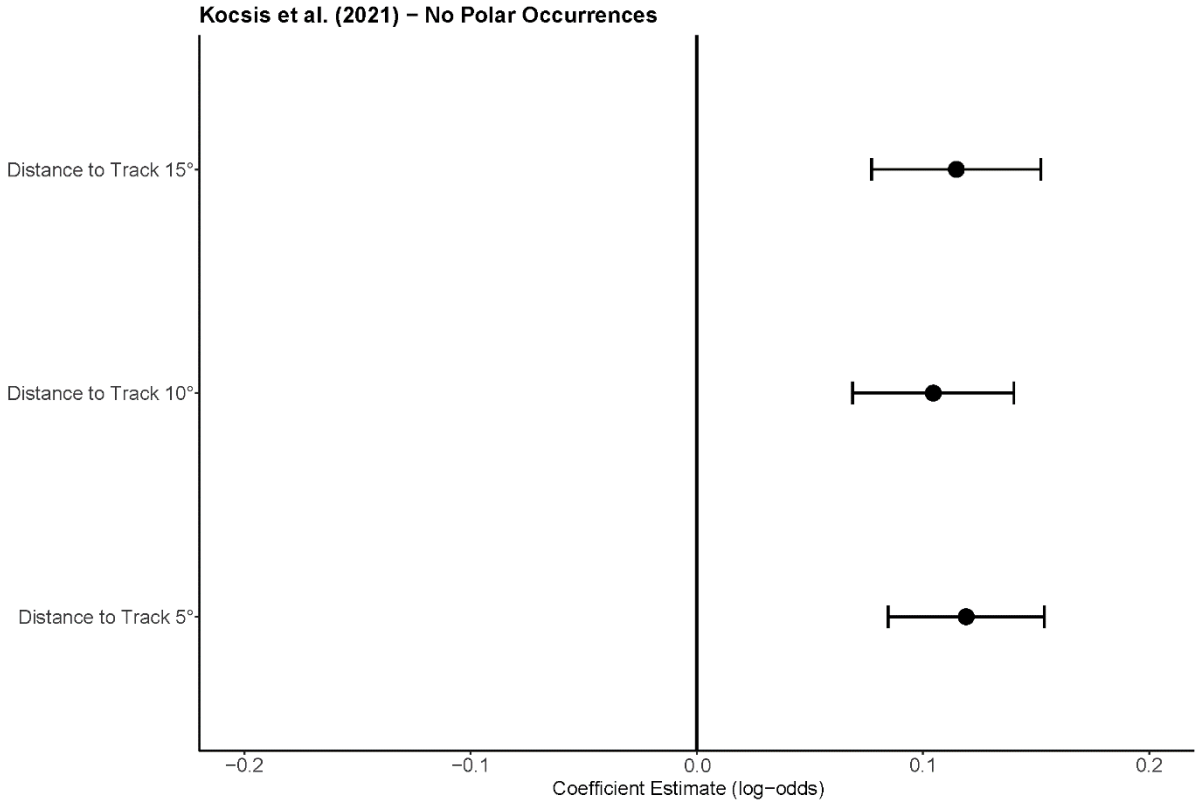

1311

1312 **Fig. S14. Coefficient estimates (log-odds) for extinction risk associated with the coastline geometry**
1313 **metric for latitudinal thresholds of 5°, 10°, and 15°, using the Kocsis et al. (2021) paleogeographic**
1314 **model with polar occurrences (absolute latitude > 60) excluded**. Each point represents the
1315 estimated coefficient for extinction risk associated with three different latitudinal thresholds, with
1316 horizontal lines representing 95% confidence intervals.

1317

1318

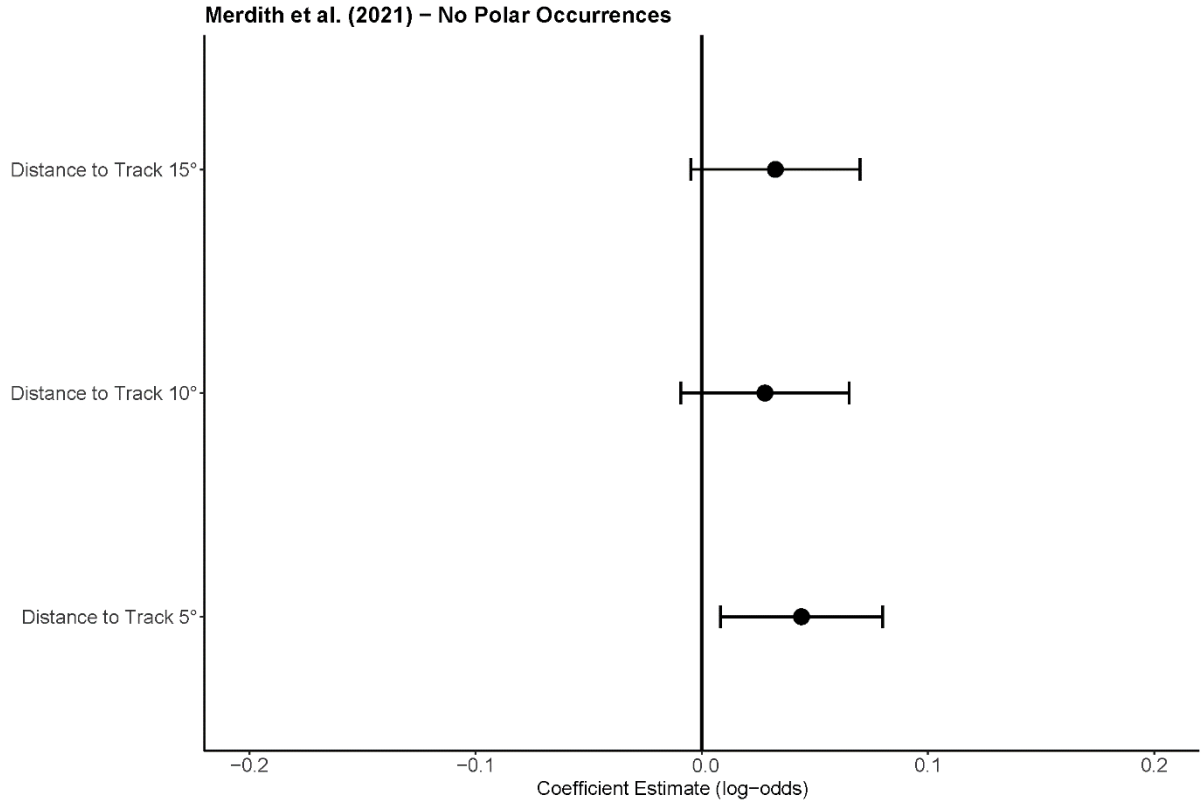

Fig. S15. Coefficient estimates (log-odds) for extinction risk associated with the coastline geometry metric for latitudinal thresholds of 5°, 10°, and 15°, using the Meredith et al. (2021) paleogeographic model with polar occurrences (absolute latitude > 60) excluded. Each point represents the estimated coefficient for extinction risk associated with three different latitudinal thresholds, with horizontal lines representing 95% confidence intervals.

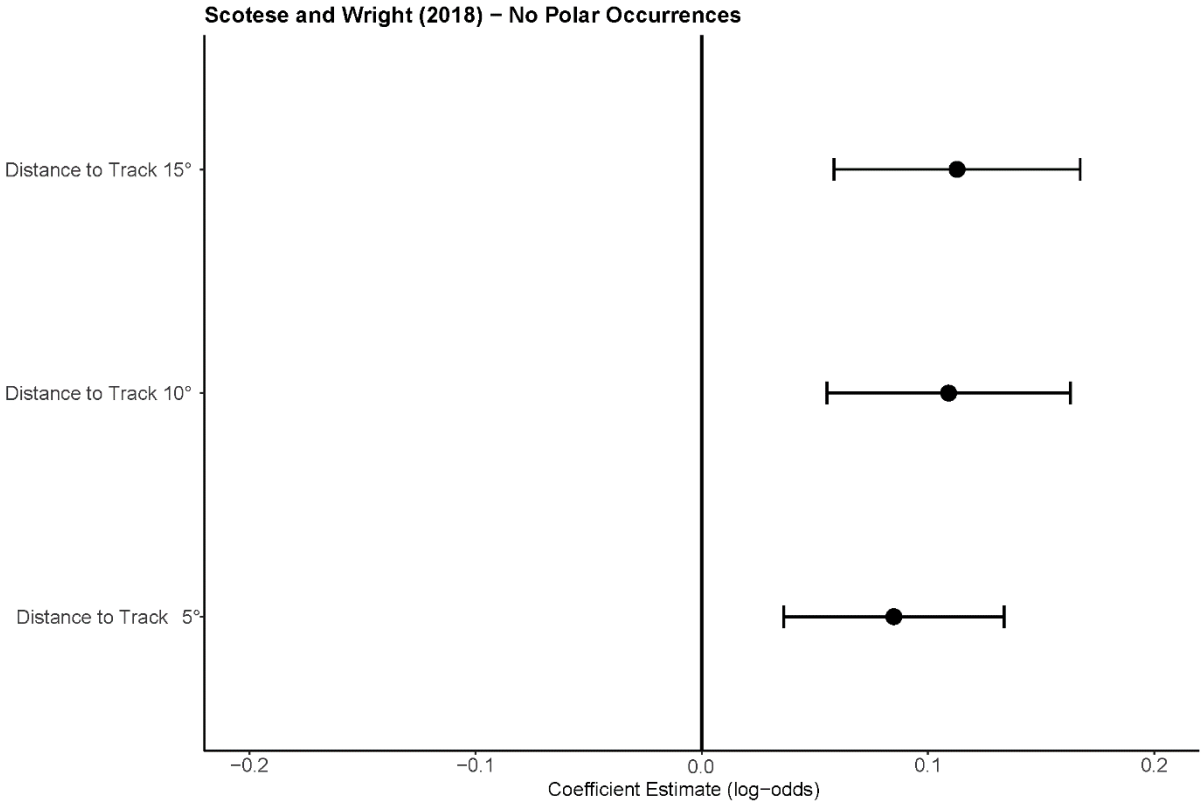

Fig. S16. Coefficient estimates (log-odds) for extinction risk associated with the coastline geometry metric for latitudinal thresholds of 5°, 10°, and 15°, using the Scotese and Wright (2018) paleogeographic model with polar occurrences (absolute latitude > 60) excluded. Each point represents the estimated coefficient for extinction risk associated with three different latitudinal thresholds, with horizontal lines representing 95% confidence intervals.

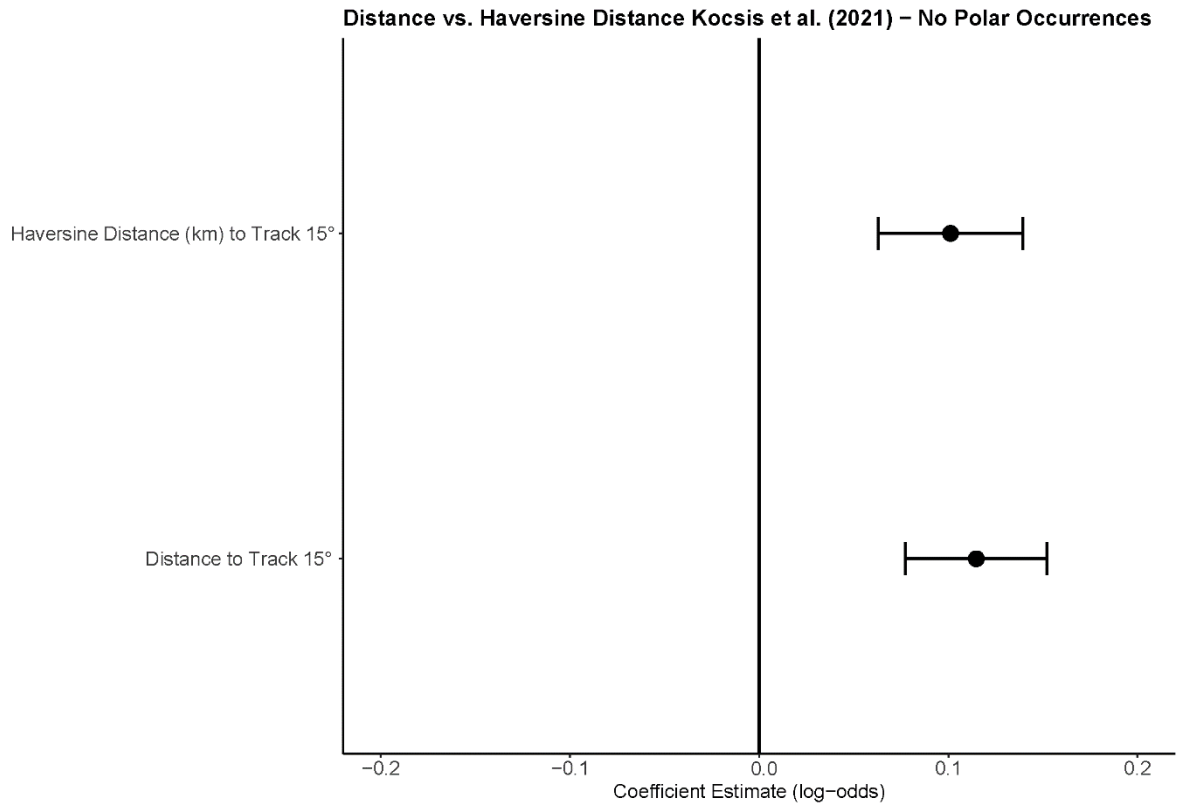

Fig. S17. Coefficient estimates (log-odds) for extinction risk associated with the coastline geometry metric for a latitudinal threshold of 15°, using the Kocsis et al. (2021) paleogeographic model, showing similarities between the steps to threshold metric and the haversine distance metric, with polar occurrences (absolute latitude > 60) excluded. Each point represents the estimated coefficient for extinction risk associated with three different latitudinal thresholds, with horizontal lines representing 95% confidence intervals.

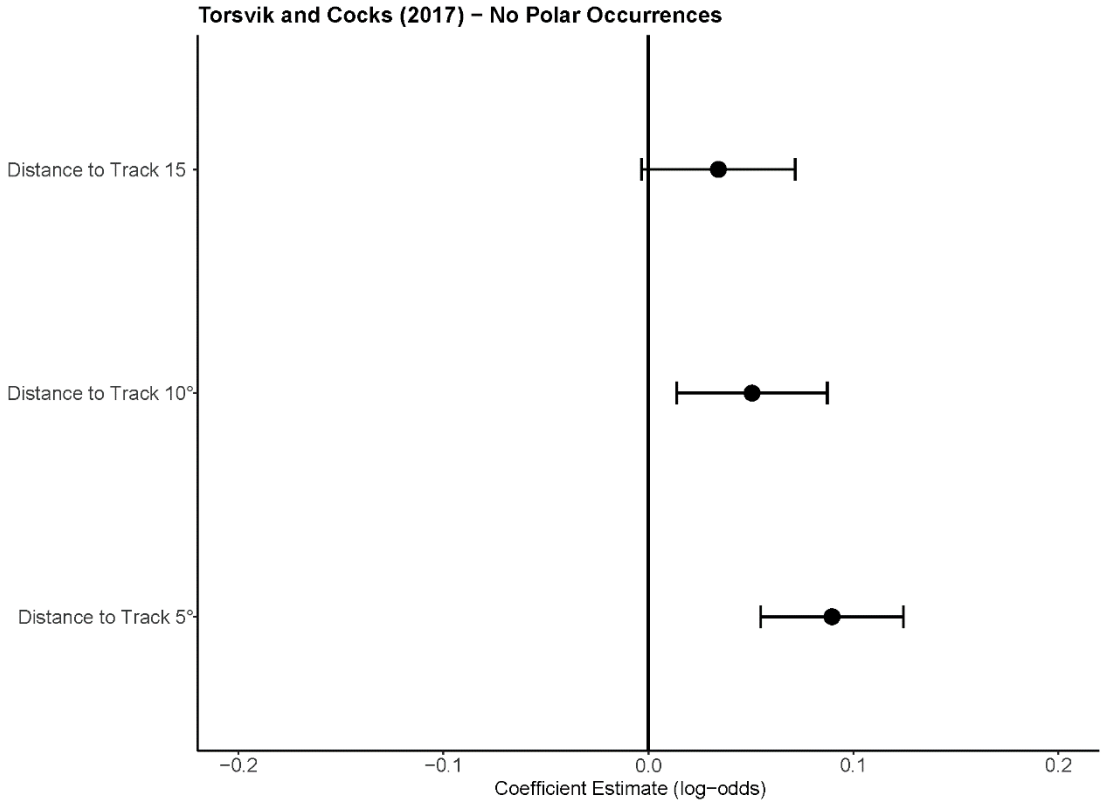

Fig. S18. Coefficient estimates (log-odds) for extinction risk associated with the coastline geometry metric for latitudinal thresholds of 5°, 10°, and 15°, using the Torsvik and Cocks (2017) paleogeographic model with polar occurrences (absolute latitude > 60) excluded. Each point represents the estimated coefficient for extinction risk associated with three different latitudinal thresholds, with horizontal lines representing 95% confidence intervals.

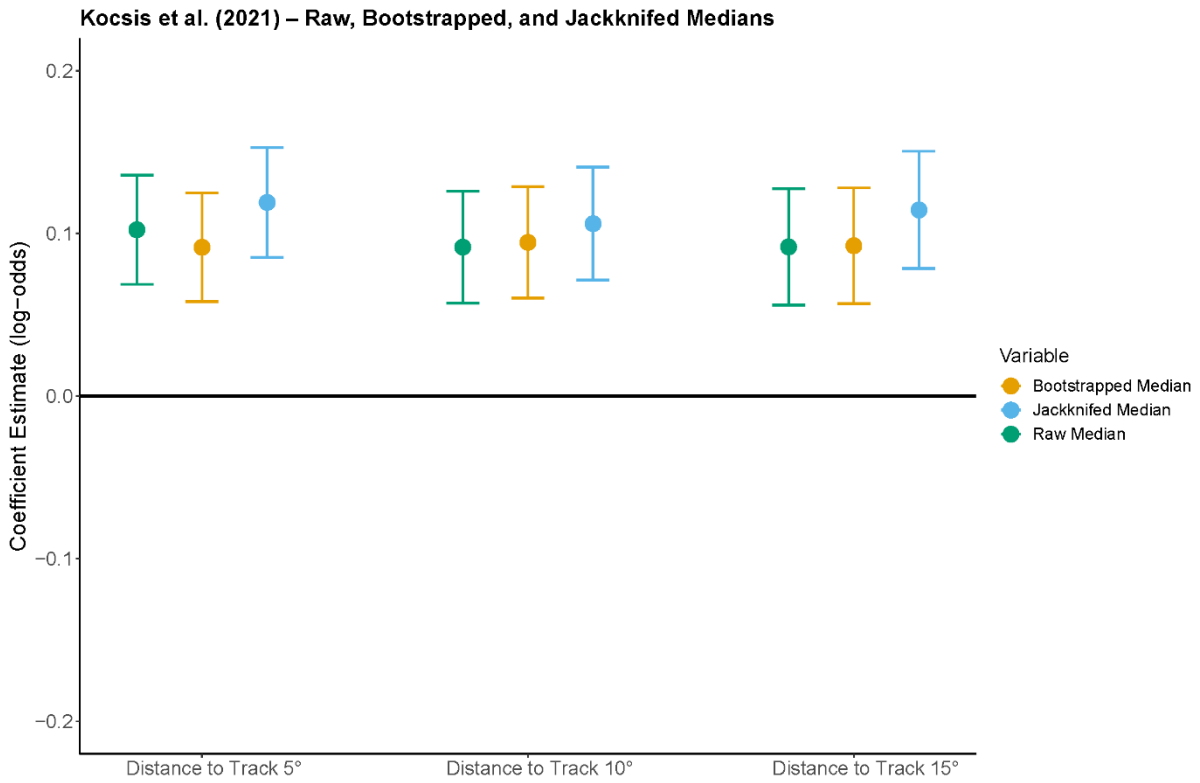

Fig. S19. Coefficient estimates (log-odds) for extinction risk associated with the coastline geometry metric for latitudinal thresholds of 5°, 10°, and 15°, using the Kocsis et al. (2021) paleogeographic model for the raw data, jackknifed subsampled median, and bootstrap subsampled median. Each point represents the estimated coefficient for extinction risk associated with three different latitudinal thresholds, with horizontal lines representing 95% confidence intervals.

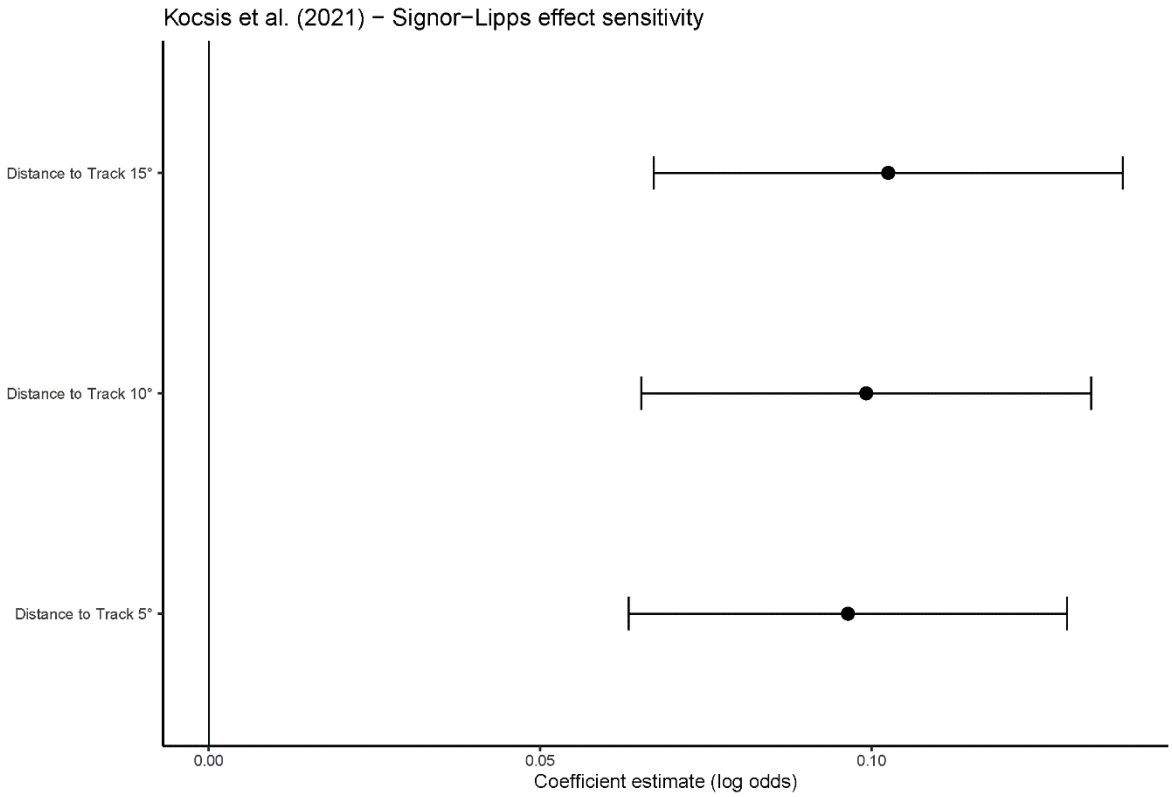

Fig. S20. Coefficient plots for the distance (grid cell steps) required to travel 5°, 10°, and 15° latitude, using the Kocsis et al. (2021) plate model, testing for sensitivity to the Signor-Lipps effect (*57*)**.** We used the approach from Reddin et al. (*7*, *43*), which implements a probabilistic response variable for extinction based on sampling completeness. Bars represent 95% confidence intervals.

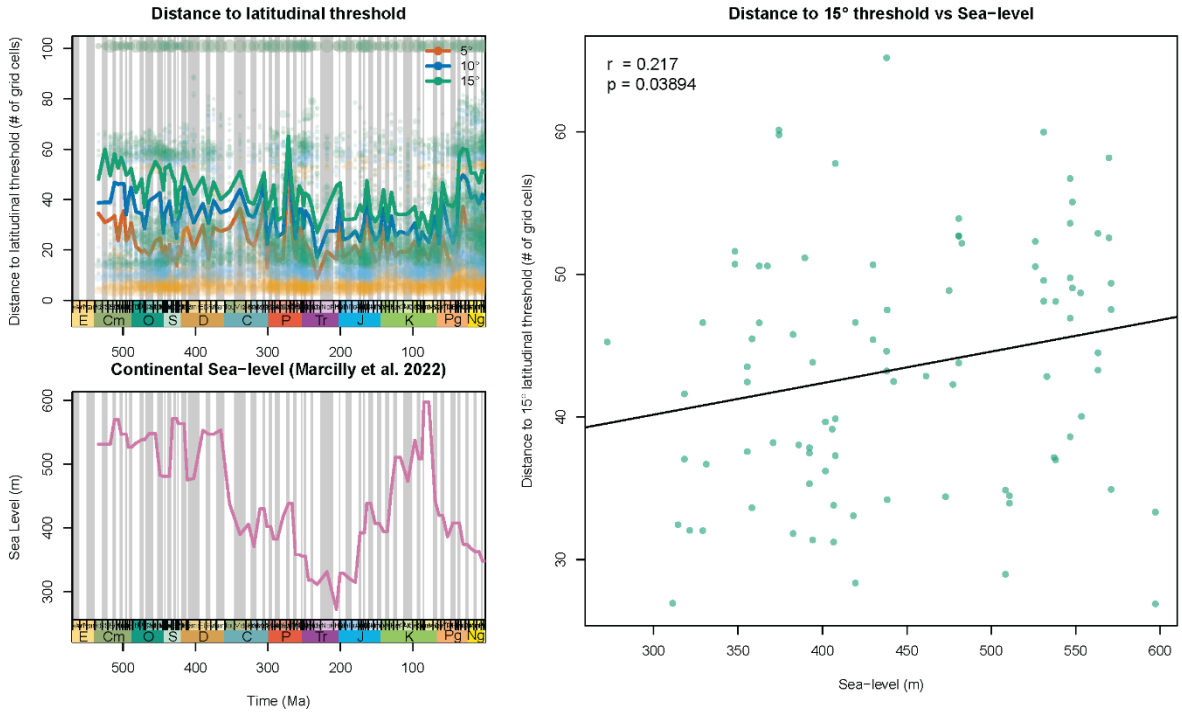

Fig. S21. Distance to track vs. sea level. The distance to track metric timeseries alongside the Phanerozoic continental sea level curve from Marcilly et al. (*45*). On the right panel is average distance to track using the 15° latitude threshold vs. sea level for each stage over the Phanerozoic. A Pearson's correlation is fitted, with *r* indicating the correlation coefficient (*rho*) and *p* denoting significance. A significant positive relationship is observed, suggesting sea level may influence the overall ability for species to track latitudinal thresholds during certain stages.

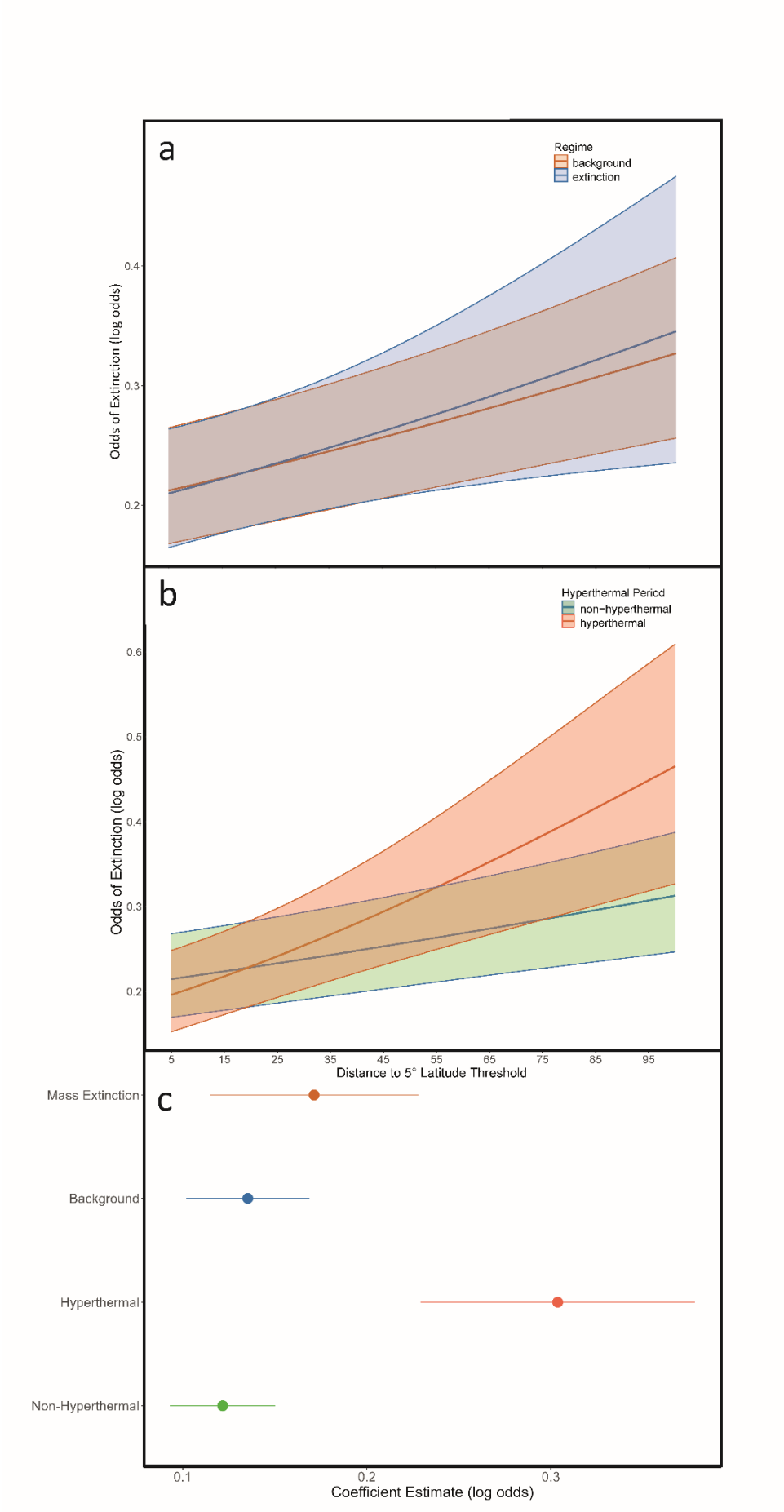
a
Regime
background
extinction
Odds of Extinction (log odds)
0.2
0.3
0.4
b
Hyperthermal Period
non−hyperthermal
hyperthermal
Odds of Extinction (log odds)
0.2
0.3
0.4
0.5
0.6
5
15
25
35
45
55
65
75
85
95
Distance to 5° Latitude Threshold
c
Mass Extinction
Background
Hyperthermal
Non-Hyperthermal
0.1
0.2
0.3
Coefficient Estimate (log odds)

1379

Fig. S22. **The relationship between coastline geometry and extinction risk across first and second order mass extinctions and hyperthermal events.** (**A**) The marginal effects for the distance (grid cell steps) to a latitudinal threshold of 5° for mass extinction versus background intervals, showing log-odds predictions with 95% confidence intervals. Mass extinctions were determined using Bond and Grasby (*51*). (**B**) The marginal effects for the distance (grid cell steps) to a latitudinal threshold of 5° for hyperthermal intervals versus non-hyperthermal intervals, showing log-odds predictions with 95% confidence intervals. (**C**) Model coefficients and 95% confidence intervals for mass extinction versus background intervals, and hyperthermal versus non-hyperthermal periods, capturing the effect of coastline geometry on extinction risk.

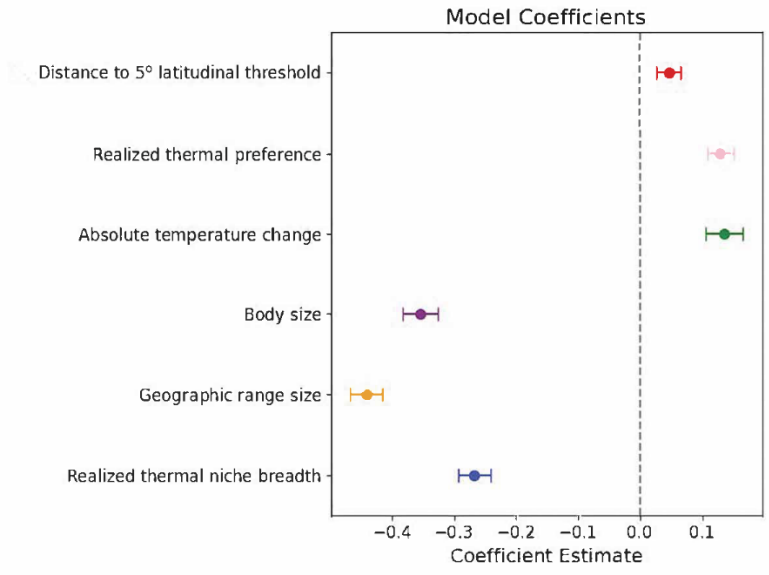

Fig. S23. Coefficient plots for the distance (grid cell steps) required to travel 5° latitude, using the Kocsis et al. (2021) plate model, compared to five other predictors from Malanoski et al. (*6*) **from the best, most saturated model shown in Table S3**. All variables are centered and standardized to facilitate the comparison of coefficients. Bars represent 95% confidence intervals.

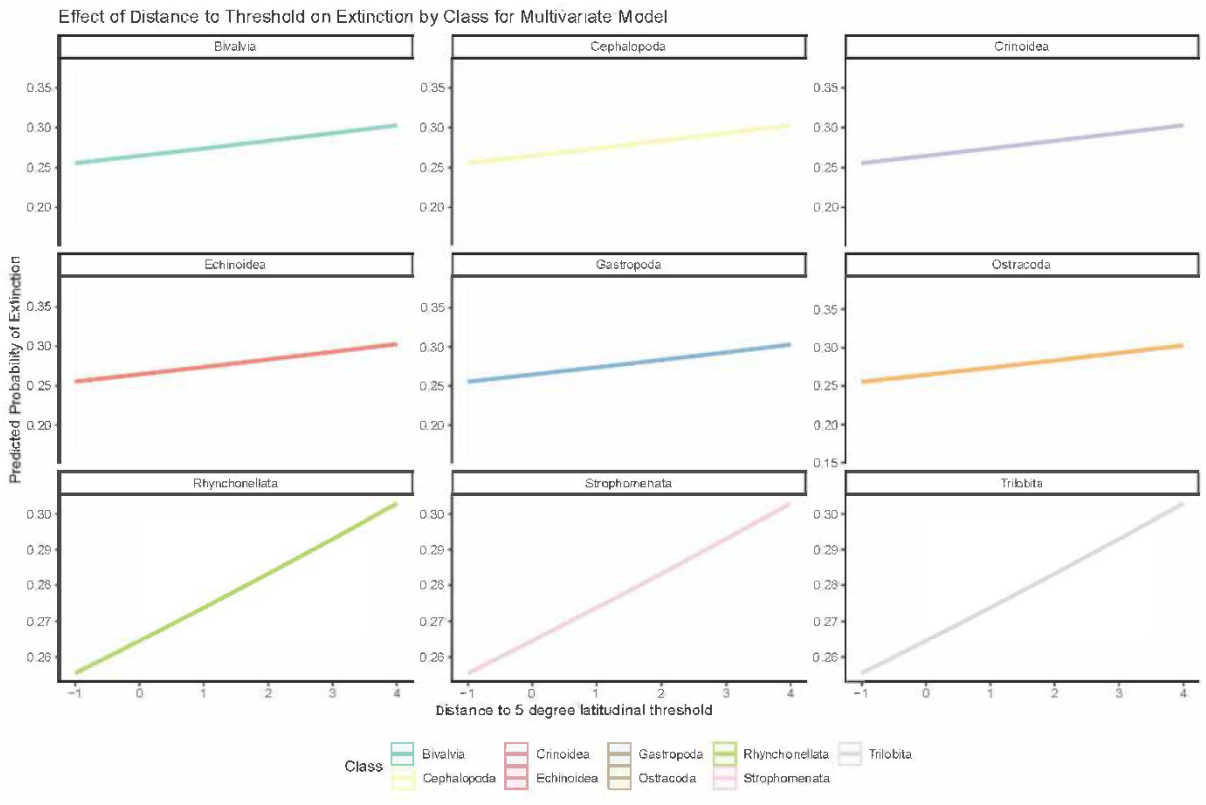

Fig. S24. Marginal effects plots for each distance (grid cell steps) of the coastline geometry metric, for different taxonomic classes. This model was generated from the saturated multivariate model for a latitudinal threshold of 5˚ using the Kocsis et al. (2021) plate model.

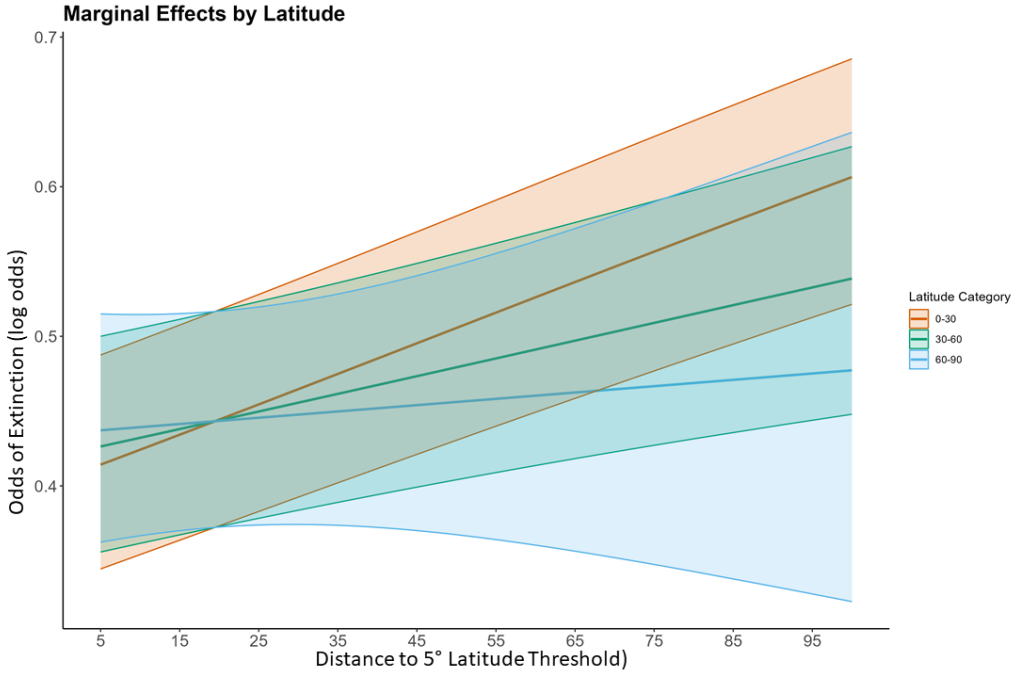

Fig. S25. Marginal effects plots for the distance (grid cell steps) required to travel 5° latitude, using the Kocsis et al. (2021) plate model, with effects shown for low latitudes (0–30°), mid latitudes (30–60°), and high latitudes (60–90°). Shaded regions represent 95% confidence intervals.

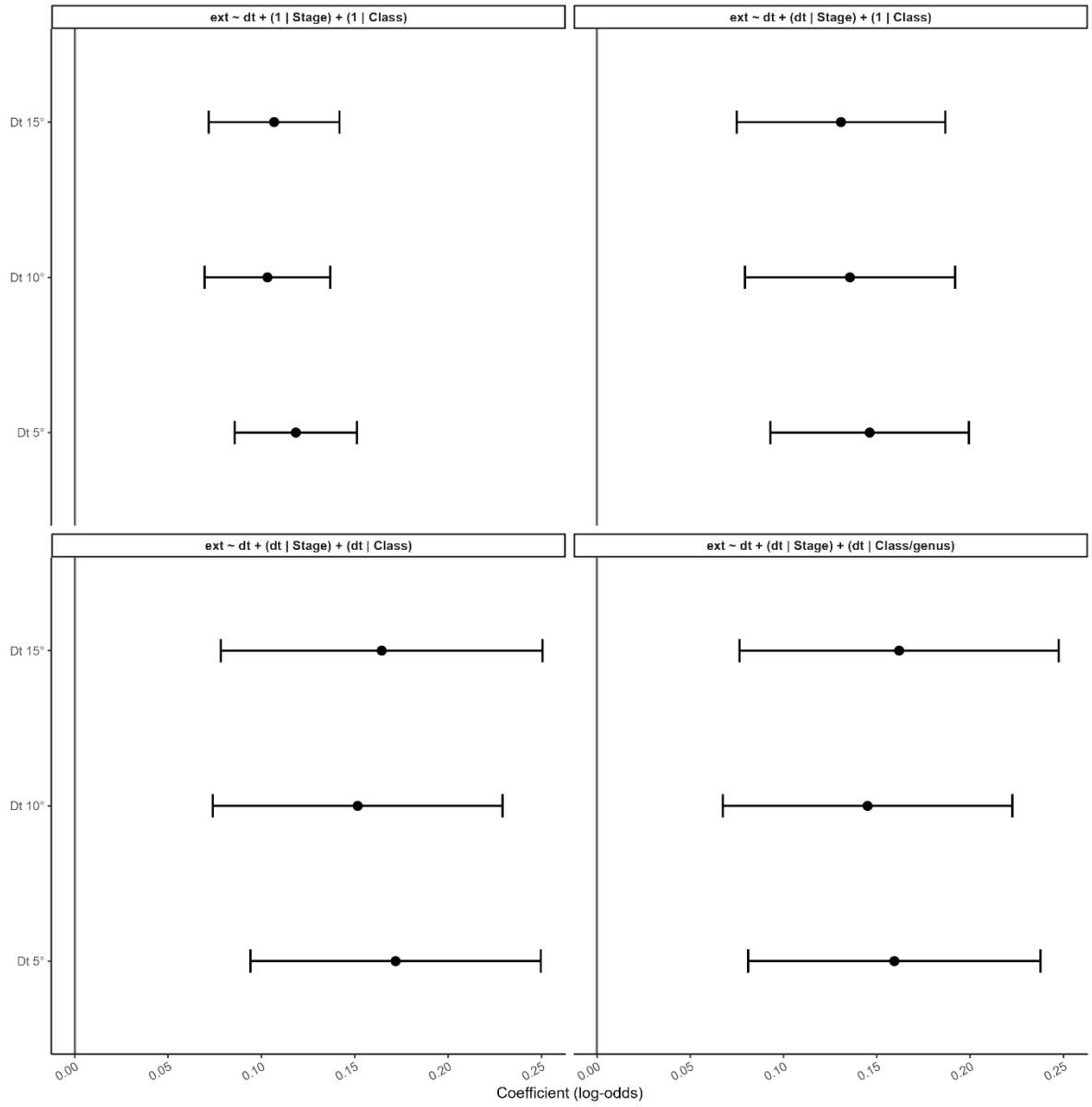

Fig. S26 Model coefficient plots for the distance (grid cell steps) required to travel 5°, 10°, and 15° latitude, using the Kocsis et al. (2021) plate model, with different random effects structures. Model equations are shown at the top of each panel, coeffients are in log odds, 95% confidence intervals are shown, and dt = distance to track.

.

System	Series	Stage	Mass extinction (Bond and Grasby, 2017)	Mass extinction (Big five)	Hyperthermals
Ediacaran	Upper Ediacaran	Avalon Assemblage	background	background	non-hyperthermal
Ediacaran	Upper Ediacaran	White Sea Assemblage	background	background	non-hyperthermal
Ediacaran	Upper Ediacaran	Nama Assemblage	background	background	non-hyperthermal
Cambrian	Terreneuvian	Fortunian	background	background	non-hyperthermal
Cambrian	Terreneuvian	Stage 2	background	background	non-hyperthermal
Cambrian	Series 2	Stage 3	background	background	non-hyperthermal
Cambrian	Series 2	Stage 4	extinction	background	non-hyperthermal
Cambrian	Maolingian	Wulian	background	background	non-hyperthermal
Cambrian	Maolingian	Drumian	background	background	non-hyperthermal
Cambrian	Maolingian	Guzhangian	extinction	background	non-hyperthermal
Cambrian	Furongian	Paibian	extinction	background	non-hyperthermal
Cambrian	Furongian	Jiangshanian	extinction	background	non-hyperthermal
Cambrian	Furongian	Stages 10	background	background	non-hyperthermal
Ordovician	Lower Ordovician	Tremadocian	background	background	non-hyperthermal
Ordovician	Lower Ordovician	Floian	background	background	non-hyperthermal
Ordovician	Middle Ordovician	Dapingian	background	background	non-hyperthermal
Ordovician	Middle Ordovician	Darriwilian	background	background	non-hyperthermal
Ordovician	Upper Ordovician	Sandbian	background	background	non-hyperthermal
Ordovician	Upper Ordovician	Katian	extinction	background	non-hyperthermal
Ordovician	Upper Ordovician	Hirnantian	extinction	extinction	non-hyperthermal
Silurian	Llandovery	Rhuddanian	extinction	background	non-hyperthermal
Silurian	Llandovery	Aeronian	background	background	non-hyperthermal
Silurian	Llandovery	Telychian	extinction	background	non-hyperthermal
Silurian	Wenlock	Sheinwoodian	extinction	background	non-hyperthermal
Silurian	Wenlock	Homerian	extinction	background	non-hyperthermal
Silurian	Ludlow	Gorstian	background	background	non-hyperthermal
Silurian	Ludlow	Ludfordian	extinction	background	non-hyperthermal
Silurian	Pridoli	Pridoli	background	background	non-hyperthermal
Devonian	Lower Devonian	Lochkovian	background	background	non-hyperthermal
Devonian	Lower Devonian	Pragian	background	background	non-hyperthermal
Devonian	Lower Devonian	Emsian	background	background	non-hyperthermal
Devonian	Middle Devonian	Eifelian	extinction	background	non-hyperthermal
Devonian	Middle Devonian	Givetian	extinction	background	non-hyperthermal
Devonian	Upper Devonian	Frasnian	extinction	extinction	non-hyperthermal
Devonian	Upper Devonian	Famennian	extinction	background	non-hyperthermal
Carboniferous	Mississippian	Tournaisian	background	background	non-hyperthermal
Carboniferous	Mississippian	Visean	background	background	non-hyperthermal
Carboniferous	Mississippian	Serpukhovian	extinction	background	non-hyperthermal
Carboniferous	Pennsylvanian	Bashkirian	background	background	non-hyperthermal
Carboniferous	Pennsylvanian	Moscovian	background	background	non-hyperthermal
Carboniferous	Pennsylvanian	Kasimovian	background	background	non-hyperthermal
Carboniferous	Pennsylvanian	Gzhelian	background	background	non-hyperthermal
Permian	Cisuralian	Asselian	background	background	non-hyperthermal
Permian	Cisuralian	Sakmarian	background	background	non-hyperthermal
Permian	Cisuralian	Artinskian	background	background	non-hyperthermal
Permian	Cisuralian	Kungurian	background	background	non-hyperthermal
Permian	Guadalupian	Roadian	background	background	non-hyperthermal
Permian	Guadalupian	Wordian	background	background	non-hyperthermal
Permian	Guadalupian	Capitanian	extinction	background	non-hyperthermal
Permian	Lopingian	Wuchiapingian	background	background	non-hyperthermal
Permian	Lopingian	Changhsingian	extinction	extinction	hyperthermal
Triassic	Lower Triassic	Induan	extinction	background	hyperthermal
Triassic	Lower Triassic	Olenekian	extinction	background	hyperthermal
Triassic	Middle Triassic	Anisian	background	background	non-hyperthermal
Triassic	Middle Triassic	Ladinian	background	background	non-hyperthermal
Triassic	Upper Triassic	Carnian	extinction	background	hyperthermal
Triassic	Upper Triassic	Norian	background	background	non-hyperthermal
Triassic	Upper Triassic	Rhaetian	extinction	extinction	hyperthermal
Jurassic	Lower Jurassic	Hettangian	extinction	background	non-hyperthermal
Jurassic	Lower Jurassic	Sinemurian	background	background	non-hyperthermal
Jurassic	Lower Jurassic	Pliensbachian	background	background	hyperthermal
Jurassic	Lower Jurassic	Toarcian	extinction	background	hyperthermal
Jurassic	Middle Jurassic	Aalenian	background	background	non-hyperthermal
Jurassic	Middle Jurassic	Bajocian	background	background	non-hyperthermal
Jurassic	Middle Jurassic	Bathonian	background	background	non-hyperthermal
Jurassic	Middle Jurassic	Callovian	background	background	non-hyperthermal

Jurassic	Upper Jurassic	Oxfordian	background	background	non-hyperthermal
Jurassic	Upper Jurassic	Kimmeridgian	background	background	non-hyperthermal
Jurassic	Upper Jurassic	Tithonian	background	background	non-hyperthermal
Cretaceous	Lower Cretaceous	Berriasian	background	background	non-hyperthermal
Cretaceous	Lower Cretaceous	Valanginian	background	background	non-hyperthermal
Cretaceous	Lower Cretaceous	Hauterivian	background	background	non-hyperthermal
Cretaceous	Lower Cretaceous	Barremian	background	background	hyperthermal
Cretaceous	Lower Cretaceous	Aptian	background	background	hyperthermal
Cretaceous	Lower Cretaceous	Albian	background	background	non-hyperthermal
Cretaceous	Upper Cretaceous	Cenomanian	background	background	hyperthermal
Cretaceous	Upper Cretaceous	Turonian	background	background	hyperthermal
Cretaceous	Upper Cretaceous	Coniacian	background	background	non-hyperthermal
Cretaceous	Upper Cretaceous	Santonian	background	background	non-hyperthermal
Cretaceous	Upper Cretaceous	Campanian	background	background	non-hyperthermal
Cretaceous	Upper Cretaceous	Maastrichtian	extinction	extinction	non-hyperthermal
Paleogene	Paleocene	Danian	extinction	background	non-hyperthermal
Paleogene	Paleocene	Selandian-Thanetian	background	background	hyperthermal
Paleogene	Eocene	Ypresian	background	background	non-hyperthermal
Paleogene	Eocene	Lutetian	background	background	non-hyperthermal
Paleogene	Eocene	Bartonian	background	background	non-hyperthermal
Paleogene	Eocene	Priabonian	background	background	non-hyperthermal
Paleogene	Oligocene	Rupelian	background	background	non-hyperthermal
Paleogene	Oligocene	Chattian	background	background	non-hyperthermal
Neogene	Miocene	Lower Miocene	background	background	non-hyperthermal
Neogene	Miocene	Middle Miocene	background	background	non-hyperthermal
Neogene	Miocene	Upper Miocene	background	background	non-hyperthermal
Neogene	Pliocene	Pliocene	background	background	non-hyperthermal
Quarternary	Pleistocene	Pleistocene	background	background	non-hyperthermal
Quarternary	Holocene	Holocene	background	background	non-hyperthermal

Table S1. Table showing mass extinction vs. background stages for the big five definition used in the main text (n=5), the Bond and Grasby (2017)(*51*) definition (n=25), and hyperthermals vs. non-hyperthermals (n=12)(*7*, *99*).

genus	phylum	class	order	family
Acanthambonia	Brachiopoda	Lingulata	Siphonotretida	Siphonotretidae
Acanthoceras	Mollusca	Cephalopoda	Ammonitida	Acanthoceratidae
Acanthodiscus	Mollusca	Cephalopoda	Ammonitida	Neocomitidae
Acanthoscaphites	Mollusca	Cephalopoda	Ammonitida	Scaphitidae
Aconeceras	Mollusca	Cephalopoda	Ammonitida	Oppeliidae
Acrioceras	Mollusca	Cephalopoda	Ammonitida	Ancyloceratidae
Acroteuthis	Mollusca	Cephalopoda	Belemnitida	Belemnitidae
Acrothele	Brachiopoda	Lingulata	Lingulida	Acrothelidae
Acrothyra	Brachiopoda	Lingulata	Acrotretida	
Acrotreta	Brachiopoda	Lingulata	Acrotretida	Acrotretidae
Actinocamax	Mollusca	Cephalopoda	Belemnitida	Belemnitellidae
Actinoceras	Mollusca	Cephalopoda	Actinocerida	Actinoceratidae
Actinosepia	Mollusca	Cephalopoda	Vampyromorphida	Actinosepiidae
Acutimitoceras	Mollusca	Cephalopoda	Goniatitida	Gattendorfiidae
Adrianites	Mollusca	Cephalopoda	Goniatitida	Adrianitidae
Agathiceras	Mollusca	Cephalopoda	Goniatitida	Agathiceratidae
Agoniatites	Mollusca	Cephalopoda	Agoniatitida	Agoniatitidae
Alligaticeras	Mollusca	Cephalopoda	Ammonitida	Perisphinctidae
Allocrioceras	Mollusca	Cephalopoda	Ammonitida	Anisoceratidae
Allumettoceras	Mollusca	Cephalopoda	Orthocerida	Tripteroceratidae
Almites	Mollusca	Cephalopoda	Goniatitida	Marathonitidae
Alocolytoceras	Mollusca	Cephalopoda	Ammonitida	Lytoceratidae
Altudoceras	Mollusca	Cephalopoda	Goniatitida	Paragastrioceratidae
Amapondella	Mollusca	Cephalopoda	Ammonitida	Nostoceratidae
Ambites	Mollusca	Cephalopoda	Ceratitida	Gyronitidae
Ammonellipsites	Mollusca	Cephalopoda	Goniatitida	Pericyclidae
Amoeboceras	Mollusca	Cephalopoda	Ammonitida	Cardioceratidae
Amphicyrtoceras	Mollusca	Cephalopoda	Oncocerida	Acleistoceratidae
Amuletum	Mollusca	Gastropoda	Neogastropoda	Turridae
Anagaudryceras	Mollusca	Cephalopoda	Ammonitida	Tetragonitidae
Anahamulina	Mollusca	Cephalopoda	Ammonoidea	Hamulinidae
Anarcestes	Mollusca	Cephalopoda	Agoniatitida	Anarcestidae
Anaspyroceras	Mollusca	Cephalopoda	Orthocerida	Dawsonoceratidae
Ancistroceras	Mollusca	Cephalopoda	Lituitida	Lituitidae
Ancyloceras	Mollusca	Cephalopoda	Ammonitida	Ancyloceratidae
Anglonautilus	Mollusca	Cephalopoda	Nautilida	Nautilidae
Angulaticeras	Mollusca	Cephalopoda	Ammonitida	Schlotheimiidae
Angulithes	Mollusca	Cephalopoda	Nautilida	Nautilidae
Anisoceras	Mollusca	Cephalopoda	Ammonitida	Anisoceratidae
Anolcites	Mollusca	Cephalopoda	Ceratitida	Trachyceratidae
Anoploceras	Mollusca	Cephalopoda	Nautilida	Tainoceratidae
Aphetoceras	Mollusca	Cephalopoda	Tarphycerida	Estonioceratidae
Aplococeras	Mollusca	Cephalopoda	Ceratitida	Aplococeratidae
Arcestes	Mollusca	Cephalopoda	Ceratitida	Arcestidae
Arcticoceras	Mollusca	Cephalopoda	Ammonitida	Cardioceratidae
Arctogymnites	Mollusca	Cephalopoda	Ceratitida	Ceratitidae
Arctoptychites	Mollusca	Cephalopoda	Ceratitida	Ptychitidae
Argonauticeras	Mollusca	Cephalopoda	Ammonitida	Tetragonitidae
Arietites	Mollusca	Cephalopoda	Ammonitida	Arietitidae
Armenoceras	Mollusca	Cephalopoda	Actinocerida	Armenoceratidae
Arpadites	Mollusca	Cephalopoda	Ceratitida	Trachyceratidae
Arrhoges	Mollusca	Gastropoda	Sorbeoconcha	Aporrhaidae
Artinskia	Mollusca	Cephalopoda	Prolecanitida	Medlicottiidae
Asklepioceras	Mollusca	Cephalopoda	Ceratitida	Trachyceratidae
Aspidoceras	Mollusca	Cephalopoda	Ammonitida	Aspidoceratidae
Atractites	Mollusca	Cephalopoda	Aulacoceratida	Xiphoteuthididae
Aturia	Mollusca	Cephalopoda	Nautilida	Aturiidae
Aturoidea	Mollusca	Cephalopoda	Nautilida	Hercoglossidae
Axonoceras	Mollusca	Cephalopoda	Ammonitida	Nostoceratidae
Bactrites	Mollusca	Cephalopoda	Bactritida	Bactritidae
Bactroceras	Mollusca	Cephalopoda	Orthocerida	Baltoceratidae
Baculites	Mollusca	Cephalopoda	Ammonitida	Baculitidae
Badouxia	Mollusca	Cephalopoda	Ammonitida	Psiloceratidae
Bamyaniceras	Mollusca	Cephalopoda	Prolecanitida	Medlicottiidae
Barremites	Mollusca	Cephalopoda	Ammonitida	Desmoceratidae
Barroisiceras (Barroisiceras)	Mollusca	Cephalopoda	Ammonitida	Collignoniceratidae
Bassleroceras	Mollusca	Cephalopoda	Ellesmerocerida	Ellesmeroceratidae
Bathmoceras	Mollusca	Cephalopoda	Ellesmerocerida	Bathmoceratidae
Belemnitella	Mollusca	Cephalopoda	Belemnitida	Belemnitellidae

Belemnites	Mollusca	Cephalopoda	Belemnitida	Belemnitidae
Belemnites (Hibolites)	Mollusca	Cephalopoda	Belemnitida	Belemnitidae
Belemnopsis	Mollusca	Cephalopoda	Belemnitida	Belemnopseidae
Beloitoceras	Mollusca	Cephalopoda	Oncocerida	Oncoceratidae
Belosaepia	Mollusca	Cephalopoda		
Berriasella	Mollusca	Cephalopoda	Ammonitida	Neocomitidae
Biarmiceras	Mollusca	Cephalopoda	Goniatitida	Mongoloceratidae
Biernatia	Brachiopoda	Lingulata	Acrotretida	Biernatidae
Billingsites	Mollusca	Cephalopoda	Ascocerida	Ascoceratidae
Billingsites	Mollusca	Cephalopoda	Ceratitida	Ceratitidae
Bisatoceras	Mollusca	Cephalopoda	Goniatitida	Bisatoceratidae
Bochianites	Mollusca	Cephalopoda	Ammonoidea	Bochianitidae
Boesites	Mollusca	Cephalopoda	Prolecanitida	Daraelitidae
Borissjakoceras	Mollusca	Cephalopoda	Ammonitida	Binneyitidae
Bostrychoceras	Mollusca	Cephalopoda	Ammonitida	Nostoceratidae
Botsfordia	Brachiopoda	Lingulata	Lingulida	Botsfordiidae
Bradfordia	Mollusca	Cephalopoda	Ammonitida	Oppeliidae
Bransonoceras	Mollusca	Cephalopoda	Goniatitida	Metalegoceratidae
Bredyia	Mollusca	Cephalopoda	Ammonitida	Hammatoceratidae
Brightia	Mollusca	Cephalopoda	Ammonitida	Oppeliidae
Broeggeria	Brachiopoda	Lingulata	Lingulida	Elkaniidae
Cadomites	Mollusca	Cephalopoda	Ammonitida	Stephanoceratidae
Cadomites (Cadomites)	Mollusca	Cephalopoda	Ammonitida	Stephanoceratidae
Calliphylloceras	Mollusca	Cephalopoda	Phylloceratida	Phylloceratidae
Cameroceras	Mollusca	Cephalopoda	Endocerida	Endoceratidae
Campbelloceras	Mollusca	Cephalopoda	Tarphycerida	Tarphyceratidae
Canadoceras	Mollusca	Cephalopoda	Ammonitida	Pachydiscidae
Canavaria	Mollusca	Cephalopoda	Ammonitida	Hildoceratidae
Cardiella	Mollusca	Cephalopoda	Goniatitida	Marathonitidae
Caveola	Mollusca	Gastropoda	Neogastropoda	Cancellariidae
Celtites	Mollusca	Cephalopoda	Ceratitida	Danubitidae
Cenoceras	Mollusca	Cephalopoda	Nautilida	Cenoceratidae
Centrocyrtoceras	Mollusca	Cephalopoda	Barrandeocerida	Barrandeoceratidae
Ceratites	Mollusca	Cephalopoda	Ceratitida	Ceratitidae
Ceratreta	Brachiopoda	Lingulata	Acrotretida	Ceratretidae
Cerithium	Mollusca	Gastropoda	Sorbeoconcha	Cerithiidae
Chieseiceras	Mollusca	Cephalopoda	Ceratitida	Ceratitidae
Chisiloceras	Mollusca	Cephalopoda	Endocerida	Endoceratidae
Choffatia	Mollusca	Cephalopoda	Ammonitida	Perisphinctidae
Choristoceras	Mollusca	Cephalopoda	Ceratitida	Choristoceratidae
Cibolites	Mollusca	Cephalopoda	Ceratitida	Paraceltitidae
Cimomia	Mollusca	Cephalopoda	Nautilida	Hercoglossidae
Cladiscites	Mollusca	Cephalopoda	Ceratitida	Cladiscitidae
Clionitites	Mollusca	Cephalopoda	Ceratitida	Clionitidae
Clioscaphites	Mollusca	Cephalopoda	Ammonitida	Scaphitidae
Clitendoceras	Mollusca	Cephalopoda	Endocerida	Proterocameroceratidae
Cochlioceras	Mollusca	Cephalopoda	Orthocerida	Baltoceratidae
Coeloceras	Mollusca	Cephalopoda	Ammonitida	Coeloceratidae
Coilopoceras	Mollusca	Cephalopoda	Ammonitida	Coilopoceratidae
Collina	Mollusca	Cephalopoda	Ammonitida	Dactylioceratidae
Conotreta	Brachiopoda	Lingulata	Acrotretida	Acrotretidae
Craspedites	Mollusca	Cephalopoda	Ammonitida	Polyptychitidae
Creniceras	Mollusca	Cephalopoda	Ammonitida	Oppeliidae
Crimites	Mollusca	Cephalopoda	Goniatitida	Adrianitidae
Crioceratites	Mollusca	Cephalopoda	Ammonitida	Crioceratitidae
Crioceratites (Emericiceras)	Mollusca	Cephalopoda	Ammonitida	Crioceratitidae
Crispoceras	Mollusca	Cephalopoda	Agoniatitida	Werneroceratidae
Curtoceras	Mollusca	Cephalopoda	Tarphycerida	Trocholitidae
Cyclendoceras	Mollusca	Cephalopoda	Endocerida	Endoceratidae
Cycloceras	Mollusca	Cephalopoda	Orthocerida	
Cyclolobus	Mollusca	Cephalopoda	Goniatitida	Cyclolobidae
Cyclostomiceras	Mollusca	Cephalopoda	NO_ORDER_SPECIFIED	Cyclostomiceratidae
Cylindroteuthis	Mollusca	Cephalopoda	Belemnitida	Belemnitidae
Cymatoceras	Mollusca	Cephalopoda	Nautilida	Nautilidae
Cymbites	Mollusca	Cephalopoda	Ammonitida	Cymbitidae
Cyrtoceras	Mollusca	Cephalopoda		
Cyrtocerina	Mollusca	Cephalopoda	Cyrtocerinida	Cyrtocerinidae
Cyrtonotreta	Brachiopoda	Lingulata	Acrotretida	Acrotretidae
Dactylioceras	Mollusca	Cephalopoda	Ammonitida	Dactylioceratidae
Damesites	Mollusca	Cephalopoda	Ammonitida	Desmoceratidae

Danubites	Mollusca	Cephalopoda	Ceratitida	Danubitidae
Daraelites	Mollusca	Cephalopoda	Prolecanitida	Daraelitidae
Dawsonoceras	Mollusca	Cephalopoda	Orthocerida	Dawsonoceratidae
Daxatina	Mollusca	Cephalopoda	Ceratitida	Trachyceratidae
Deltoidonautilus	Mollusca	Cephalopoda	Nautilida	Hercoglossidae
Desmoceras	Mollusca	Cephalopoda	Ammonitida	Desmoceratidae
Desmoceras (Desmoceras)	Mollusca	Cephalopoda	Ammonitida	Desmoceratidae
Desmoceras (Pseudouhligella)	Mollusca	Cephalopoda	Ammonitida	Desmoceratidae
Desmophyllites	Mollusca	Cephalopoda	Ammonitida	Desmoceratidae
Diandongia	Brachiopoda	Lingulata	Lingulida	Botsfordiidae
Dicellomus	Brachiopoda	Lingulata	Lingulida	Obolidae
Dictyoconites	Mollusca	Cephalopoda	Aulacocerida	Aulacoceratidae
Dideroceras	Mollusca	Cephalopoda	Endocerida	Endoceratidae
Didymoceras	Mollusca	Cephalopoda	Ammonitida	Nostoceratidae
Diestoceras	Mollusca	Cephalopoda	Oncocerida	Diestoceratidae
Dimitobelus	Mollusca	Cephalopoda	Belemnitida	Dimitobelidae
Dimitobelus (Dimitobelus)	Mollusca	Cephalopoda	Belemnitida	Dimitobelidae
Dimorphoceras	Mollusca	Cephalopoda	Goniatitida	Dimorphoceratidae
Diplomoceras	Mollusca	Cephalopoda	Ammonitida	Diplomoceratidae
Discinisca	Brachiopoda	Lingulata	Discinida	Discinidae
Discoceras	Mollusca	Cephalopoda	Tarphycerida	Trocholitidae
Discophyllites	Mollusca	Cephalopoda	Phylloceratida	Discophyllitidae
Discoscaphites	Mollusca	Cephalopoda	Ammonitida	Scaphitidae
Discosorus	Mollusca	Cephalopoda	Discosorida	Discosoridae
Dolorthoceras	Mollusca	Cephalopoda	Pseudorthocerida	Pseudorthoceratidae
Domatoceras	Mollusca	Cephalopoda	Nautilida	Grypoceratidae
Dombarites	Mollusca	Cephalopoda	Goniatitida	Delepinoceratidae
Douvilleiceras	Mollusca	Cephalopoda	Ammonitida	Douvilleiceratidae
Drepanochilus	Mollusca	Gastropoda	Sorbeoconcha	Aporrhaidae
Drilluta	Mollusca	Gastropoda	Neogastropoda	Fasciolariidae
Duvalia	Mollusca	Cephalopoda	Belemnitida	Duvaliidae
Ectenoglossa	Brachiopoda	Lingulata	Lingulida	Obolidae
Eleniceras	Mollusca	Cephalopoda	Ammonitida	Neocomitidae
Elliptoglossa	Brachiopoda	Lingulata	Lingulida	Obolidae
Emilites	Mollusca	Cephalopoda	Goniatitida	Adrianitidae
Endoceras	Mollusca	Cephalopoda	Endocerida	Endoceratidae
Engonoceras	Mollusca	Cephalopoda	Ammonitida	Engonoceratidae
Eoasianites	Mollusca	Cephalopoda	Goniatitida	Neoicoceratidae
Eoconulus	Brachiopoda	Lingulata	Acrotretida	Eoconulidae
Eoderoceras	Mollusca	Cephalopoda	Ammonitida	Eoderoceratidae
Eogaudryceras	Mollusca	Cephalopoda	Ammonitida	Tetragonitidae
Eogaudryceras (Eotetragonites)	Mollusca	Cephalopoda	Ammonitida	Tetragonitidae
Eogunnarites	Mollusca	Cephalopoda	Ammonitida	Kossmaticeratidae
Eoobolus	Brachiopoda	Lingulata	Lingulida	Eoobolidae
Eophyllites	Mollusca	Cephalopoda	Phylloceratida	Palaeophyllitidae
Eoprotrachyceras	Mollusca	Cephalopoda	Ceratitida	Trachyceratidae
Eosiphonotreta	Brachiopoda	Lingulata	Siphonotretida	Siphonotretidae
Eosomichelinoceras	Mollusca	Cephalopoda	Orthocerida	Baltoceratidae
Eothele	Brachiopoda	Lingulata	Lingulida	Acrothelidae
Eothinites	Mollusca	Cephalopoda	Goniatitida	Metalegoceratidae
Ephippelasma	Brachiopoda	Lingulata	Acrotretida	Ephippelasmatidae
Ephippioceras	Mollusca	Cephalopoda	Nautilida	Ephippioceratidae
Ephippiorthoceras	Mollusca	Cephalopoda	Orthocerida	Proteoceratidae
Epicanites	Mollusca	Cephalopoda	Prolecanitida	Daraelitidae
Epigymnites	Mollusca	Cephalopoda	Ceratitida	Gymnitidae
Epistroboceras	Mollusca	Cephalopoda	Nautilida	Trigonoceratidae
Erycites	Mollusca	Cephalopoda	Ammonitida	Hammatoceratidae
Euaptetoceras	Mollusca	Cephalopoda	Ammonitida	Hammatoceratidae
Euaspidoceras	Mollusca	Cephalopoda	Ammonitida	Aspidoceratidae
Eubostrychoceras	Mollusca	Cephalopoda	Ammonitida	Nostoceratidae
Euciphoceras	Mollusca	Cephalopoda	Nautilida	Nautilidae
Eucymatoceras	Mollusca	Cephalopoda	Nautilida	Nautilidae
Eulima	Mollusca	Gastropoda	Sorbeoconcha	Eulimidae
Eulophoceras	Mollusca	Cephalopoda	Ammonitida	Sphenodiscidae
Eumedlicottia	Mollusca	Cephalopoda	Prolecanitida	Medlicottiidae
Eumorphoceras	Mollusca	Cephalopoda	Goniatitida	Girtyoceratidae
Euomphaloceras	Mollusca	Cephalopoda	Ammonitida	Acanthoceratidae
Eupachydiscus	Mollusca	Cephalopoda	Ammonitida	Pachydiscidae

Euphylloceras	Mollusca	Cephalopoda	Phylloceratida	Phylloceratidae
Euspira	Mollusca	Gastropoda	Sorbeoconcha	Naticidae
Eutrephoceras	Mollusca	Cephalopoda	Nautilida	Nautilidae
Eutrephoceras (Simplicioceras)	Mollusca	Cephalopoda	Nautilida	Nautilidae
Exiteloceras	Mollusca	Cephalopoda	Ammonitida	Nostoceratidae
Fagesia	Mollusca	Cephalopoda	Ammonitida	Vascoceratidae
Fauriella	Mollusca	Cephalopoda	Ammonitida	Neocomitidae
Ficheuria	Mollusca	Cephalopoda	Ammonitida	Flickiidae
Flexoptychites	Mollusca	Cephalopoda	Ceratitida	Ptychitidae
Fontanelliceras	Mollusca	Cephalopoda	Ammonitida	Hildoceratidae
Fontannesia	Mollusca	Cephalopoda	Ammonitida	Sonniniidae
Foordiceras	Mollusca	Cephalopoda	Nautilida	Tainoceratidae
Frankites	Mollusca	Cephalopoda	Ceratitida	Trachyceratidae
Fresvillia	Mollusca	Cephalopoda	Ammonitida	Baculitidae
Gastrioceras	Mollusca	Cephalopoda	Goniatitida	Gastrioceratidae
Gaudryceras	Mollusca	Cephalopoda	Ammonitida	Tetragonitidae
Gaudryceras (Gaudryceras)	Mollusca	Cephalopoda	Ammonitida	Tetragonitidae
Geisonoceras	Mollusca	Cephalopoda	Dissidocerida	Geisonoceratidae
Gemmellaroceras	Mollusca	Cephalopoda	Ammonitida	Polymorphitidae
Germanonautilus	Mollusca	Cephalopoda	Nautilida	Tainoceratidae
Girtyoceras	Mollusca	Cephalopoda	Goniatitida	Girtyoceratidae
Glaphyrites	Mollusca	Cephalopoda	Goniatitida	Glaphyritidae
Gleviceras	Mollusca	Cephalopoda	Ammonitida	Oxynoticeratidae
Glochiceras	Mollusca	Cephalopoda	Ammonitida	Oppeliidae
Glochiceras (Glochiceras)	Mollusca	Cephalopoda	Ammonitida	Oppeliidae
Glossella	Brachiopoda	Lingulata	Lingulida	Obolidae
Glottidia	Brachiopoda	Lingulata	Lingulida	Lingulidae
Glyphiolobus	Mollusca	Cephalopoda	Goniatitida	Dimorphoceratidae
Glyphiteuthis	Mollusca	Cephalopoda	Octopoda	Trachyteuthididae
Glyptophiceras	Mollusca	Cephalopoda	Ceratitida	Xenoceltitidae
Glyptoxoceras	Mollusca	Cephalopoda	Ammonitida	Diplomoceratidae
Gonioceras	Mollusca	Cephalopoda	Actinocerida	Gonioceratidae
Gonioloboceras	Mollusca	Cephalopoda	Goniatitida	Gonioloboceratidae
Gonionotites	Mollusca	Cephalopoda	Ceratitida	Juvavitidae
Gorbyoceras	Mollusca	Cephalopoda	Orthocerida	Proteoceratidae
Graciliala	Mollusca	Gastropoda	Sorbeoconcha	Aporrhaidae
Grammoceras	Mollusca	Cephalopoda	Ammonitida	Hildoceratidae
Graphoceras	Mollusca	Cephalopoda	Ammonitida	Graphoceratidae
Griesbachites	Mollusca	Cephalopoda	Ceratitida	Juvavitidae
Grypoceras	Mollusca	Cephalopoda	Nautilida	Grypoceratidae
Gryponautilus	Mollusca	Cephalopoda	Nautilida	Grypoceratidae
Gunnarites	Mollusca	Cephalopoda	Ammonitida	Kossmaticeratidae
Gymnites	Mollusca	Cephalopoda	Ceratitida	Gymnitidae
Gymnotoceras	Mollusca	Cephalopoda	Ceratitida	Ceratitidae
Gyrodes	Mollusca	Gastropoda	Sorbeoconcha	Naticidae
Gyronites	Mollusca	Cephalopoda	Ceratitida	Gyronitidae
Gyrophiceras	Mollusca	Cephalopoda	Ceratitida	Gyronitidae
Gzheloceras	Mollusca	Cephalopoda	Nautilida	Gzheloceratidae
Hadrotreta	Brachiopoda	Lingulata	Acrotretida	
Hamites	Mollusca	Cephalopoda	Ammonitida	Hamitidae
Hammatoceras	Mollusca	Cephalopoda	Ammonitida	Hammatoceratidae
Hamulinites	Mollusca	Cephalopoda	Ammonitida	Leptoceratoididae
Hantkeniceras	Mollusca	Cephalopoda	Phylloceratida	Phylloceratidae
Haploceras	Mollusca	Cephalopoda	Ammonitida	Haploceratidae
Hauericeras	Mollusca	Cephalopoda	Ammonitida	Desmoceratidae
Hauericeras (Gardeniceras)	Mollusca	Cephalopoda	Ammonitida	Desmoceratidae
Haustator	Mollusca	Gastropoda	Sorbeoconcha	Turritellidae
Hecticoceras	Mollusca	Cephalopoda	Ammonitida	Oppeliidae
Hemiliroceras	Mollusca	Cephalopoda	Nautilida	Liroceratidae
Heminautilus	Mollusca	Cephalopoda	Nautilida	Cenoceratidae
Hemitissotia	Mollusca	Cephalopoda	Ammonitida	Vascoceratidae
Hercoglossa	Mollusca	Cephalopoda	Nautilida	Hercoglossidae
Hibolithes	Mollusca	Cephalopoda	Belemnitida	Mesohibolitidae
Hisingerella	Brachiopoda	Lingulata	Acrotretida	Acrotretidae
Holcophylloceras	Mollusca	Cephalopoda	Phylloceratida	Phylloceratidae
Homolsomites	Mollusca	Cephalopoda	Ammonitida	Polyptychitidae
Hoplites	Mollusca	Cephalopoda	Ammonitida	Hoplitidae
Hoploscaphites	Mollusca	Cephalopoda	Ammonitida	Scaphitidae

Huananoceras	Mollusca	Cephalopoda	Ceratitida	Huananoceratidae
Hulenites	Mollusca	Cephalopoda	Ammonitida	Kossmaticeratidae
Hungarites	Mollusca	Cephalopoda	Ceratitida	Hungaritidae
Hybonoticeras	Mollusca	Cephalopoda	Ammonitida	Aspidoceratidae
Hypacanthoplites	Mollusca	Cephalopoda	Ammonitida	Parahoplitidae
Hyphantoceras	Mollusca	Cephalopoda	Ammonitida	Nostoceratidae
Hyphoplites	Mollusca	Cephalopoda	Ammonitida	Hoplitidae
Hypocladiscites	Mollusca	Cephalopoda	Ceratitida	Cladiscitidae
Hypolissoceras	Mollusca	Cephalopoda	Ammonitida	Haploceratidae
Hysteroceras	Mollusca	Cephalopoda	Ammonitida	Brancoceratidae
Idanoceras	Mollusca	Cephalopoda	Ammonitida	Labeceratidae
Idiohamites	Mollusca	Cephalopoda	Ammonitida	Anisoceratidae
Idoceras	Mollusca	Cephalopoda	Ammonitida	Perisphinctidae
Imbricatoceras	Mollusca	Cephalopoda	Orthocerida	Orthoceratidae
Imitoceras	Mollusca	Cephalopoda	Goniatitida	Prionoceratidae
Indigirophyllites	Mollusca	Cephalopoda	Phylloceratida	Discophyllitidae
Indonautilus	Mollusca	Cephalopoda	Nautilida	Paranautilidae
Iniskinites	Mollusca	Cephalopoda	Ammonitida	Sphaeroceratidae
Isorthoceras	Mollusca	Cephalopoda	Orthocerida	Proteoceratidae
Japonites	Mollusca	Cephalopoda	Ceratitida	Japonitidae
Jeanthieuloyites	Mollusca	Cephalopoda	Ammonitida	Holcodiscidae
Jeletzkytes	Mollusca	Cephalopoda	Ammonitida	Scaphitidae
Jimboiceras	Mollusca	Cephalopoda	Ammonitida	Desmoceratidae
Joannites	Mollusca	Cephalopoda	Ceratitida	Joannitidae
Juraphyllites	Mollusca	Cephalopoda	Phylloceratida	Juraphyllitidae
Juresanites	Mollusca	Cephalopoda	Goniatitida	Metalegoceratidae
Juvavites	Mollusca	Cephalopoda	Ceratitida	Juvavitidae
Kamerunoceras	Mollusca	Cephalopoda	Ammonitida	Acanthoceratidae
Kargalites	Mollusca	Cephalopoda	Goniatitida	Marathonitidae
Katroliceras	Mollusca	Cephalopoda	Ammonitida	Ataxioceratidae
Kazakhoceras	Mollusca	Cephalopoda	Goniatitida	Berkhoceratidae
Keyserlingites	Mollusca	Cephalopoda	Ceratitida	Keyserlingitidae
Kilianella	Mollusca	Cephalopoda	Ammonitida	Neocomitidae
Kilianiceras	Mollusca	Cephalopoda	Ammonitida	Olcostephanidae
Kingites	Mollusca	Cephalopoda	Ceratitida	Gyronitidae
Kionoceras	Mollusca	Cephalopoda	Orthocerida	Kionoceratidae
Kitchinites	Mollusca	Cephalopoda	Ammonitida	Desmoceratidae
Knightoceras	Mollusca	Cephalopoda	Nautilida	Koninckioceratidae
Koninckites	Mollusca	Cephalopoda	Ceratitida	Paranoritidae
Kosmoceras	Mollusca	Cephalopoda	Ammonitida	Kosmoceratidae
Kossmatia	Mollusca	Cephalopoda	Ammonitida	Neocomitidae
Kummelonautilus	Mollusca	Cephalopoda	Nautilida	Nautilidae
Kyrshabaktella	Brachiopoda	Lingulata	Lingulida	Kyrshabaktellidae
Lagonibelus	Mollusca	Cephalopoda	Belemnitida	
Lamanskya	Brachiopoda	Lingulata	Lingulida	Elkaniidae
Lambeoceras	Mollusca	Cephalopoda	Actinocerida	Gonioceratidae
Lamellaptychus	Mollusca	Cephalopoda		
Laxispira	Mollusca	Gastropoda	Sorbeoconcha	Turritellidae
Lecanites	Mollusca	Cephalopoda	Ceratitida	Lecanitidae
Lechites (Lechites)	Mollusca	Cephalopoda	Ammonitida	Baculitidae
Leiophyllites	Mollusca	Cephalopoda	Phylloceratida	Palaeophyllitidae
Lenotropites	Mollusca	Cephalopoda	Ceratitida	Longobarditidae
Leptobolus	Brachiopoda	Lingulata	Lingulida	Obolidae
Leptoceras	Mollusca	Cephalopoda	Ammonoidea	Protancyloceratidae
Lewyites	Mollusca	Cephalopoda	Ammonitida	Diplomoceratidae
Libycoceras	Mollusca	Cephalopoda	Ammonitida	Sphenodiscidae
Lilloettia	Mollusca	Cephalopoda	Ammonitida	Sphaeroceratidae
Lingula	Brachiopoda	Lingulata	Lingulida	Lingulidae
Lingularia	Brachiopoda	Lingulata	Lingulida	Lingulidae
Lingulasma	Brachiopoda	Lingulata	Lingulida	Lingulasmatidae
Lingulella	Brachiopoda	Lingulata	Lingulida	Obolidae
Lingulellotreta	Brachiopoda	Lingulata	Lingulida	Lingulellotretidae
Lingulepis	Brachiopoda	Lingulata	Lingulida	Obolidae
Lingulipora	Brachiopoda	Lingulata	Lingulida	
Linnarssonia	Brachiopoda	Lingulata	Acrotretida	Acrotretidae
Lioceratoides	Mollusca	Cephalopoda	Ammonitida	Hildoceratidae
Lioceratoides (Lioceratoides)	Mollusca	Cephalopoda	Ammonitida	Hildoceratidae
Liroceras	Mollusca	Cephalopoda	Nautilida	Liroceratidae
Lissoceras	Mollusca	Cephalopoda	Ammonitida	Lissoceratidae
Lithacoceras	Mollusca	Cephalopoda	Ammonitida	Ataxioceratidae

Lituites	Mollusca	Cephalopoda	Lituitida	Lituitidae
Lobites	Mollusca	Cephalopoda	Ceratitida	Lobitidae
Lobobactrites	Mollusca	Cephalopoda	Bactritida	Bactritidae
Lobotornoceras	Mollusca	Cephalopoda	Goniatitida	Tornoceratidae
Longibelus	Mollusca	Cephalopoda		
Longobardites	Mollusca	Cephalopoda	Ceratitida	Longobarditidae
Lopingoceras	Mollusca	Cephalopoda	Pseudorthocerida	Spyroceratidae
Lyrogoniatites	Mollusca	Cephalopoda	Goniatitida	Cravenoceratidae
Lytoceras	Mollusca	Cephalopoda	Ammonitida	Lytoceratidae
Macrocephalites	Mollusca	Cephalopoda	Ammonitida	Macrocephalitidae
Macroscaphites	Mollusca	Cephalopoda	Ammonoidea	Macroscaphitidae
Manchuroceras	Mollusca	Cephalopoda	Bisonocerida	Manchuroceratidae
Maorites	Mollusca	Cephalopoda	Ammonitida	Kossmaticeratidae
Mariceras	Mollusca	Cephalopoda	Nautilida	Scyphoceratidae
Mariella	Mollusca	Cephalopoda	Ammonitida	Turrilitidae
Mariella (Mariella)	Mollusca	Cephalopoda	Ammonitida	Turrilitidae
Marshallites	Mollusca	Cephalopoda	Ammonitida	Kossmaticeratidae
Mcqueenoceras	Mollusca	Cephalopoda	Endocerida	Proterocameroceratidae
Medlicottia	Mollusca	Cephalopoda	Prolecanitida	Medlicottiidae
Meekoceras	Mollusca	Cephalopoda	Ceratitida	Prionitidae
Megalytoceras	Mollusca	Cephalopoda	Ammonitida	Lytoceratidae
Megaphyllites	Mollusca	Cephalopoda	Ceratitida	Megaphyllitidae
Megapronorites	Mollusca	Cephalopoda	Prolecanitida	Pronoritidae
Melchiorites	Mollusca	Cephalopoda	Ammonitida	Desmoceratidae
Menuites	Mollusca	Cephalopoda	Ammonitida	Pachydiscidae
Mesopuzosia	Mollusca	Cephalopoda	Ammonitida	Desmoceratidae
Metacoceras	Mollusca	Cephalopoda	Nautilida	Tainoceratidae
Metalegoceras	Mollusca	Cephalopoda	Goniatitida	Metalegoceratidae
Metapeltoceras	Mollusca	Cephalopoda	Ammonitida	Aspidoceratidae
Metaperrinites	Mollusca	Cephalopoda	Goniatitida	Perrinitidae
Metapronorites	Mollusca	Cephalopoda	Prolecanitida	Pronoritidae
Metaptychoceras	Mollusca	Cephalopoda	Ammonitida	Hamitidae
Metasibirites	Mollusca	Cephalopoda	Ceratitida	Metasibiritidae
Metengonoceras	Mollusca	Cephalopoda	Ammonitida	Engonoceratidae
Metoicoceras	Mollusca	Cephalopoda	Ammonitida	Acanthoceratidae
Mexicoceras	Mollusca	Cephalopoda	Goniatitida	Cyclolobidae
Michelinoceras	Mollusca	Cephalopoda	Orthocerida	Orthoceratidae
Microderoceras	Mollusca	Cephalopoda	Ammonitida	Eoderoceratidae
Miklukhoceras	Mollusca	Cephalopoda	Prolecanitida	Medlicottiidae
Mimagoniatites	Mollusca	Cephalopoda	Agoniatitida	Mimagoniatitidae
Mimimitoceras	Mollusca	Cephalopoda	Goniatitida	Prionoceratidae
Mitorthoceras	Mollusca	Cephalopoda	Pseudorthocerida	Pseudorthoceratidae
Mojsisovicsteuthis	Mollusca	Cephalopoda	Aulacoceratida	Xiphoteuthididae
Monophyllites	Mollusca	Cephalopoda	Phylloceratida	Ussuritidae
Mortoniceras	Mollusca	Cephalopoda	Ammonitida	Brancoceratidae
Muensteroceras	Mollusca	Cephalopoda	Goniatitida	Muensteroceratidae
Myotreta	Brachiopoda	Lingulata	Acrotretida	Ephippelasmatidae
Nathorstites	Mollusca	Cephalopoda	Ceratitida	Nathorstitidae
Nautilus	Mollusca	Cephalopoda	Nautilida	Nautilidae
Neoaganides	Mollusca	Cephalopoda	Goniatitida	Pseudohaloritidae
Neocampylites	Mollusca	Cephalopoda	Ammonitida	Oppeliidae
Neocomites	Mollusca	Cephalopoda	Ammonitida	Neocomitidae
Neocomites (Teschenites)	Mollusca	Cephalopoda	Ammonitida	Neocomitidae
Neocrimites	Mollusca	Cephalopoda	Goniatitida	Adrianitidae
Neocycloceras	Mollusca	Cephalopoda	Pseudorthocerida	Pseudorthoceratidae
Neodeshayesites	Mollusca	Cephalopoda	Ammonitida	Parahoplitidae
Neodimorphoceras	Mollusca	Cephalopoda	Goniatitida	Neodimorphoceratidae
Neogastroplites	Mollusca	Cephalopoda	Ammonitida	Hoplitidae
Neogeoceras	Mollusca	Cephalopoda	Prolecanitida	Medlicottiidae
Neoglyphioceras	Mollusca	Cephalopoda	Goniatitida	Goniatitidae
Neogoniatites	Mollusca	Cephalopoda	Goniatitida	Goniatitidae
Neohibolites	Mollusca	Cephalopoda	Belemnitida	Belemnopseidae
Neolioceratoides	Mollusca	Cephalopoda	Ammonitida	Hildoceratidae
Neolissoceras	Mollusca	Cephalopoda	Ammonitida	Haploceratidae
Neophlycticeras (Neophlycticeras)	Mollusca	Cephalopoda	Ammonitida	Lyelliceratidae
Neophylloceras	Mollusca	Cephalopoda	Phylloceratida	Phylloceratidae
Neopopanoceras	Mollusca	Cephalopoda	Goniatitida	Popanoceratidae
Neopronorites	Mollusca	Cephalopoda	Prolecanitida	Pronoritidae
Neouddenites	Mollusca	Cephalopoda	Prolecanitida	Medlicottiidae
Nevadaphyllites	Mollusca	Cephalopoda	Phylloceratida	Juraphyllitidae

Nigericeras	Mollusca	Cephalopoda	Ammonitida	Acanthoceratidae
Norites	Mollusca	Cephalopoda	Ceratitida	Noritidae
Nostoceras	Mollusca	Cephalopoda	Ammonitida	Nostoceratidae
Nostoceras (Nostoceras)	Mollusca	Cephalopoda	Ammonitida	Nostoceratidae
Nowakites	Mollusca	Cephalopoda	Ammonitida	Pachydiscidae
Nybyoceras	Mollusca	Cephalopoda	Actinocerida	Armenoceratidae
Obolus	Brachiopoda	Lingulata	Lingulida	Obolidae
Olcostephanus	Mollusca	Cephalopoda	Ammonitida	Olcostephanidae
Olcostephanus (Olcostephanus)	Mollusca	Cephalopoda	Ammonitida	Olcostephanidae
Onychoceras	Mollusca	Cephalopoda	NO_ORDER_SPECIFIED	Basslerocerati dae
Onychoceras	Mollusca	Cephalopoda	Ammonitida	Hammatoceratidae
Oosterella	Mollusca	Cephalopoda	Ammonitida	Oosterellidae
Ophiceras	Mollusca	Cephalopoda	Ceratitida	Ophiceratidae
Ophionautilus	Mollusca	Cephalopoda	Nautilida	Cenoceratidae
Oppelia	Mollusca	Cephalopoda	Ammonitida	Oppeliidae
Orbiculoidea	Brachiopoda	Lingulata	Lingulida	Discinidae
Ormoceras	Mollusca	Cephalopoda	Actinocerida	Ormoceratidae
Ornopsis	Mollusca	Gastropoda	Neogastropoda	Buccinidae
Orthoceras	Mollusca	Cephalopoda	Orthocerida	Orthoceratidae
Orthocycloceras	Mollusca	Cephalopoda	Orthocerida	Orthoceratidae
Orthosphinctes	Mollusca	Cephalopoda	Ammonitida	Ataxioceratidae
Ostlingoceras	Mollusca	Cephalopoda	Ammonitida	Turrilitidae
Otoceras	Mollusca	Cephalopoda	Ceratitida	Otoceratidae
Oxycerites	Mollusca	Cephalopoda	Ammonitida	Oppeliidae
Pachydesmoceras	Mollusca	Cephalopoda	Ammonitida	Desmoceratidae
Pachydiscus	Mollusca	Cephalopoda	Ammonitida	Pachydiscidae
Pachydiscus (Neodesmoceras)	Mollusca	Cephalopoda	Ammonitida	Pachydiscidae
Pachydiscus (Pachydiscus)	Mollusca	Cephalopoda	Ammonitida	Pachydiscidae
Pachyglossella	Brachiopoda	Lingulata	Lingulida	Obolidae
Pachyteuthis	Mollusca	Cephalopoda	Belemnitida	
Palaeoglossa	Brachiopoda	Lingulata	Lingulida	Obolidae
Paraceltites	Mollusca	Cephalopoda	Ceratitida	Paraceltitidae
Paracenoceras	Mollusca	Cephalopoda	Nautilida	Paracenoceratidae
Paracladiscites	Mollusca	Cephalopoda	Ceratitida	Cladiscitidae
Paracrochordiceras	Mollusca	Cephalopoda	Ceratitida	Acrochordiceratidae
Paradasyceras	Mollusca	Cephalopoda	Phylloceratida	Juraphyllitidae
Paradimorphoceras	Mollusca	Cephalopoda	Goniatitida	Dimorphoceratidae
Paragastrioceras	Mollusca	Cephalopoda	Goniatitida	Paragastrioceratidae
Parahoplites	Mollusca	Cephalopoda	Ammonitida	Parahoplitidae
Paralegoceras	Mollusca	Cephalopoda	Goniatitida	Schistoceratidae
Paramicroderoceras	Mollusca	Cephalopoda	Ammonitida	Eoderoceratidae
Paranautilus	Mollusca	Cephalopoda	Nautilida	Liroceratidae
Paranorites	Mollusca	Cephalopoda	Ceratitida	Paranoritidae
Parapenascoceras	Mollusca	Cephalopoda	Nautilida	Grypoceratidae
Parapronorites	Mollusca	Cephalopoda	Prolecanitida	Pronoritidae
Parapuzosia	Mollusca	Cephalopoda	Ammonitida	Desmoceratidae
Parapuzosia (Austiniceras)	Mollusca	Cephalopoda	Ammonitida	Desmoceratidae
Parapuzosia (Parapuzosia)	Mollusca	Cephalopoda	Ammonitida	Desmoceratidae
Paraschistoceras	Mollusca	Cephalopoda	Goniatitida	Schistoceratidae
Paraspiticeras	Mollusca	Cephalopoda	Ammonitida	
Parasturia	Mollusca	Cephalopoda	Ceratitida	Sturiidae
Paratirolites	Mollusca	Cephalopoda	Ceratitida	Dzhulfitidae
Paratrachyceras	Mollusca	Cephalopoda	Ceratitida	Trachyceratidae
Parkinsonia	Mollusca	Cephalopoda	Ammonitida	Stephanoceratidae
Parkinsonia (Durotrigensia)	Mollusca	Cephalopoda	Ammonitida	Stephanoceratidae
Parkinsonia (Gonolkites)	Mollusca	Cephalopoda	Ammonitida	Stephanoceratidae
Partschiceras	Mollusca	Cephalopoda	Phylloceratida	Phylloceratidae
Pashtunites	Mollusca	Cephalopoda	Ceratitida	Paranoritidae
Paterula	Brachiopoda	Lingulata	Lingulida	Paterulidae
Peltoceras	Mollusca	Cephalopoda	Ammonitida	Aspidoceratidae
Peltoceratoides	Mollusca	Cephalopoda	Ammonitida	Aspidoceratidae
Pericyclus	Mollusca	Cephalopoda	Goniatitida	Pericyclidae
Peripetoceras	Mollusca	Cephalopoda	Nautilida	Liroceratidae
Perisphinctes	Mollusca	Cephalopoda	Ammonitida	Perisphinctidae

Perrinites	Mollusca	Cephalopoda	Goniatitida	Perrinitidae
Phaneroceras	Mollusca	Cephalopoda	Goniatitida	Pseudoparalegoceratidae
Phoenixites	Mollusca	Cephalopoda	Goniatitida	Tornoceratidae
Phylloceras	Mollusca	Cephalopoda	Phylloceratida	Phylloceratidae
Phylloceras (Hypophylloceras)	Mollusca	Cephalopoda	Phylloceratida	Phylloceratidae
Phyllopachyceras	Mollusca	Cephalopoda	Phylloceratida	Phylloceratidae
Physodoceras	Mollusca	Cephalopoda	Ammonitida	Aspidoceratidae
Pinacoceras	Mollusca	Cephalopoda	Ceratitida	Pinacoceratidae
Placenticeras	Mollusca	Cephalopoda	Ammonitida	Placenticeratidae
Placites	Mollusca	Cephalopoda	Ceratitida	Gymnitidae
Planammatoceras	Mollusca	Cephalopoda	Ammonitida	Hammatoceratidae
Platygoniatites	Mollusca	Cephalopoda	Goniatitida	Delepinoceratidae
Plectoceras	Mollusca	Cephalopoda	Barrandeocerida	Plectoceratidae
Pleurofrechites	Mollusca	Cephalopoda	Ceratitida	Ceratitidae
Pleurolytoceras	Mollusca	Cephalopoda	Ammonitida	Lytoceratidae
Pleuronautilus	Mollusca	Cephalopoda	Nautilida	Tainoceratidae
Polinices	Mollusca	Gastropoda	Sorbeoconcha	Naticidae
Polygrammoceras	Mollusca	Cephalopoda	Orthocerida	Kionoceratidae
Polyptychoceras	Mollusca	Cephalopoda	Ammonitida	Diplomoceratidae
Ponticeras	Mollusca	Cephalopoda	Agoniatitida	Acanthoclymeniidae
Popanoceras	Mollusca	Cephalopoda	Goniatitida	Popanoceratidae
Praedaraelites	Mollusca	Cephalopoda	Prolecanitida	Daraelitidae
Praeoppelia	Mollusca	Cephalopoda	Ammonitida	Oppeliidae
Praestrigites	Mollusca	Cephalopoda	Ammonitida	Strigoceratidae
Prionolobus	Mollusca	Cephalopoda	Ceratitida	Proptychitidae
Proarcestes	Mollusca	Cephalopoda	Ceratitida	Arcestidae
Procarnites	Mollusca	Cephalopoda	Ceratitida	Procarnitidae
Procheloniceras	Mollusca	Cephalopoda	Ammonitida	Douvilleiceratidae
Procladiscites	Mollusca	Cephalopoda	Ceratitida	Cladiscitidae
Proclydonautilus	Mollusca	Cephalopoda	Nautilida	Clydonautilidae
Prolecanites	Mollusca	Cephalopoda	Prolecanitida	Prolecanitidae
Properisphinctes	Mollusca	Cephalopoda	Ammonitida	Perisphinctidae
Properrinites	Mollusca	Cephalopoda	Goniatitida	Perrinitidae
Propinacoceras	Mollusca	Cephalopoda	Prolecanitida	Medlicottiidae
Proplacenticeras	Mollusca	Cephalopoda	Ammonitida	Placenticeratidae
Proptychites	Mollusca	Cephalopoda	Ceratitida	Proptychitidae
Proshumardites	Mollusca	Cephalopoda	Goniatitida	Delepinoceratidae
Prostacheoceras	Mollusca	Cephalopoda	Goniatitida	Vidrioceratidae
Protacanthodiscus	Mollusca	Cephalopoda	Ammonitida	Himalayitidae
Protancyloceras	Mollusca	Cephalopoda	Ammonoidea	Protancyloceratidae
Proteoceras	Mollusca	Cephalopoda	Orthocerida	Proteoceratidae
Proterocameroceras	Mollusca	Cephalopoda	Endocerida	Proterocameroceratidae
Protetragonites	Mollusca	Cephalopoda	Ammonitida	Protetragonitidae
Protexanites	Mollusca	Cephalopoda	Ammonitida	Collignoniceratidae
Prothalassoceras	Mollusca	Cephalopoda	Goniatitida	Thalassoceratidae
Protocycloceras	Mollusca	Cephalopoda	Ellesmerocerida	Protocycloceratidae
Protogrammoceras	Mollusca	Cephalopoda	Ammonitida	Hildoceratidae
Prototreta	Brachiopoda	Lingulata	Acrotretida	Acrotretidae
Protrachyceras	Mollusca	Cephalopoda	Ceratitida	Trachyceratidae
Pseudaganides	Mollusca	Cephalopoda	Nautilida	Pseudonautilidae
Pseudaptetoceras	Mollusca	Cephalopoda	Ammonitida	Hammatoceratidae
Pseudaspidoceras	Mollusca	Cephalopoda	Ammonitida	Acanthoceratidae
Pseudhelicoceras	Mollusca	Cephalopoda	Ammonitida	Turrilitidae
Pseudobelus	Mollusca	Cephalopoda	Belemnitida	Duvaliidae
Pseudocenoceras	Mollusca	Cephalopoda	Nautilida	Nautilidae
Pseudogastrioceras	Mollusca	Cephalopoda	Goniatitida	Paragastrioceratidae
Pseudohaploceras	Mollusca	Cephalopoda	Ammonitida	Desmoceratidae
Pseudokossmaticeras	Mollusca	Cephalopoda	Ammonitida	Kossmaticeratidae
Pseudolingula	Brachiopoda	Lingulata	Lingulida	Pseudolingulidae
Pseudolioceras	Mollusca	Cephalopoda	Ammonitida	Hildoceratidae
Pseudolioceras (Tugurites)	Mollusca	Cephalopoda	Ammonitida	Hildoceratidae
Pseudophyllites	Mollusca	Cephalopoda	Ammonitida	Tetragonitidae
Pseudopronorites	Mollusca	Cephalopoda	Prolecanitida	Pronoritidae
Pseudorthoceras	Mollusca	Cephalopoda	Pseudorthocerida	Pseudorthoceratidae
Pseudosageceras	Mollusca	Cephalopoda	Ceratitida	Hedenstroemiidae
Pseudoschloenbachia (Pseudoschloenbachia)	Mollusca	Cephalopoda	Ammonitida	Muniericeratidae
Pseudosubplanites	Mollusca	Cephalopoda	Ammonitida	Ataxioceratidae
Pseudotitanoceras	Mollusca	Cephalopoda	Nautilida	Grypoceratidae
Pseudoxybeloceras	Mollusca	Cephalopoda	Ammonitida	Diplomoceratidae

Pterocerella	Mollusca	Gastropoda	Sorbeoconcha	Aporrhaidae
Ptychites	Mollusca	Cephalopoda	Ceratitida	Ptychitidae
Ptychoceras	Mollusca	Cephalopoda	Ammonitida	Ptychoceratidae
Ptychophylloceras	Mollusca	Cephalopoda	Phylloceratida	Phylloceratidae
Pugnellus	Mollusca	Gastropoda	Sorbeoconcha	Aporrhaidae
Putealiceras	Mollusca	Cephalopoda	Ammonitida	Oppeliidae
Puzosia	Mollusca	Cephalopoda	Ammonitida	Desmoceratidae
Puzosia (Anapuzosia)	Mollusca	Cephalopoda	Ammonitida	Desmoceratidae
Puzosia (Puzosia)	Mollusca	Cephalopoda	Ammonitida	Desmoceratidae
Quenstedtoceras	Mollusca	Cephalopoda	Ammonitida	Cardioceratidae
Radioceras	Mollusca	Cephalopoda	Ceratitida	Paranoritidae
Radstockiceras	Mollusca	Cephalopoda	Ammonitida	Oxynoticeratidae
Rayonnoceras	Mollusca	Cephalopoda	Actinocerida	Carbactinoceratidae
Reitziites	Mollusca	Cephalopoda	Ceratitida	Ceratitidae
Reticycloceras	Mollusca	Cephalopoda	Pseudorthocerida	Spyroceratidae
Rhabdoceras	Mollusca	Cephalopoda	Ceratitida	Choristoceratidae
Rhacophyllites	Mollusca	Cephalopoda	Phylloceratida	Discophyllitidae
Rhynchorthoceras	Mollusca	Cephalopoda	Lituitida	Sinoceratidae
Riccardiceras	Mollusca	Cephalopoda	Ammonitida	Stephanoceratidae
Richardsonoceras	Mollusca	Cephalopoda	Oncocerida	Oncoceratidae
Richterella	Mollusca	Cephalopoda	Ammonitida	Ataxioceratidae
Rineceras	Mollusca	Cephalopoda	Nautilida	Trigonoceratidae
Rioceras	Mollusca	Cephalopoda	Ellesmerocerida	Rioceratidae
Roadoceras	Mollusca	Cephalopoda	Goniatitida	Paragastrioceratidae
Rollieria	Mollusca	Cephalopoda	Ammonitida	Oppeliidae
Rowellella	Brachiopoda	Lingulata	Lingulida	Obolidae
Sactoceras	Mollusca	Cephalopoda	Orthocerida	Sactoceratidae
Sageceras	Mollusca	Cephalopoda	Ceratitida	Sageceratidae
Sagenites	Mollusca	Cephalopoda	Ceratitida	Haloritidae
Saghalinites	Mollusca	Cephalopoda	Ammonitida	Tetragonitidae
Saloceras	Mollusca	Cephalopoda	Ellesmerocerida	Eothinoceratidae
Sanmartinoceras	Mollusca	Cephalopoda	Ammonitida	Oppeliidae
Sarasinella	Mollusca	Cephalopoda	Ammonitida	Neocomitidae
Scalarites	Mollusca	Cephalopoda	Ammonitida	Diplomoceratidae
Scaphelasma	Brachiopoda	Lingulata	Acrotretida	Scaphelasmatidae
Scaphites	Mollusca	Cephalopoda	Ammonitida	Scaphitidae
Scaphites (Scaphites)	Mollusca	Cephalopoda	Ammonitida	Scaphitidae
Schistoceras	Mollusca	Cephalopoda	Goniatitida	Schistoceratidae
Schizambon	Brachiopoda	Lingulata	Siphonotretida	Siphonotretidae
Schizocrania	Brachiopoda	Lingulata	Lingulida	Trematidae
Schizotreta	Brachiopoda	Lingulata	Lingulida	Discinidae
Schloenbachia	Mollusca	Cephalopoda	Ammonitida	Schloenbachiidae
Schmidtites	Brachiopoda	Lingulata	Lingulida	Obolidae
Schuchertoceras	Mollusca	Cephalopoda	Ascocerida	Ascoceratidae
Sciponoceras	Mollusca	Cephalopoda	Ammonitida	Baculitidae
Semilingula	Brachiopoda	Lingulata	Lingulida	Lingulidae
Shasticrioceras	Mollusca	Cephalopoda	Ammonoidea	Megacrioceratidae
Shevyrevites	Mollusca	Cephalopoda	Ceratitida	Xenodiscidae
Sibyllonautilus	Mollusca	Cephalopoda	Nautilida	Tainoceratidae
Silesites	Mollusca	Cephalopoda	Ammonitida	Silesitidae
Sinoceras	Mollusca	Cephalopoda	Orthocerida	Orthoceratidae
Sinoglottidia	Brachiopoda	Lingulata	Lingulida	Lingulidae
Solenoceras	Mollusca	Cephalopoda	Ammonitida	Diplomoceratidae
Somoholites	Mollusca	Cephalopoda	Goniatitida	Somoholitidae
Sowerbyceras	Mollusca	Cephalopoda	Phylloceratida	Phylloceratidae
Sphenodiscus	Mollusca	Cephalopoda	Ammonitida	Sphenodiscidae
Spiticeras	Mollusca	Cephalopoda	Ammonitida	Olcostephanidae
Spitidiscus	Mollusca	Cephalopoda	Ammonitida	Holcodiscidae
Spondylotreta	Brachiopoda	Lingulata	Acrotretida	Acrotretidae
Spyroceras	Mollusca	Cephalopoda	Pseudorthocerida	Spyroceratidae
Stacheoceras	Mollusca	Cephalopoda	Goniatitida	Vidrioceratidae
Stearoceras	Mollusca	Cephalopoda	Nautilida	Grypoceratidae
Stenarcestes	Mollusca	Cephalopoda	Ceratitida	Arcestidae
Stenoglaphyrites	Mollusca	Cephalopoda	Goniatitida	Glaphyritidae
Stenolobulites	Mollusca	Cephalopoda	Goniatitida	Paragastrioceratidae
Stenopoceras	Mollusca	Cephalopoda	Nautilida	Grypoceratidae
Stenopronorites	Mollusca	Cephalopoda	Prolecanitida	Pronoritidae
Stoliczkaiella	Mollusca	Cephalopoda	Ammonitida	Lyelliceratidae
Stoliczkaiella (Stoliczkaiella)	Mollusca	Cephalopoda	Ammonitida	Lyelliceratidae
Stolleyites	Mollusca	Cephalopoda	Ceratitida	Nathorstitidae

Stomohamites	Mollusca	Cephalopoda	Ammonitida	Hamitidae
Striatocycloceras	Mollusca	Cephalopoda	Orthocerida	Orthoceratidae
Strigogoniatites	Mollusca	Cephalopoda	Goniatitida	Paragastrioceratidae
Stroboceras	Mollusca	Cephalopoda	Nautilida	Trigonoceratidae
Sturia	Mollusca	Cephalopoda	Ceratitida	Sturiidae
Subcraspedites	Mollusca	Cephalopoda	Ammonitida	Polyptychitidae
Subdichotomoceras	Mollusca	Cephalopoda	Ammonitida	Perisphinctidae
Submortoniceras	Mollusca	Cephalopoda	Ammonitida	Collignoniceratidae
Subplanites	Mollusca	Cephalopoda	Ammonitida	Perisphinctidae
Substeueroceras	Mollusca	Cephalopoda	Ammonitida	Neocomitidae
Sudeticeras	Mollusca	Cephalopoda	Goniatitida	Anthracoceratidae
Sulcogirtyoceras	Mollusca	Cephalopoda	Goniatitida	Girtyoceratidae
Surites (Bojarkia)	Mollusca	Cephalopoda	Ammonitida	Polyptychitidae
Surites (Surites)	Mollusca	Cephalopoda	Ammonitida	Polyptychitidae
Sutneria	Mollusca	Cephalopoda	Ammonitida	Aspidoceratidae
Syngastrioceras	Mollusca	Cephalopoda	Goniatitida	Glaphyritidae
Syringoceras	Mollusca	Cephalopoda	Nautilida	Syringonautilidae
Syringonautilus	Mollusca	Cephalopoda	Nautilida	Syringonautilidae
Tainionautilus	Mollusca	Cephalopoda	Nautilida	Tainoceratidae
Tainoceras	Mollusca	Cephalopoda	Nautilida	Tainoceratidae
Taramelliceras	Mollusca	Cephalopoda	Ammonitida	Oppeliidae
Taramelliceras (Metahaploceras)	Mollusca	Cephalopoda	Ammonitida	Oppeliidae
Taramelliceras (Taramelliceras)	Mollusca	Cephalopoda	Ammonitida	Oppeliidae
Tarphyceras	Mollusca	Cephalopoda	Tarphycerida	Tarphyceratidae
Temnocheilus	Mollusca	Cephalopoda	Nautilida	Temnocheilidae
Tetragonites	Mollusca	Cephalopoda	Ammonitida	Tetragonitidae
Tetragonites (Tetragonites)	Mollusca	Cephalopoda	Ammonitida	Tetragonitidae
Tetraspidoceras	Mollusca	Cephalopoda	Ammonitida	Coeloceratidae
Texanites	Mollusca	Cephalopoda	Ammonitida	Collignoniceratidae
Thalassoceras	Mollusca	Cephalopoda	Goniatitida	Thalassoceratidae
Thambites	Mollusca	Cephalopoda	Ammonitida	Thamboceratidae
Thisbites	Mollusca	Cephalopoda	Ceratitida	Thisbitidae
Thomasites	Mollusca	Cephalopoda	Ammonitida	Pseudotissotiidae
Thurmanniceras	Mollusca	Cephalopoda	Ammonitida	Neocomitidae
Tiltoniceras	Mollusca	Cephalopoda	Ammonitida	Hildoceratidae
Timorites	Mollusca	Cephalopoda	Goniatitida	Cyclolobidae
Tirnovella	Mollusca	Cephalopoda	Ammonitida	Neocomitidae
Tollia	Mollusca	Cephalopoda	Ammonitida	Polyptychitidae
Tollia (Tollia)	Mollusca	Cephalopoda	Ammonitida	Polyptychitidae
Tongoboryceras	Mollusca	Cephalopoda	Ammonitida	Pachydiscidae
Tornoceras	Mollusca	Cephalopoda	Goniatitida	Tornoceratidae
Torquatisphinctes	Mollusca	Cephalopoda	Ammonitida	Perisphinctidae
Toxoceratoides	Mollusca	Cephalopoda	Ammonitida	Acrioceratidae
Trachyceras	Mollusca	Cephalopoda	Ceratitida	Trachyceratidae
Trachyscaphites	Mollusca	Cephalopoda	Ammonitida	Scaphitidae
Trematis	Brachiopoda	Lingulata	Lingulida	Trematidae
Trematoceras	Mollusca	Cephalopoda	Orthocerida	Orthoceratidae
Trimarginites	Mollusca	Cephalopoda	Ammonitida	Oppeliidae
Tripteroceras	Mollusca	Cephalopoda	Orthocerida	Tripteroceratidae
Trocholites	Mollusca	Cephalopoda	Tarphycerida	Trocholitidae
Tropaeum	Mollusca	Cephalopoda	Ammonitida	Ancyloceratidae
Tropiceltites	Mollusca	Cephalopoda	Ceratitida	Tropiceltitidae
Truyolsoceras	Mollusca	Cephalopoda	Goniatitida	Tornoceratidae
Turrilites	Mollusca	Cephalopoda	Ammonitida	Turrilitidae
Turrilitoides	Mollusca	Cephalopoda	Ammonitida	Nostoceratidae
Turritella	Mollusca	Gastropoda	Sorbeoconcha	Turritellidae
Tylonautilus	Mollusca	Cephalopoda	Nautilida	Tainoceratidae
Uhligella	Mollusca	Cephalopoda	Ammonitida	Desmoceratidae
Ungula	Brachiopoda	Lingulata	Lingulida	Obolidae
Unio	Mollusca	Bivalvia	Unionida	Unionidae
Uraloceras	Mollusca	Cephalopoda	Goniatitida	Paragastrioceratidae
Ussurites	Mollusca	Cephalopoda	Phylloceratida	Ussuritidae
Vaginoceras	Mollusca	Cephalopoda	Endocerida	Endoceratidae
Valcouroceras	Mollusca	Cephalopoda	Oncocerida	Valcouroceratidae
Valdedorsella	Mollusca	Cephalopoda	Ammonitida	Desmoceratidae
Vascoceras	Mollusca	Cephalopoda	Ammonitida	Vascoceratidae
Vermiceras	Mollusca	Cephalopoda	Ammonitida	Arietitidae
Vermiceras (Paracaloceras)	Mollusca	Cephalopoda	Ammonitida	Arietitidae

Veruzhites	Mollusca	Cephalopoda	Goniatitida	Adrianitidae
Villania	Mollusca	Cephalopoda	Ammonitida	Phricodoceratidae
Waagenoceras	Mollusca	Cephalopoda	Goniatitida	Cyclolobidae
Wadiglossa	Brachiopoda	Lingulata	Lingulida	Pseudolingulidae
Walcottoceras	Mollusca	Cephalopoda	Ellesmerocerida	Ellesmeroceratidae
Westonia	Brachiopoda	Lingulata	Lingulida	Obolidae
Wiedeyoceras	Mollusca	Cephalopoda	Goniatitida	Wiedeyoceratidae
Winnipegoceras	Mollusca	Cephalopoda	Discosorida	Westonoceratidae
Xenocephalites	Mollusca	Cephalopoda	Ammonitida	Sphaeroceratidae
Xenodiscoides	Mollusca	Cephalopoda	Ceratitida	Flemingitidae
Xenodiscus	Mollusca	Cephalopoda	Ceratitida	Xenodiscidae
Xenophora	Mollusca	Gastropoda	Sorbeoconcha	Xenophoridae
Yezoites	Mollusca	Cephalopoda	Ammonitida	Scaphitidae
Zelandites	Mollusca	Cephalopoda	Ammonitida	Tetragonitidae
Zestoceras	Mollusca	Cephalopoda	Ceratitida	Trachyceratidae
Zetoceras	Mollusca	Cephalopoda	Phylloceratida	Phylloceratidae
Zittelloceras	Mollusca	Cephalopoda	Oncocerida	Oncoceratidae

Table S2. Table showing taxa which have been characterized in the literature as good dispersers(*21*, *92–95*).

Model rank	ATC	BSZ	GRS	RTNB	RTP	STLT_5	df	AICc	delta	weight
1	0.14	-0.35	-0.44	-0.27	0.13	0.05	9	17152.60	0.00	0.86
2	0.13	-0.36	-0.45	-0.27	0.13	NA	8	17156.26	3.66	0.14
3	NA	-0.35	-0.45	-0.26	0.14	0.04	8	17171.70	19.10	0.00
4	NA	-0.36	-0.45	-0.26	0.13	NA	7	17174.81	22.21	0.00
5	0.15	-0.34	-0.46	-0.26	NA	0.05	8	17186.83	34.23	0.00
6	0.15	-0.34	-0.47	-0.26	NA	NA	7	17190.05	37.45	0.00
7	NA	-0.34	-0.47	-0.25	NA	0.04	7	17209.66	57.06	0.00
8	NA	-0.34	-0.48	-0.25	NA	NA	6	17212.27	59.67	0.00
9	0.12	-0.37	-0.59	NA	0.11	0.05	8	17255.06	102.46	0.00
10	0.12	-0.37	-0.60	NA	0.11	NA	7	17260.22	107.62	0.00
11	NA	-0.37	-0.60	NA	0.12	0.05	7	17271.00	118.40	0.00
12	NA	-0.37	-0.60	NA	0.12	NA	6	17275.59	122.99	0.00
13	0.14	-0.36	-0.60	NA	NA	0.05	7	17281.95	129.35	0.00
14	0.13	-0.36	-0.61	NA	NA	NA	6	17286.64	134.04	0.00
15	NA	-0.36	-0.61	NA	NA	0.05	6	17301.23	148.63	0.00
16	NA	-0.36	-0.62	NA	NA	NA	5	17305.27	152.67	0.00
17	0.14	NA	-0.45	-0.29	0.11	0.05	8	17308.94	156.34	0.00
18	0.14	NA	-0.46	-0.29	0.11	NA	7	17314.15	161.55	0.00
19	NA	NA	-0.46	-0.28	0.12	0.05	7	17328.76	176.17	0.00
20	NA	NA	-0.47	-0.28	0.12	NA	6	17333.39	180.79	0.00
21	0.15	NA	-0.47	-0.28	NA	0.05	7	17334.77	182.17	0.00
22	0.15	NA	-0.48	-0.28	NA	NA	6	17339.44	186.84	0.00
23	NA	NA	-0.48	-0.27	NA	0.05	6	17357.87	205.27	0.00
24	NA	NA	-0.49	-0.27	NA	NA	5	17361.88	209.28	0.00
25	0.13	NA	-0.62	NA	0.10	0.06	7	17427.94	275.34	0.00
26	0.12	NA	-0.63	NA	0.09	NA	6	17435.10	282.50	0.00
27	NA	NA	-0.62	NA	0.10	0.06	6	17444.32	291.72	0.00
28	0.13	NA	-0.63	NA	NA	0.06	6	17446.80	294.20	0.00
29	0.17	-0.38	NA	-0.53	0.18	0.08	8	17447.42	294.82	0.00
30	NA	NA	-0.63	NA	0.10	NA	5	17450.88	298.28	0.00
31	0.13	NA	-0.64	NA	NA	NA	5	17453.38	300.79	0.00
32	0.17	-0.38	NA	-0.54	0.18	NA	7	17463.86	311.26	0.00
33	NA	NA	-0.63	NA	NA	0.06	5	17466.00	313.40	0.00
34	NA	NA	-0.64	NA	NA	NA	4	17471.90	319.30	0.00
35	NA	-0.38	NA	-0.53	0.19	0.08	7	17478.77	326.18	0.00
36	NA	-0.38	NA	-0.54	0.18	NA	6	17494.35	341.75	0.00
37	0.18	-0.36	NA	-0.53	NA	0.08	7	17515.56	362.96	0.00
38	0.18	-0.36	NA	-0.54	NA	NA	6	17531.91	379.31	0.00
39	NA	-0.36	NA	-0.53	NA	0.08	6	17554.12	401.53	0.00
40	NA	-0.37	NA	-0.54	NA	NA	5	17569.42	416.82	0.00
41	0.17	NA	NA	-0.56	0.16	0.09	7	17627.79	475.19	0.00
42	0.17	NA	NA	-0.57	0.16	NA	6	17647.88	495.28	0.00
43	NA	NA	NA	-0.56	0.17	0.09	6	17660.54	507.94	0.00

44	NA	NA	NA	-0.57	0.17	NA	5	17679.77	527.17	0.00
45	0.19	NA	NA	-0.56	NA	0.09	6	17684.34	531.74	0.00
46	0.18	NA	NA	-0.57	NA	NA	5	17704.02	551.42	0.00
47	NA	NA	NA	-0.56	NA	0.09	5	17723.72	571.12	0.00
48	NA	NA	NA	-0.57	NA	NA	4	17742.33	589.73	0.00
49	0.17	-0.45	NA	NA	0.18	0.14	7	18065.83	913.24	0.00
50	NA	-0.45	NA	NA	0.19	0.14	6	18097.78	945.18	0.00
51	0.16	-0.46	NA	NA	0.18	NA	6	18118.00	965.40	0.00
52	0.19	-0.43	NA	NA	NA	0.14	6	18143.30	990.70	0.00
53	NA	-0.46	NA	NA	0.19	NA	5	18148.81	996.21	0.00
54	NA	-0.43	NA	NA	NA	0.14	5	18183.74	1031.14	0.00
55	0.18	-0.44	NA	NA	NA	NA	5	18196.27	1043.67	0.00
56	NA	-0.44	NA	NA	NA	NA	4	18235.34	1082.74	0.00
57	0.17	NA	NA	NA	0.17	0.15	6	18335.51	1182.91	0.00
58	NA	NA	NA	NA	0.18	0.15	5	18368.93	1216.33	0.00
59	0.17	NA	NA	NA	0.17	NA	5	18399.58	1246.98	0.00
60	0.19	NA	NA	NA	NA	0.15	5	18400.04	1247.44	0.00
61	NA	NA	NA	NA	0.17	NA	4	18431.93	1279.33	0.00
62	NA	NA	NA	NA	NA	0.15	4	18441.38	1288.79	0.00
63	0.18	NA	NA	NA	NA	NA	4	18464.19	1311.59	0.00
64	NA	NA	NA	NA	NA	NA	3	18504.23	1351.63	0.00

Table S3. Model selection results for the distance (grid cell steps) required to travel 5° latitude. ATC = Absolute temperature change, BSZ = Body size, GRS = Geographic range size, RTNB = Realized thermal niche breadth, RTP = Realized thermal preference, STLT = Distance to latitudinal threshold

Model rank	ATC	BSZ	GRS	RTNB	RTP	STLT_5	df	AICc	delta	weight
1	0.13	-0.35	-0.44	-0.27	0.13	0.04	9	17154.38	0.00	0.72
2	0.13	-0.36	-0.45	-0.27	0.13	NA	8	17156.26	1.88	0.28
3	NA	-0.35	-0.45	-0.26	0.13	0.04	8	17173.23	18.85	0.00
4	NA	-0.36	-0.45	-0.26	0.13	NA	7	17174.81	20.42	0.00
5	0.15	-0.34	-0.46	-0.26	NA	0.04	8	17186.98	32.59	0.00
6	0.15	-0.34	-0.47	-0.26	NA	NA	7	17190.05	35.67	0.00
7	NA	-0.34	-0.47	-0.25	NA	0.04	7	17209.53	55.14	0.00
8	NA	-0.34	-0.48	-0.25	NA	NA	6	17212.27	57.88	0.00
9	0.12	-0.37	-0.59	NA	0.11	0.04	8	17257.97	103.59	0.00
10	0.12	-0.37	-0.60	NA	0.11	NA	7	17260.22	105.83	0.00
11	NA	-0.37	-0.60	NA	0.12	0.04	7	17273.63	119.24	0.00
12	NA	-0.37	-0.60	NA	0.12	NA	6	17275.59	121.21	0.00
13	0.13	-0.36	-0.61	NA	NA	0.05	7	17283.28	128.90	0.00
14	0.13	-0.36	-0.61	NA	NA	NA	6	17286.64	132.25	0.00
15	NA	-0.36	-0.61	NA	NA	0.04	6	17302.21	147.83	0.00
16	NA	-0.36	-0.62	NA	NA	NA	5	17305.27	150.88	0.00
17	0.14	NA	-0.46	-0.29	0.11	0.04	8	17311.22	156.84	0.00
18	0.14	NA	-0.46	-0.29	0.11	NA	7	17314.15	159.77	0.00
19	NA	NA	-0.46	-0.28	0.11	0.04	7	17330.77	176.39	0.00
20	NA	NA	-0.47	-0.28	0.12	NA	6	17333.39	179.01	0.00
21	0.15	NA	-0.47	-0.28	NA	0.05	7	17335.44	181.05	0.00
22	0.15	NA	-0.48	-0.28	NA	NA	6	17339.44	185.06	0.00
23	NA	NA	-0.48	-0.27	NA	0.05	6	17358.20	203.82	0.00
24	NA	NA	-0.49	-0.27	NA	NA	5	17361.88	207.50	0.00
25	0.12	NA	-0.62	NA	0.09	0.05	7	17431.65	277.26	0.00
26	0.12	NA	-0.63	NA	0.09	NA	6	17435.10	280.72	0.00
27	NA	NA	-0.62	NA	0.10	0.05	6	17447.71	293.33	0.00
28	0.13	NA	-0.63	NA	NA	0.05	6	17448.97	294.59	0.00
29	NA	NA	-0.63	NA	0.10	NA	5	17450.88	296.50	0.00
30	0.17	-0.38	NA	-0.53	0.17	0.07	8	17452.60	298.21	0.00
31	0.13	NA	-0.64	NA	NA	NA	5	17453.38	299.00	0.00
32	0.17	-0.38	NA	-0.54	0.18	NA	7	17463.86	309.48	0.00
33	NA	NA	-0.64	NA	NA	0.05	5	17467.77	313.39	0.00
34	NA	NA	-0.64	NA	NA	NA	4	17471.90	317.52	0.00
35	NA	-0.38	NA	-0.53	0.18	0.07	7	17483.49	329.11	0.00
36	NA	-0.38	NA	-0.54	0.18	NA	6	17494.35	339.97	0.00

37	0.18	-0.36	NA	-0.53	NA	0.08	7	17516.81	362.42	0.00
38	0.18	-0.36	NA	-0.54	NA	NA	6	17531.91	377.52	0.00
39	NA	-0.36	NA	-0.53	NA	0.08	6	17554.71	400.32	0.00
40	NA	-0.37	NA	-0.54	NA	NA	5	17569.42	415.04	0.00
41	0.17	NA	NA	-0.56	0.16	0.08	7	17634.08	479.70	0.00
42	0.17	NA	NA	-0.57	0.16	NA	6	17647.88	493.50	0.00
43	NA	NA	NA	-0.56	0.16	0.08	6	17666.33	511.94	0.00
44	NA	NA	NA	-0.57	0.17	NA	5	17679.77	525.39	0.00
45	0.18	NA	NA	-0.56	NA	0.09	6	17686.72	532.33	0.00
46	0.18	NA	NA	-0.57	NA	NA	5	17704.02	549.64	0.00
47	NA	NA	NA	-0.56	NA	0.08	5	17725.34	570.96	0.00
48	NA	NA	NA	-0.57	NA	NA	4	17742.33	587.94	0.00
49	0.16	-0.45	NA	NA	0.18	0.11	7	18086.38	932.00	0.00
50	NA	-0.45	NA	NA	0.19	0.11	6	18117.60	963.21	0.00
51	0.16	-0.46	NA	NA	0.18	NA	6	18118.00	963.61	0.00
52	NA	-0.46	NA	NA	0.19	NA	5	18148.81	994.43	0.00
53	0.18	-0.44	NA	NA	NA	0.12	6	18157.90	1003.51	0.00
54	0.18	-0.44	NA	NA	NA	NA	5	18196.27	1041.89	0.00
55	NA	-0.44	NA	NA	NA	0.12	5	18197.20	1042.82	0.00
56	NA	-0.44	NA	NA	NA	NA	4	18235.34	1080.96	0.00
57	0.17	NA	NA	NA	0.16	0.12	6	18360.73	1206.34	0.00
58	NA	NA	NA	NA	0.17	0.12	5	18393.35	1238.96	0.00
59	0.17	NA	NA	NA	0.17	NA	5	18399.58	1245.19	0.00
60	0.18	NA	NA	NA	NA	0.13	5	18419.20	1264.81	0.00
61	NA	NA	NA	NA	0.17	NA	4	18431.93	1277.55	0.00
62	NA	NA	NA	NA	NA	0.13	4	18459.30	1304.91	0.00
63	0.18	NA	NA	NA	NA	NA	4	18464.19	1309.81	0.00
64	NA	NA	NA	NA	NA	NA	3	18504.23	1349.85	0.00

Table S4. Model selection results for the distance (grid cell steps) required to travel 10° latitude. ATC = Absolute temperature change, BSZ = Body size, GRS = Geographic range size, RTNB = Realized thermal niche breadth, RTP = Realized thermal preference, STLT = Distance to latitudinal threshold.

Model rank	ATC	BSZ	GRS	RTNB	RTP	STLT_5	df	AICc	delta	weight
1	0.13	-0.36	-0.44	-0.27	0.13	0.04	9	17110.63	0	0.72
2	0.13	-0.36	-0.45	-0.27	0.13	NA	8	17112.48	1.84	0.28
3	NA	-0.36	-0.45	-0.27	0.13	0.04	8	17129.31	18.67	0
4	NA	-0.36	-0.46	-0.27	0.14	NA	7	17130.74	20.1	0
5	0.15	-0.35	-0.46	-0.26	NA	0.05	8	17143.47	32.83	0
6	0.14	-0.35	-0.47	-0.26	NA	NA	7	17148.42	37.79	0
7	NA	-0.35	-0.47	-0.26	NA	0.05	7	17165.98	55.34	0
8	NA	-0.35	-0.48	-0.25	NA	NA	6	17170.48	59.84	0
9	0.12	-0.37	-0.6	NA	0.11	0.04	8	17216.08	105.44	0
10	0.12	-0.38	-0.6	NA	0.12	NA	7	17217.17	106.53	0
11	NA	-0.38	-0.6	NA	0.12	0.03	7	17231.59	120.95	0
12	NA	-0.38	-0.61	NA	0.12	NA	6	17232.35	121.72	0
13	0.13	-0.37	-0.61	NA	NA	0.05	7	17241.76	131.13	0
14	0.13	-0.36	-0.62	NA	NA	NA	6	17245.39	134.75	0
15	NA	-0.36	-0.62	NA	NA	0.05	6	17260.67	150.04	0
16	NA	-0.36	-0.62	NA	NA	NA	5	17263.96	153.32	0
17	0.14	NA	-0.46	-0.29	0.11	0.04	8	17270.03	159.39	0
18	0.14	NA	-0.46	-0.29	0.11	NA	7	17272.31	161.68	0
19	NA	NA	-0.47	-0.29	0.12	0.04	7	17289.51	178.88	0
20	NA	NA	-0.47	-0.28	0.12	NA	6	17291.37	180.74	0
21	0.15	NA	-0.47	-0.28	NA	0.05	7	17294.31	183.68	0
22	0.15	NA	-0.48	-0.28	NA	NA	6	17299.32	188.69	0
23	NA	NA	-0.48	-0.28	NA	0.05	6	17317.14	206.51	0
24	NA	NA	-0.49	-0.27	NA	NA	5	17321.72	211.08	0
25	0.12	NA	-0.63	NA	0.09	0.04	7	17392.75	282.11	0
26	0.12	NA	-0.63	NA	0.1	NA	6	17394.18	283.55	0
27	NA	NA	-0.63	NA	0.1	0.04	6	17408.79	298.15	0
28	NA	NA	-0.63	NA	0.1	NA	5	17409.89	299.25	0
29	0.13	NA	-0.64	NA	NA	0.05	6	17410.25	299.61	0
30	0.17	-0.38	NA	-0.54	0.17	0.07	8	17412.17	301.53	0
31	0.13	NA	-0.64	NA	NA	NA	5	17413.82	303.19	0
32	0.17	-0.38	NA	-0.54	0.18	NA	7	17421.5	310.86	0
33	NA	NA	-0.64	NA	NA	0.05	5	17429.14	318.51	0
34	NA	NA	-0.65	NA	NA	NA	4	17432.4	321.76	0
35	NA	-0.38	NA	-0.54	0.18	0.07	7	17443.03	332.4	0
36	NA	-0.38	NA	-0.54	0.19	NA	6	17451.66	341.03	0
37	0.18	-0.37	NA	-0.54	NA	0.09	7	17475.84	365.2	0
38	0.18	-0.37	NA	-0.54	NA	NA	6	17493.02	382.38	0
39	NA	-0.37	NA	-0.54	NA	0.09	6	17513.87	403.24	0

40	NA	-0.37	NA	-0.54	NA	NA	5	17530.45	419.81	0
41	0.17	NA	NA	-0.57	0.16	0.07	7	17596.57	485.93	0
42	0.17	NA	NA	-0.57	0.16	NA	6	17607.15	496.51	0
43	NA	NA	NA	-0.57	0.16	0.07	6	17628.97	518.34	0
44	NA	NA	NA	-0.57	0.17	NA	5	17638.84	528.21	0
45	0.18	NA	NA	-0.57	NA	0.09	6	17648.42	537.78	0
46	0.18	NA	NA	-0.57	NA	NA	5	17666.16	555.53	0
47	NA	NA	NA	-0.57	NA	0.09	5	17687.36	576.73	0
48	NA	NA	NA	-0.57	NA	NA	4	17704.55	593.91	0
49	0.17	-0.46	NA	NA	0.18	0.09	7	18061.04	950.4	0
50	0.16	-0.46	NA	NA	0.19	NA	6	18077.57	966.94	0
51	NA	-0.46	NA	NA	0.19	0.08	6	18092.59	981.95	0
52	NA	-0.46	NA	NA	0.2	NA	5	18108.28	997.65	0
53	0.18	-0.44	NA	NA	NA	0.11	6	18132.16	1021.52	0
54	0.18	-0.44	NA	NA	NA	NA	5	18159.27	1048.63	0
55	NA	-0.44	NA	NA	NA	0.11	5	18172.06	1061.43	0
56	NA	-0.44	NA	NA	NA	NA	4	18198.55	1087.92	0
57	0.17	NA	NA	NA	0.16	0.09	6	18341.55	1230.92	0
58	0.17	NA	NA	NA	0.17	NA	5	18360.71	1250.07	0
59	NA	NA	NA	NA	0.17	0.09	5	18374.86	1264.23	0
60	NA	NA	NA	NA	0.18	NA	4	18393.19	1282.56	0
61	0.19	NA	NA	NA	NA	0.11	5	18399.07	1288.44	0
62	0.18	NA	NA	NA	NA	NA	4	18427.94	1317.31	0
63	NA	NA	NA	NA	NA	0.11	4	18440.12	1329.49	0
64	NA	NA	NA	NA	NA	NA	3	18468.44	1357.8	0

Table S5. Model selection results for the distance (grid cell steps) required to travel 15° latitude. ATC = Absolute temperature change, BSZ = Body size, GRS = Geographic range size, RTNB = Realized thermal niche breadth, RTP = Realized thermal preference, STLT = Distance to latitudinal threshold.

Model rank	ATC	BSZ	GRS	RTNB	RTP	STLT_5	df	AICc	delta	weight
1	0.13	-0.36	-0.45	0.05	-0.27	0.19	9	16304.14	0.00	0.84
2	0.13	-0.36	-0.46	NA	-0.27	0.19	8	16307.52	3.38	0.16
3	NA	-0.36	-0.46	0.04	-0.27	0.19	8	16320.06	15.91	0.00
4	NA	-0.36	-0.46	NA	-0.27	0.19	7	16322.89	18.74	0.00
5	0.14	-0.35	-0.47	0.05	-0.25	NA	8	16346.49	42.35	0.00
6	0.14	-0.35	-0.48	NA	-0.26	NA	7	16349.82	45.67	0.00
7	NA	-0.35	-0.48	0.04	-0.25	NA	7	16364.29	60.15	0.00
8	NA	-0.35	-0.49	NA	-0.25	NA	6	16367.03	62.89	0.00
9	0.12	-0.37	-0.60	0.05	NA	0.16	8	16396.72	92.58	0.00
10	0.12	-0.37	-0.61	NA	NA	0.16	7	16401.77	97.62	0.00
11	NA	-0.37	-0.61	0.05	NA	0.17	7	16409.15	105.00	0.00
12	NA	-0.37	-0.61	NA	NA	0.17	6	16413.63	109.48	0.00
13	0.13	-0.36	-0.61	0.05	NA	NA	7	16427.84	123.69	0.00
14	0.13	-0.37	-0.62	NA	NA	NA	6	16432.72	128.57	0.00
15	NA	-0.36	-0.62	0.05	NA	NA	6	16442.10	137.95	0.00
16	NA	-0.37	-0.63	NA	NA	NA	5	16446.37	142.23	0.00
17	0.13	NA	-0.46	0.05	-0.29	0.17	8	16455.22	151.07	0.00
18	0.13	NA	-0.47	NA	-0.29	0.17	7	16459.76	155.62	0.00
19	NA	NA	-0.47	0.05	-0.29	0.18	7	16471.43	167.28	0.00
20	NA	NA	-0.48	NA	-0.29	0.18	6	16475.40	171.25	0.00
21	0.14	NA	-0.48	0.05	-0.27	NA	7	16490.86	186.72	0.00
22	0.14	NA	-0.49	NA	-0.28	NA	6	16495.30	191.16	0.00
23	NA	NA	-0.49	0.05	-0.27	NA	6	16508.85	204.71	0.00
24	NA	NA	-0.50	NA	-0.27	NA	5	16512.67	208.53	0.00
25	0.12	NA	-0.63	0.06	NA	0.14	7	16563.77	259.63	0.00
26	0.12	NA	-0.64	NA	NA	0.14	6	16570.41	266.27	0.00
27	NA	NA	-0.63	0.06	NA	0.15	6	16576.16	272.02	0.00
28	NA	NA	-0.64	NA	NA	0.15	5	16582.22	278.07	0.00
29	0.13	NA	-0.64	0.06	NA	NA	6	16588.29	284.15	0.00
30	0.18	-0.38	NA	0.08	-0.55	0.26	8	16591.13	286.99	0.00
31	0.12	NA	-0.65	NA	NA	NA	5	16594.70	290.56	0.00
32	NA	NA	-0.64	0.06	NA	NA	5	16602.37	298.22	0.00

33	0.17	-0.38	NA	NA	-0.56	0.26	7	16605.89	301.75	0.00
34	NA	NA	-0.65	NA	NA	NA	4	16608.15	304.01	0.00
35	NA	-0.38	NA	0.08	-0.55	0.26	7	16620.86	316.71	0.00
36	NA	-0.38	NA	NA	-0.56	0.26	6	16634.71	330.56	0.00
37	0.19	-0.36	NA	0.08	-0.55	NA	7	16672.13	367.99	0.00
38	0.18	-0.37	NA	NA	-0.56	NA	6	16688.04	383.89	0.00
39	NA	-0.37	NA	0.08	-0.55	NA	6	16706.18	402.04	0.00
40	NA	-0.37	NA	NA	-0.56	NA	5	16721.07	416.93	0.00
41	0.18	NA	NA	0.09	-0.58	0.24	7	16763.57	459.43	0.00
42	0.17	NA	NA	NA	-0.59	0.24	6	16781.03	476.89	0.00
43	NA	NA	NA	0.09	-0.58	0.25	6	16794.20	490.06	0.00
44	NA	NA	NA	NA	-0.59	0.25	5	16810.76	506.62	0.00
45	0.19	NA	NA	0.09	-0.58	NA	6	16835.88	531.74	0.00
46	0.19	NA	NA	NA	-0.59	NA	5	16854.34	550.20	0.00
47	NA	NA	NA	0.09	-0.58	NA	5	16870.70	566.56	0.00
48	NA	NA	NA	NA	-0.59	NA	4	16888.14	583.99	0.00
49	0.17	-0.45	NA	0.14	NA	0.24	7	17191.45	887.30	0.00
50	NA	-0.45	NA	0.14	NA	0.25	6	17221.28	917.14	0.00
51	0.17	-0.46	NA	NA	NA	0.24	6	17241.90	937.75	0.00
52	0.18	-0.44	NA	0.14	NA	NA	6	17268.22	964.08	0.00
53	NA	-0.46	NA	NA	NA	0.25	5	17270.55	966.41	0.00
54	NA	-0.44	NA	0.14	NA	NA	5	17302.85	998.71	0.00
55	0.18	-0.45	NA	NA	NA	NA	5	17320.82	1016.67	0.00
56	NA	-0.45	NA	NA	NA	NA	4	17354.21	1050.06	0.00
57	0.17	NA	NA	0.15	NA	0.22	6	17450.42	1146.27	0.00
58	NA	NA	NA	0.15	NA	0.23	5	17481.13	1176.99	0.00
59	0.17	NA	NA	NA	NA	0.23	5	17511.01	1206.86	0.00
60	0.19	NA	NA	0.16	NA	NA	5	17518.32	1214.17	0.00
61	NA	NA	NA	NA	NA	0.23	4	17540.60	1236.45	0.00
62	NA	NA	NA	0.15	NA	NA	4	17553.82	1249.67	0.00
63	0.18	NA	NA	NA	NA	NA	4	17580.78	1276.64	0.00
64	NA	NA	NA	NA	NA	NA	3	17615.10	1310.95	0.00

Table S6. Model selection results for the distance (grid cell steps) required to travel 5° latitude with no polar occurrences. ATC = Absolute temperature change, BSZ = Body size, GRS = Geographic range size, RTNB = Realized thermal niche breadth, RTP = Realized thermal preference, STLT = Distance to latitudinal threshold.

Model rank	ATC	BSZ	GRS	RTNB	RTP	STLT_5	df	AICc	delta	weight
1	0.12	-0.22	-0.37	0.05	-0.21	0.12	10	15506.78	0.00	0.83
2	0.11	-0.22	-0.38	NA	-0.21	0.12	9	15510.03	3.24	0.16
3	NA	-0.22	-0.38	0.05	-0.21	0.13	9	15518.93	12.15	0.00
4	NA	-0.23	-0.38	NA	-0.21	0.13	8	15521.78	15.00	0.00
5	0.13	-0.21	-0.39	0.05	-0.20	NA	9	15534.91	28.13	0.00
6	0.12	-0.21	-0.40	NA	-0.20	NA	8	15537.69	30.91	0.00
7	NA	-0.21	-0.40	0.04	-0.19	NA	8	15550.00	43.21	0.00
8	NA	-0.21	-0.40	NA	-0.20	NA	7	15552.33	45.54	0.00
9	0.12	NA	-0.38	0.05	-0.22	0.11	9	15559.65	52.87	0.00
10	0.11	-0.23	-0.48	0.05	NA	0.11	9	15560.67	53.88	0.00
11	0.11	NA	-0.38	NA	-0.22	0.11	8	15563.97	57.19	0.00
12	0.11	-0.24	-0.49	NA	NA	0.11	8	15564.95	58.16	0.00
13	NA	-0.23	-0.49	0.05	NA	0.12	8	15570.83	64.05	0.00
14	NA	NA	-0.38	0.05	-0.21	0.12	8	15572.06	65.28	0.00
15	NA	-0.24	-0.50	NA	NA	0.12	7	15574.70	67.92	0.00
16	NA	NA	-0.39	NA	-0.22	0.12	7	15575.96	69.18	0.00
17	0.13	NA	-0.40	0.05	-0.21	NA	8	15582.80	76.02	0.00
18	0.12	-0.22	-0.50	0.05	NA	NA	8	15583.45	76.67	0.00
19	0.12	NA	-0.40	NA	-0.21	NA	7	15586.59	79.81	0.00
20	0.12	-0.22	-0.51	NA	NA	NA	7	15587.23	80.45	0.00
21	NA	-0.22	-0.50	0.05	NA	NA	7	15596.22	89.44	0.00
22	NA	NA	-0.40	0.05	-0.20	NA	7	15597.93	91.14	0.00
23	NA	-0.22	-0.51	NA	NA	NA	6	15599.53	92.75	0.00
24	NA	NA	-0.41	NA	-0.21	NA	6	15601.22	94.44	0.00
25	0.11	NA	-0.50	0.06	NA	0.10	8	15618.98	112.20	0.00
26	0.11	NA	-0.51	NA	NA	0.10	7	15624.55	117.77	0.00
27	NA	NA	-0.50	0.06	NA	0.10	7	15629.34	122.56	0.00
28	NA	NA	-0.51	NA	NA	0.10	6	15634.46	127.68	0.00

29	0.12	NA	-0.51	0.06	NA	NA	7	15636.85	130.07	0.00
30	0.11	NA	-0.52	NA	NA	NA	6	15641.85	135.06	0.00
31	NA	NA	-0.51	0.05	NA	NA	6	15649.56	142.78	0.00
32	NA	NA	-0.52	NA	NA	NA	5	15654.04	147.26	0.00
33	0.14	-0.24	NA	0.08	-0.43	0.16	9	15689.82	183.04	0.00
34	0.14	-0.24	NA	NA	-0.44	0.16	8	15701.75	194.97	0.00
35	NA	-0.24	NA	0.08	-0.43	0.17	8	15709.67	202.88	0.00
36	NA	-0.24	NA	NA	-0.44	0.17	7	15721.07	214.29	0.00
37	0.16	-0.23	NA	0.08	-0.43	NA	8	15742.32	235.53	0.00
38	0.14	NA	NA	0.08	-0.44	0.15	8	15752.35	245.57	0.00
39	0.16	-0.23	NA	NA	-0.44	NA	7	15753.95	247.17	0.00
40	0.14	NA	NA	NA	-0.45	0.15	7	15766.46	259.68	0.00
41	NA	-0.23	NA	0.07	-0.43	NA	7	15767.62	260.84	0.00
42	NA	NA	NA	0.08	-0.44	0.16	7	15772.65	265.87	0.00
43	NA	-0.23	NA	NA	-0.44	NA	6	15778.60	271.82	0.00
44	NA	NA	NA	NA	-0.45	0.16	6	15786.19	279.41	0.00
45	0.16	NA	NA	0.08	-0.44	NA	7	15798.09	291.31	0.00
46	0.16	NA	NA	NA	-0.45	NA	6	15811.72	304.94	0.00
47	NA	NA	NA	0.08	-0.44	NA	6	15823.56	316.77	0.00
48	NA	NA	NA	NA	-0.45	NA	5	15836.49	329.71	0.00
49	0.14	-0.29	NA	0.12	NA	0.17	8	16031.29	524.50	0.00
50	NA	-0.29	NA	0.12	NA	0.17	7	16050.98	544.20	0.00
51	0.14	-0.29	NA	NA	NA	0.17	7	16063.51	556.73	0.00
52	NA	-0.29	NA	NA	NA	0.17	6	16082.49	575.71	0.00
53	0.16	-0.27	NA	0.12	NA	NA	7	16087.48	580.70	0.00
54	NA	-0.27	NA	0.12	NA	NA	6	16112.89	606.11	0.00
55	0.15	-0.28	NA	NA	NA	NA	6	16119.54	612.76	0.00
56	0.14	NA	NA	0.13	NA	0.15	7	16124.14	617.36	0.00
57	NA	-0.28	NA	NA	NA	NA	5	16144.07	637.29	0.00
58	NA	NA	NA	0.13	NA	0.16	6	16144.39	637.61	0.00
59	0.14	NA	NA	NA	NA	0.15	6	16161.80	655.02	0.00
60	0.16	NA	NA	0.13	NA	NA	6	16172.21	665.43	0.00
61	NA	NA	NA	NA	NA	0.16	5	16181.29	674.50	0.00
62	NA	NA	NA	0.12	NA	NA	5	16197.86	691.07	0.00
63	0.15	NA	NA	NA	NA	NA	5	16209.34	702.56	0.00
64	NA	NA	NA	NA	NA	NA	4	16234.04	727.26	0.00

Table S7. Model selection results for the distance (grid cell steps) required to travel 5° latitude with number of species per genera as a random effect. ATC = Absolute temperature change, BSZ = Body size, GRS = Geographic range size, RTNB = Realized thermal niche breadth, RTP = Realized thermal preference, STLT = Distance to latitudinal threshold.

Model Rank	ATC	BSZ	GRZ	STLT	RTNB	RTP	MASS	MASS:STLT	df	AICc	delta	weight
1	0.13	-0.35	-0.44	0.05	-0.27	0.13	+	NA	10	17143.31	0.00	0.65
2	0.13	-0.35	-0.44	0.05	-0.27	0.13	+	+	11	17145.29	1.98	0.24
3	0.13	-0.35	-0.45	NA	-0.27	0.13	+	NA	9	17147.15	3.84	0.10
4	0.14	-0.35	-0.44	0.05	-0.27	0.13	NA	NA	9	17152.60	9.29	0.01
5	0.13	-0.36	-0.45	NA	-0.27	0.13	NA	NA	8	17156.26	12.95	0.00
6	NA	-0.35	-0.45	0.05	-0.26	0.14	+	NA	9	17161.48	18.18	0.00
7	NA	-0.35	-0.45	0.05	-0.26	0.14	+	+	10	17163.41	20.10	0.00
8	NA	-0.35	-0.45	NA	-0.26	0.13	+	NA	8	17164.79	21.48	0.00
9	NA	-0.35	-0.45	0.04	-0.26	0.14	NA	NA	8	17171.70	28.39	0.00
10	NA	-0.36	-0.45	NA	-0.26	0.13	NA	NA	7	17174.81	31.50	0.00
11	0.14	-0.34	-0.46	0.05	-0.26	NA	+	NA	9	17178.13	34.83	0.00
12	0.14	-0.34	-0.46	0.04	-0.26	NA	+	+	10	17180.09	36.78	0.00

13	0.14	-0.34	-0.47	NA	-0.26	NA	+	NA	8	17181.52	38.22	0.00
14	0.15	-0.34	-0.46	0.05	-0.26	NA	NA	NA	8	17186.83	43.52	0.00
15	0.15	-0.34	-0.47	NA	-0.26	NA	NA	NA	7	17190.05	46.75	0.00
16	NA	-0.34	-0.47	0.04	-0.25	NA	+	NA	8	17200.04	56.73	0.00
17	NA	-0.34	-0.47	0.04	-0.25	NA	+	+	9	17202.04	58.73	0.00
18	NA	-0.34	-0.47	NA	-0.25	NA	+	NA	7	17202.83	59.52	0.00
19	NA	-0.34	-0.47	0.04	-0.25	NA	NA	NA	7	17209.66	66.35	0.00
20	NA	-0.34	-0.48	NA	-0.25	NA	NA	NA	6	17212.27	68.96	0.00
21	0.12	-0.37	-0.59	0.05	NA	0.12	+	NA	9	17245.66	102.36	0.00
22	0.12	-0.37	-0.59	0.06	NA	0.12	+	+	10	17247.61	104.31	0.00
23	0.12	-0.37	-0.60	NA	NA	0.11	+	NA	8	17251.02	107.72	0.00
24	0.12	-0.37	-0.59	0.05	NA	0.11	NA	NA	8	17255.06	111.75	0.00
25	0.12	-0.37	-0.60	NA	NA	0.11	NA	NA	7	17260.22	116.91	0.00
26	NA	-0.37	-0.59	0.05	NA	0.12	+	NA	8	17260.73	117.42	0.00
27	NA	-0.37	-0.59	0.05	NA	0.12	+	+	9	17262.60	119.30	0.00
28	NA	-0.37	-0.60	NA	NA	0.12	+	NA	7	17265.54	122.23	0.00
29	NA	-0.37	-0.60	0.05	NA	0.12	NA	NA	7	17271.00	127.70	0.00
30	0.13	-0.36	-0.60	0.05	NA	NA	+	NA	8	17273.06	129.75	0.00
31	0.13	-0.36	-0.60	0.05	NA	NA	+	+	9	17275.05	131.75	0.00
32	NA	-0.37	-0.60	NA	NA	0.12	NA	NA	6	17275.59	132.28	0.00
33	0.13	-0.36	-0.61	NA	NA	NA	+	NA	7	17277.93	134.63	0.00
34	0.14	-0.36	-0.60	0.05	NA	NA	NA	NA	7	17281.95	138.64	0.00
35	0.13	-0.36	-0.61	NA	NA	NA	NA	NA	6	17286.64	143.33	0.00
36	NA	-0.36	-0.61	0.05	NA	NA	+	NA	7	17291.44	148.13	0.00
37	NA	-0.36	-0.61	0.05	NA	NA	+	+	8	17293.44	150.13	0.00
38	NA	-0.36	-0.62	NA	NA	NA	+	NA	6	17295.68	152.38	0.00
39	0.13	NA	-0.45	0.05	-0.29	0.11	+	NA	9	17298.76	155.45	0.00
40	0.13	NA	-0.45	0.06	-0.29	0.11	+	+	10	17300.71	157.41	0.00
41	NA	-0.36	-0.61	0.05	NA	NA	NA	NA	6	17301.23	157.92	0.00
42	0.13	NA	-0.46	NA	-0.29	0.11	+	NA	8	17304.17	160.86	0.00
43	NA	-0.36	-0.62	NA	NA	NA	NA	NA	5	17305.27	161.96	0.00
44	0.14	NA	-0.45	0.05	-0.29	0.11	NA	NA	8	17308.94	165.63	0.00
45	0.14	NA	-0.46	NA	-0.29	0.11	NA	NA	7	17314.15	170.84	0.00
46	NA	NA	-0.46	0.05	-0.28	0.12	+	NA	8	17317.60	174.30	0.00
47	NA	NA	-0.46	0.05	-0.28	0.12	+	+	9	17319.48	176.17	0.00
48	NA	NA	-0.47	NA	-0.28	0.12	+	NA	7	17322.45	179.14	0.00
49	0.14	NA	-0.47	0.05	-0.28	NA	+	NA	8	17325.14	181.83	0.00
50	0.14	NA	-0.47	0.05	-0.28	NA	+	+	9	17327.13	183.82	0.00
51	NA	NA	-0.46	0.05	-0.28	0.12	NA	NA	7	17328.76	185.46	0.00
52	0.14	NA	-0.48	NA	-0.28	NA	+	NA	7	17330.00	186.69	0.00

53	NA	NA	-0.47	NA	-0.28	0.12	NA	NA	6	17333.39	190.08	0.00
54	0.15	NA	-0.47	0.05	-0.28	NA	NA	NA	7	17334.77	191.46	0.00
55	0.15	NA	-0.48	NA	-0.28	NA	NA	NA	6	17339.44	196.14	0.00
56	NA	NA	-0.48	0.05	-0.27	NA	+	NA	7	17347.25	203.94	0.00
57	NA	NA	-0.48	0.05	-0.27	NA	+	+	8	17349.25	205.94	0.00
58	NA	NA	-0.49	NA	-0.27	NA	+	NA	6	17351.47	208.16	0.00
59	NA	NA	-0.48	0.05	-0.27	NA	NA	NA	6	17357.87	214.56	0.00
60	NA	NA	-0.49	NA	-0.27	NA	NA	NA	5	17361.88	218.57	0.00
61	0.12	NA	-0.62	0.06	NA	0.10	+	NA	8	17417.62	274.32	0.00
62	0.12	NA	-0.62	0.06	NA	0.10	+	+	9	17419.52	276.22	0.00
63	0.12	NA	-0.63	NA	NA	0.10	+	NA	7	17425.00	281.70	0.00
64	0.13	NA	-0.62	0.06	NA	0.10	NA	NA	7	17427.94	284.63	0.00
65	NA	NA	-0.62	0.06	NA	0.10	+	NA	7	17433.07	289.76	0.00
66	NA	NA	-0.62	0.06	NA	0.10	+	+	8	17434.87	291.56	0.00
67	0.12	NA	-0.63	NA	NA	0.09	NA	NA	6	17435.10	291.79	0.00
68	0.13	NA	-0.63	0.06	NA	NA	+	NA	7	17436.91	293.61	0.00
69	0.16	-0.37	NA	0.08	-0.53	0.18	+	NA	9	17438.09	294.78	0.00
70	0.13	NA	-0.63	0.06	NA	NA	+	+	8	17438.91	295.61	0.00
71	NA	NA	-0.63	NA	NA	0.10	+	NA	6	17439.87	296.56	0.00
72	0.16	-0.37	NA	0.08	-0.53	0.18	+	+	10	17440.09	296.78	0.00
73	0.13	NA	-0.64	NA	NA	NA	+	NA	6	17443.71	300.41	0.00
74	NA	NA	-0.62	0.06	NA	0.10	NA	NA	6	17444.32	301.02	0.00
75	0.13	NA	-0.63	0.06	NA	NA	NA	NA	6	17446.80	303.49	0.00
76	0.17	-0.38	NA	0.08	-0.53	0.18	NA	NA	8	17447.42	304.11	0.00
77	NA	NA	-0.63	NA	NA	0.10	NA	NA	5	17450.88	307.57	0.00
78	0.13	NA	-0.64	NA	NA	NA	NA	NA	5	17453.38	310.08	0.00
79	0.16	-0.38	NA	NA	-0.54	0.18	+	NA	8	17454.87	311.56	0.00
80	NA	NA	-0.63	0.06	NA	NA	+	NA	6	17455.16	311.85	0.00
81	NA	NA	-0.63	0.06	NA	NA	+	+	7	17457.13	313.83	0.00
82	NA	NA	-0.64	NA	NA	NA	+	NA	5	17461.30	317.99	0.00
83	0.17	-0.38	NA	NA	-0.54	0.18	NA	NA	7	17463.86	320.55	0.00
84	NA	NA	-0.63	0.06	NA	NA	NA	NA	5	17466.00	322.69	0.00
85	NA	-0.38	NA	0.08	-0.53	0.19	+	NA	8	17468.15	324.84	0.00
86	NA	-0.38	NA	0.08	-0.53	0.19	+	+	9	17470.13	326.82	0.00
87	NA	NA	-0.64	NA	NA	NA	NA	NA	4	17471.90	328.59	0.00
88	NA	-0.38	NA	0.08	-0.53	0.19	NA	NA	7	17478.77	335.47	0.00
89	NA	-0.38	NA	NA	-0.54	0.19	+	NA	7	17484.10	340.79	0.00
90	NA	-0.38	NA	NA	-0.54	0.18	NA	NA	6	17494.35	351.05	0.00
91	0.18	-0.36	NA	0.08	-0.53	NA	+	NA	8	17507.16	363.85	0.00
92	0.18	-0.36	NA	0.08	-0.53	NA	+	+	9	17508.89	365.58	0.00
93	0.18	-0.36	NA	0.08	-0.53	NA	NA	NA	7	17515.56	372.25	0.00
94	0.18	-0.36	NA	NA	-0.54	NA	+	NA	7	17523.84	380.54	0.00
95	0.18	-0.36	NA	NA	-0.54	NA	NA	NA	6	17531.91	388.60	0.00
96	NA	-0.36	NA	0.08	-0.53	NA	+	NA	7	17544.44	401.13	0.00
97	NA	-0.36	NA	0.08	-0.53	NA	+	+	8	17546.33	403.02	0.00
98	NA	-0.36	NA	0.08	-0.53	NA	NA	NA	6	17554.12	410.82	0.00
99	NA	-0.36	NA	NA	-0.54	NA	+	NA	6	17560.11	416.81	0.00

100	NA	-0.37	NA	NA	-0.54	NA	NA	NA	5	17569.42	426.11	0.00
101	0.17	NA	NA	0.09	-0.56	0.16	+	NA	8	17617.43	474.13	0.00
102	0.17	NA	NA	0.09	-0.56	0.16	+	+	9	17619.43	476.13	0.00
103	0.17	NA	NA	0.09	-0.56	0.16	NA	NA	7	17627.79	484.48	0.00
104	0.16	NA	NA	NA	-0.57	0.16	+	NA	7	17637.89	494.58	0.00
105	0.17	NA	NA	NA	-0.57	0.16	NA	NA	6	17647.88	504.58	0.00
106	NA	NA	NA	0.09	-0.56	0.17	+	NA	7	17648.78	505.48	0.00
107	NA	NA	NA	0.09	-0.56	0.17	+	+	8	17650.72	507.42	0.00
108	NA	NA	NA	0.09	-0.56	0.17	NA	NA	6	17660.54	517.24	0.00
109	NA	NA	NA	NA	-0.57	0.17	+	NA	6	17668.41	525.10	0.00
110	0.18	NA	NA	0.09	-0.56	NA	+	NA	7	17674.87	531.56	0.00
111	0.18	NA	NA	0.09	-0.56	NA	+	+	8	17676.72	533.41	0.00
112	NA	NA	NA	NA	-0.57	0.17	NA	NA	5	17679.77	536.46	0.00
113	0.19	NA	NA	0.09	-0.56	NA	NA	NA	6	17684.34	541.04	0.00
114	0.18	NA	NA	NA	-0.57	NA	+	NA	6	17694.90	551.60	0.00
115	0.18	NA	NA	NA	-0.57	NA	NA	NA	5	17704.02	560.71	0.00
116	NA	NA	NA	0.09	-0.56	NA	+	NA	6	17712.85	569.54	0.00
117	NA	NA	NA	0.09	-0.56	NA	+	+	7	17714.81	571.50	0.00
118	NA	NA	NA	0.09	-0.56	NA	NA	NA	5	17723.72	580.41	0.00
119	NA	NA	NA	NA	-0.57	NA	+	NA	5	17731.86	588.56	0.00
120	NA	NA	NA	NA	-0.57	NA	NA	NA	4	17742.33	599.02	0.00
121	0.16	-0.45	NA	0.14	NA	0.19	+	NA	8	18056.16	912.85	0.00
122	0.16	-0.45	NA	0.14	NA	0.19	+	+	9	18058.14	914.83	0.00
123	0.17	-0.45	NA	0.14	NA	0.18	NA	NA	7	18065.83	922.53	0.00
124	NA	-0.45	NA	0.14	NA	0.19	+	NA	7	18086.49	943.18	0.00
125	NA	-0.45	NA	0.14	NA	0.19	+	+	8	18088.40	945.09	0.00
126	NA	-0.45	NA	0.14	NA	0.19	NA	NA	6	18097.78	954.47	0.00
127	0.16	-0.45	NA	NA	NA	0.18	+	NA	7	18108.91	965.60	0.00
128	0.16	-0.46	NA	NA	NA	0.18	NA	NA	6	18118.00	974.69	0.00
129	0.18	-0.43	NA	0.14	NA	NA	+	NA	7	18134.46	991.15	0.00
130	0.18	-0.43	NA	0.14	NA	NA	+	+	8	18136.32	993.02	0.00
131	NA	-0.46	NA	NA	NA	0.19	+	NA	6	18138.18	994.87	0.00
132	0.19	-0.43	NA	0.14	NA	NA	NA	NA	6	18143.30	999.99	0.00
133	NA	-0.46	NA	NA	NA	0.19	NA	NA	5	18148.81	1005.51	0.00
134	NA	-0.43	NA	0.14	NA	NA	+	NA	6	18173.19	1029.88	0.00
135	NA	-0.43	NA	0.14	NA	NA	+	+	7	18175.16	1031.85	0.00
136	NA	-0.43	NA	0.14	NA	NA	NA	NA	5	18183.74	1040.43	0.00
137	0.18	-0.44	NA	NA	NA	NA	+	NA	6	18188.04	1044.73	0.00
138	0.18	-0.44	NA	NA	NA	NA	NA	NA	5	18196.27	1052.96	0.00
139	NA	-0.44	NA	NA	NA	NA	+	NA	5	18225.48	1082.18	0.00
140	NA	-0.44	NA	NA	NA	NA	NA	NA	4	18235.34	1092.03	0.00
141	0.16	NA	NA	0.15	NA	0.17	+	NA	7	18324.53	1181.22	0.00
142	0.16	NA	NA	0.16	NA	0.17	+	+	8	18326.45	1183.14	0.00
143	0.17	NA	NA	0.15	NA	0.17	NA	NA	6	18335.51	1192.21	0.00
144	NA	NA	NA	0.15	NA	0.18	+	NA	6	18356.15	1212.84	0.00
145	NA	NA	NA	0.16	NA	0.18	+	+	7	18357.94	1214.63	0.00

146	NA	NA	NA	0.15	NA	0.18	NA	NA	5	18368.93	1225.62	0.00
147	0.16	NA	NA	NA	NA	0.17	+	NA	6	18389.19	1245.89	0.00
148	0.18	NA	NA	0.15	NA	NA	+	NA	6	18389.80	1246.50	0.00
149	0.18	NA	NA	0.15	NA	NA	+	+	7	18391.77	1248.47	0.00
150	0.17	NA	NA	NA	NA	0.17	NA	NA	5	18399.58	1256.27	0.00
151	0.19	NA	NA	0.15	NA	NA	NA	NA	5	18400.04	1256.73	0.00
152	NA	NA	NA	NA	NA	0.17	+	NA	5	18419.82	1276.51	0.00
153	NA	NA	NA	0.15	NA	NA	+	NA	5	18429.24	1285.94	0.00
154	NA	NA	NA	0.15	NA	NA	+	+	6	18431.25	1287.94	0.00
155	NA	NA	NA	NA	NA	0.17	NA	NA	4	18431.93	1288.63	0.00
156	NA	NA	NA	0.15	NA	NA	NA	NA	4	18441.38	1298.08	0.00
157	0.18	NA	NA	NA	NA	NA	+	NA	5	18454.58	1311.27	0.00
158	0.18	NA	NA	NA	NA	NA	NA	NA	4	18464.19	1320.89	0.00
159	NA	NA	NA	NA	NA	NA	+	NA	4	18492.80	1349.49	0.00
160	NA	NA	NA	NA	NA	NA	NA	NA	3	18504.23	1360.92	0.00

Table S8. Model selection results for the distance (grid cell steps) required to travel 5° latitude with mass extinctions added as an interaction term. ATC = Absolute temperature change, BSZ = Body size, GRS = Geographic range size, RTNB = Realized thermal niche breadth, RTP = Realized thermal preference, STLT = Distance to latitudinal threshold, MASS = Mass extinctions, MASS:STLT = Interaction between mass extinctions and distance to latitudinal threshold.

Model Rank	ATC	BSZ	GRZ	STLT	RTNB	RTP	HYP	HYP:STLT	df	AICc	delta	weight
1	0.13	-0.35	-0.44	-0.05	-0.27	0.13	+	+	11	17149.26	0.00	0.48
2	0.13	-0.35	-0.44	0.05	-0.27	0.13	+	NA	10	17149.83	0.57	0.36
3	0.14	-0.35	-0.44	0.05	-0.27	0.13	NA	NA	9	17152.60	3.34	0.09
4	0.13	-0.36	-0.45	NA	-0.27	0.13	+	NA	9	17153.59	4.33	0.06
5	0.13	-0.36	-0.45	NA	-0.27	0.13	NA	NA	8	17156.26	7.00	0.01
6	NA	-0.35	-0.45	-0.06	-0.26	0.14	+	+	10	17167.88	18.62	0.00
7	NA	-0.35	-0.45	0.05	-0.26	0.13	+	NA	9	17168.70	19.44	0.00
8	NA	-0.35	-0.45	0.04	-0.26	0.14	NA	NA	8	17171.70	22.43	0.00
9	NA	-0.36	-0.45	NA	-0.26	0.13	+	NA	8	17171.91	22.65	0.00

10	NA	-0.36	-0.45	NA	-0.26	0.13	NA	NA	7	17174.81	25.54	0.00
11	0.15	-0.34	-0.46	0.05	-0.26	NA	+	NA	9	17183.96	34.69	0.00
12	0.15	-0.34	-0.46	-0.03	-0.26	NA	+	+	10	17184.44	35.18	0.00
13	0.15	-0.34	-0.46	0.05	-0.26	NA	NA	NA	8	17186.83	37.57	0.00
14	0.14	-0.34	-0.47	NA	-0.26	NA	+	NA	8	17187.28	38.02	0.00
15	0.15	-0.34	-0.47	NA	-0.26	NA	NA	NA	7	17190.05	40.79	0.00
16	NA	-0.34	-0.47	0.04	-0.25	NA	+	NA	8	17206.55	57.29	0.00
17	NA	-0.34	-0.47	-0.04	-0.25	NA	+	+	9	17206.86	57.60	0.00
18	NA	-0.34	-0.47	NA	-0.25	NA	+	NA	7	17209.26	59.99	0.00
19	NA	-0.34	-0.47	0.04	-0.25	NA	NA	NA	7	17209.66	60.40	0.00
20	NA	-0.34	-0.48	NA	-0.25	NA	NA	NA	6	17212.27	63.00	0.00
21	0.12	-0.37	-0.59	-0.03	NA	0.12	+	+	10	17252.59	103.33	0.00
22	0.12	-0.37	-0.59	0.05	NA	0.11	+	NA	9	17252.63	103.37	0.00
23	0.12	-0.37	-0.59	0.05	NA	0.11	NA	NA	8	17255.06	105.79	0.00
24	0.12	-0.37	-0.60	NA	NA	0.11	+	NA	8	17257.90	108.64	0.00
25	0.12	-0.37	-0.60	NA	NA	0.11	NA	NA	7	17260.22	110.95	0.00
26	NA	-0.37	-0.60	-0.04	NA	0.12	+	+	9	17268.11	118.85	0.00
27	NA	-0.37	-0.60	0.05	NA	0.12	+	NA	8	17268.37	119.11	0.00
28	NA	-0.37	-0.60	0.05	NA	0.12	NA	NA	7	17271.00	121.74	0.00
29	NA	-0.37	-0.60	NA	NA	0.12	+	NA	7	17273.07	123.81	0.00
30	NA	-0.37	-0.60	NA	NA	0.12	NA	NA	6	17275.59	126.33	0.00
31	0.13	-0.36	-0.60	0.05	NA	NA	+	NA	8	17279.40	130.14	0.00
32	0.13	-0.36	-0.60	-0.02	NA	NA	+	+	9	17280.18	130.92	0.00
33	0.14	-0.36	-0.60	0.05	NA	NA	NA	NA	7	17281.95	132.69	0.00
34	0.13	-0.36	-0.61	NA	NA	NA	+	NA	7	17284.20	134.94	0.00
35	0.13	-0.36	-0.61	NA	NA	NA	NA	NA	6	17286.64	137.37	0.00
36	NA	-0.36	-0.61	0.05	NA	NA	+	NA	7	17298.45	149.19	0.00
37	NA	-0.36	-0.61	-0.02	NA	NA	+	+	8	17299.08	149.81	0.00
38	NA	-0.36	-0.61	0.05	NA	NA	NA	NA	6	17301.23	151.97	0.00
39	NA	-0.36	-0.62	NA	NA	NA	+	NA	6	17302.60	153.34	0.00
40	0.14	NA	-0.45	-0.06	-0.29	0.11	+	+	10	17304.77	155.51	0.00
41	NA	-0.36	-0.62	NA	NA	NA	NA	NA	5	17305.27	156.00	0.00
42	0.14	NA	-0.45	0.05	-0.29	0.11	+	NA	9	17306.27	157.01	0.00
43	0.14	NA	-0.45	0.05	-0.29	0.11	NA	NA	8	17308.94	159.68	0.00
44	0.13	NA	-0.46	NA	-0.29	0.11	+	NA	8	17311.59	162.33	0.00
45	0.14	NA	-0.46	NA	-0.29	0.11	NA	NA	7	17314.15	164.89	0.00
46	NA	NA	-0.46	-0.07	-0.28	0.12	+	+	9	17324.07	174.81	0.00
47	NA	NA	-0.46	0.05	-0.28	0.12	+	NA	8	17325.88	176.62	0.00
48	NA	NA	-0.46	0.05	-0.28	0.12	NA	NA	7	17328.76	179.50	0.00
49	NA	NA	-0.47	NA	-0.28	0.12	+	NA	7	17330.62	181.36	0.00
50	0.15	NA	-0.47	-0.04	-0.28	NA	+	+	9	17331.65	182.38	0.00
51	0.15	NA	-0.47	0.05	-0.28	NA	+	NA	8	17332.02	182.76	0.00
52	NA	NA	-0.47	NA	-0.28	0.12	NA	NA	6	17333.39	184.13	0.00
53	0.15	NA	-0.47	0.05	-0.28	NA	NA	NA	7	17334.77	185.51	0.00
54	0.14	NA	-0.48	NA	-0.28	NA	+	NA	7	17336.80	187.54	0.00
55	0.15	NA	-0.48	NA	-0.28	NA	NA	NA	6	17339.44	190.18	0.00
56	NA	NA	-0.48	-0.05	-0.27	NA	+	+	8	17354.29	205.03	0.00
57	NA	NA	-0.48	0.05	-0.27	NA	+	NA	7	17354.88	205.62	0.00
58	NA	NA	-0.48	0.05	-0.27	NA	NA	NA	6	17357.87	208.61	0.00
59	NA	NA	-0.49	NA	-0.27	NA	+	NA	6	17359.01	209.75	0.00
60	NA	NA	-0.49	NA	-0.27	NA	NA	NA	5	17361.88	212.62	0.00
61	0.12	NA	-0.62	-0.04	NA	0.10	+	+	9	17424.85	275.59	0.00
62	0.12	NA	-0.62	0.06	NA	0.10	+	NA	8	17425.65	276.39	0.00
63	0.13	NA	-0.62	0.06	NA	0.10	NA	NA	7	17427.94	278.68	0.00
64	0.12	NA	-0.63	NA	NA	0.09	+	NA	7	17432.93	283.67	0.00
65	0.12	NA	-0.63	NA	NA	0.09	NA	NA	6	17435.10	285.84	0.00
66	NA	NA	-0.62	-0.05	NA	0.10	+	+	8	17440.76	291.49	0.00
67	NA	NA	-0.62	0.06	NA	0.10	+	NA	7	17441.83	292.57	0.00
68	NA	NA	-0.62	0.06	NA	0.10	NA	NA	6	17444.32	295.06	0.00
69	0.13	NA	-0.63	0.06	NA	NA	+	NA	7	17444.40	295.14	0.00
70	0.17	-0.38	NA	0.08	-0.53	0.18	+	NA	9	17444.45	295.18	0.00
71	0.13	NA	-0.63	-0.03	NA	NA	+	+	8	17444.45	295.19	0.00
72	0.17	-0.37	NA	0.01	-0.53	0.18	+	+	10	17444.97	295.71	0.00
73	0.13	NA	-0.63	0.06	NA	NA	NA	NA	6	17446.80	297.53	0.00
74	0.17	-0.38	NA	0.08	-0.53	0.18	NA	NA	8	17447.42	298.15	0.00
75	NA	NA	-0.63	NA	NA	0.10	+	NA	6	17448.51	299.25	0.00

76	NA	NA	-0.63	NA	NA	0.10	NA	NA	5	17450.88	301.62	0.00
77	0.13	NA	-0.64	NA	NA	NA	+	NA	6	17451.11	301.85	0.00
78	0.13	NA	-0.64	NA	NA	NA	NA	NA	5	17453.38	304.12	0.00
79	0.16	-0.38	NA	NA	-0.54	0.18	+	NA	8	17461.07	311.81	0.00
80	NA	NA	-0.63	-0.03	NA	NA	+	+	7	17463.23	313.97	0.00
81	NA	NA	-0.63	0.06	NA	NA	+	NA	6	17463.38	314.12	0.00
82	0.17	-0.38	NA	NA	-0.54	0.18	NA	NA	7	17463.86	314.60	0.00
83	NA	NA	-0.63	0.06	NA	NA	NA	NA	5	17466.00	316.73	0.00
84	NA	NA	-0.64	NA	NA	NA	+	NA	5	17469.41	320.15	0.00
85	NA	NA	-0.64	NA	NA	NA	NA	NA	4	17471.90	322.64	0.00
86	NA	-0.38	NA	0.08	-0.53	0.18	+	NA	8	17475.47	326.20	0.00
87	NA	-0.38	NA	0.00	-0.53	0.19	+	+	9	17475.78	326.51	0.00
88	NA	-0.38	NA	0.08	-0.53	0.19	NA	NA	7	17478.77	329.51	0.00
89	NA	-0.38	NA	NA	-0.54	0.18	+	NA	7	17491.23	341.97	0.00
90	NA	-0.38	NA	NA	-0.54	0.18	NA	NA	6	17494.35	345.09	0.00
91	0.18	-0.36	NA	0.08	-0.53	NA	+	NA	8	17512.44	363.17	0.00
92	0.18	-0.36	NA	0.04	-0.53	NA	+	+	9	17513.97	364.71	0.00
93	0.18	-0.36	NA	0.08	-0.53	NA	NA	NA	7	17515.56	366.29	0.00
94	0.18	-0.36	NA	NA	-0.54	NA	+	NA	7	17528.98	379.72	0.00
95	0.18	-0.36	NA	NA	-0.54	NA	NA	NA	6	17531.91	382.65	0.00
96	NA	-0.36	NA	0.08	-0.53	NA	+	NA	7	17550.64	401.38	0.00
97	NA	-0.36	NA	0.04	-0.53	NA	+	+	8	17552.08	402.82	0.00
98	NA	-0.36	NA	0.08	-0.53	NA	NA	NA	6	17554.12	404.86	0.00
99	NA	-0.37	NA	NA	-0.54	NA	+	NA	6	17566.14	416.88	0.00
100	NA	-0.37	NA	NA	-0.54	NA	NA	NA	5	17569.42	420.16	0.00
101	0.17	NA	NA	0.00	-0.56	0.16	+	+	9	17624.66	475.40	0.00
102	0.17	NA	NA	0.09	-0.56	0.16	+	NA	8	17624.93	475.67	0.00
103	0.17	NA	NA	0.09	-0.56	0.16	NA	NA	7	17627.79	478.53	0.00
104	0.17	NA	NA	NA	-0.57	0.16	+	NA	7	17645.21	495.95	0.00
105	0.17	NA	NA	NA	-0.57	0.16	NA	NA	6	17647.88	498.62	0.00
106	NA	NA	NA	-0.01	-0.56	0.17	+	+	8	17656.80	507.54	0.00
107	NA	NA	NA	0.09	-0.56	0.17	+	NA	7	17657.36	508.09	0.00
108	NA	NA	NA	0.09	-0.56	0.17	NA	NA	6	17660.54	511.28	0.00
109	NA	NA	NA	NA	-0.57	0.17	+	NA	6	17676.78	527.52	0.00
110	NA	NA	NA	NA	-0.57	0.17	NA	NA	5	17679.77	530.51	0.00
111	0.18	NA	NA	0.09	-0.56	NA	+	NA	7	17681.35	532.09	0.00
112	0.18	NA	NA	0.03	-0.56	NA	+	+	8	17682.32	533.06	0.00
113	0.19	NA	NA	0.09	-0.56	NA	NA	NA	6	17684.34	535.08	0.00
114	0.18	NA	NA	NA	-0.57	NA	+	NA	6	17701.22	551.96	0.00
115	0.18	NA	NA	NA	-0.57	NA	NA	NA	5	17704.02	554.76	0.00
116	NA	NA	NA	0.09	-0.56	NA	+	NA	6	17720.37	571.10	0.00
117	NA	NA	NA	0.02	-0.56	NA	+	+	7	17721.19	571.93	0.00
118	NA	NA	NA	0.09	-0.56	NA	NA	NA	5	17723.72	574.45	0.00
119	NA	NA	NA	NA	-0.57	NA	+	NA	5	17739.19	589.93	0.00
120	NA	NA	NA	NA	-0.57	NA	NA	NA	4	17742.33	593.07	0.00
121	0.17	-0.45	NA	0.14	NA	0.18	+	NA	8	18063.92	914.66	0.00
122	0.17	-0.45	NA	0.12	NA	0.18	+	+	9	18065.81	916.55	0.00
123	0.17	-0.45	NA	0.14	NA	0.18	NA	NA	7	18065.83	916.57	0.00
124	NA	-0.45	NA	0.14	NA	0.19	+	NA	7	18095.51	946.24	0.00
125	NA	-0.45	NA	0.11	NA	0.19	+	+	8	18097.33	948.07	0.00
126	NA	-0.45	NA	0.14	NA	0.19	NA	NA	6	18097.78	948.52	0.00
127	0.16	-0.46	NA	NA	NA	0.18	+	NA	7	18116.40	967.13	0.00
128	0.16	-0.46	NA	NA	NA	0.18	NA	NA	6	18118.00	968.74	0.00
129	0.18	-0.43	NA	0.14	NA	NA	+	NA	7	18141.14	991.87	0.00
130	0.18	-0.44	NA	0.15	NA	NA	+	+	8	18143.09	993.83	0.00
131	0.19	-0.43	NA	0.14	NA	NA	NA	NA	6	18143.30	994.04	0.00
132	NA	-0.46	NA	NA	NA	0.19	+	NA	6	18146.87	997.61	0.00
133	NA	-0.46	NA	NA	NA	0.19	NA	NA	5	18148.81	999.55	0.00
134	NA	-0.44	NA	0.14	NA	NA	+	NA	6	18181.14	1031.88	0.00
135	NA	-0.44	NA	0.15	NA	NA	+	+	7	18183.12	1033.86	0.00
136	NA	-0.43	NA	0.14	NA	NA	NA	NA	5	18183.74	1034.47	0.00
137	0.18	-0.44	NA	NA	NA	NA	+	NA	6	18194.45	1045.19	0.00
138	0.18	-0.44	NA	NA	NA	NA	NA	NA	5	18196.27	1047.01	0.00
139	NA	-0.44	NA	NA	NA	NA	+	NA	5	18233.12	1083.86	0.00
140	NA	-0.44	NA	NA	NA	NA	NA	NA	4	18235.34	1086.08	0.00
141	0.17	NA	NA	0.15	NA	0.17	+	NA	7	18333.84	1184.57	0.00

142	0.17	NA	NA	0.12	NA	0.17	+	+	8	18335.49	1186.23	0.00
143	0.17	NA	NA	0.15	NA	0.17	NA	NA	6	18335.51	1186.25	0.00
144	NA	NA	NA	0.15	NA	0.17	+	NA	6	18366.91	1217.64	0.00
145	NA	NA	NA	0.11	NA	0.18	+	+	7	18368.44	1219.17	0.00
146	NA	NA	NA	0.15	NA	0.18	NA	NA	5	18368.93	1219.67	0.00
147	0.18	NA	NA	0.15	NA	NA	+	NA	6	18398.13	1248.87	0.00
148	0.16	NA	NA	NA	NA	0.17	+	NA	6	18398.21	1248.95	0.00
149	0.17	NA	NA	NA	NA	0.17	NA	NA	5	18399.58	1250.32	0.00
150	0.19	NA	NA	0.15	NA	NA	NA	NA	5	18400.04	1250.78	0.00
151	0.18	NA	NA	0.15	NA	NA	+	+	7	18400.13	1250.86	0.00
152	NA	NA	NA	NA	NA	0.17	+	NA	5	18430.25	1280.99	0.00
153	NA	NA	NA	NA	NA	0.17	NA	NA	4	18431.93	1282.67	0.00
154	NA	NA	NA	0.15	NA	NA	+	NA	5	18439.07	1289.80	0.00
155	NA	NA	NA	0.14	NA	NA	+	+	6	18441.04	1291.78	0.00
156	NA	NA	NA	0.15	NA	NA	NA	NA	4	18441.38	1292.12	0.00
157	0.18	NA	NA	NA	NA	NA	+	NA	5	18462.63	1313.37	0.00
158	0.18	NA	NA	NA	NA	NA	NA	NA	4	18464.19	1314.93	0.00
159	NA	NA	NA	NA	NA	NA	+	NA	4	18502.29	1353.03	0.00
160	NA	NA	NA	NA	NA	NA	NA	NA	3	18504.23	1354.97	0.00

Table S9. Model selection results for the distance (grid cell steps) required to travel 5° latitude with hyperthermals added as an interaction term. ATC = Absolute temperature change, BSZ = Body size, GRS = Geographic range size, RTNB = Realized thermal niche breadth, RTP = Realized thermal preference, STLT = Distance to latitudinal threshold, HYP = Hyperthermals, HYP:STLT = Interaction between hyperthermals and distance to latitudinal threshold.

Data S1. Dryad data repository containing all data for the main analyses in this paper.

All data and code to run the main text analyses are included on the Dryad repository at 10.5061/dryad.9ghx3ffts.